U. S. DEPARTMENT OF THE INTERIOR
GEOLOGICAL SURVEY

RESULTS OF GEOPHYSICAL INVESTIGATIONS NEAR THE NORMAN, OKLAHOMA, MUNICIPAL LANDFILL, 1995

Jeffrey E. Lucius[1] and Robert J. Bisdorf[1]

Open-File Report 95-825

October 1995

[1] Golden, CO, USA

CONTENTS

FIGURES

TABLES

RESULTS OF GEOPHYSICAL INVESTIGATIONS NEAR THE NORMAN, OKLAHOMA, MUNICIPAL LANDFILL, 1995

by

Jeffrey E. Lucius and Robert J. Bisdorf

INTRODUCTION

In 1994, the Toxic Substances Hydrology Program (TSHP) of the United States Geological Survey (USGS), Water Resources Division (WRD), selected a new study area to be the focus of the program. It was the municipal landfill for the city of Norman in the central part of Oklahoma. This report presents the results of ground-based surface geophysical surveys at the Norman Municipal Landfill conducted during January and February 1995. The purpose of these surveys was to determine the horizontal and vertical extent of the electrically conductive part of the contaminant plume emanating from the landfill. The surveys were performed by Jeff Lucius, Bob Bisdorf, Jackie Williams, and Roy Kipfinger of the USGS, Geologic Division (GD). Scott Christenson and James Greer, of the WRD, assisted in various aspects of the surveys, including the collection and processing of global positioning system (GPS) data used to locate the stations.

The Norman Landfill was selected by the TSHP because it offers unique opportunities for scientific research in an exceptionally dynamic hydrologic system (Callender and others, 1993). The hydrology near the landfill includes dynamic interactions between ground water and surface water (both natural and anthropogenic), complex permeability structure in a lithologically heterogeneous aquifer, and processes of degradation and geochemical interaction in a ground-water environment (Callender and others, 1993).

In 1994, the WRD Oklahoma District Site Coordinator, Scott Christenson, requested geophysical investigations at the site to address the following problems:

- vertical and horizontal extent of the leachate plume,
- alluvial aquifer geometry,
- identification of lithology and sedimentary structures,
- location and size of buried objects that might be hazardous to drilling operations,
- determination of hydraulic properties, such as porosity and conductivity, and
- identification of geochemical interactions between aquifer fluids and sediments.

Because very little information was available for this site concerning the extent of the leachate plume emanating from the landfill, that was the first problem addressed. In January 1995, electromagnetic (EM) induction (conductivity) surveys were performed around the perimeter of the landfill to determine the flow direction of the conductive (inorganic) part of the plume. It was determined that the plume was flowing primarily to the south and southwest, toward the Canadian River. In February, extensive EM conductivity and direct current (DC) resistivity surveys were performed to determine the extent of the plume and its

vertical stratification. Ground penetrating radar (GPR) data were collected south of the landfill, on the alluvium, to evaluate the suitability of that method to solve some of the problems mentioned above.

Site Location

The landfill is located south of Norman, OK on the wide alluvial-filled valley created by the Canadian River (fig. 1). The landfill occupies approximately 20 hectares and is currently about 600 meters (m) from the river. As recently as 1983, the meandering Canadian River was within 70 m of the landfill (Adrian and others, 1990). The landfill is divided into two mounds or cells. The larger cell covers about 18 hectares. The smaller cell is southeast of the larger one. Treated sewage from Norman is discharged toward the Canadian River from between the two cells (fig. 2). The Norman Asphalt Company is located adjacent to the larger cell and mines the alluvium near the landfill for road construction materials. The base of the landfill is approximately 335 m above sea level (U.S. Geological Survey, 1983). The Norman area receives about 0.84 m of precipitation annually (Wood and Burton, 1968).

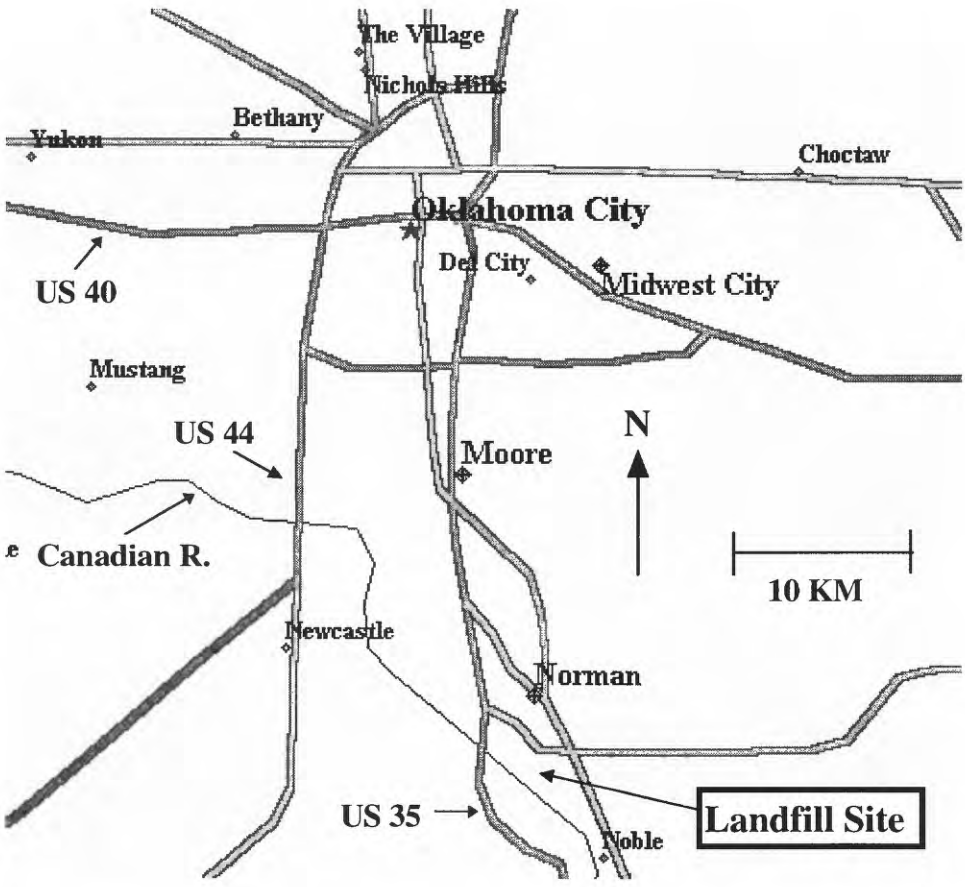

Figure 1. Site location map.

Site History

The landfill received waste from 1922 to 1985. Solid wastes were deposited at first on the ground surface, then in trenches dug by a gravel company, and finally onto the mounds. There were no restrictions on the type of material dumped in the landfill (Callender and others, 1993). In 1985, the landfill mounds were covered with a clay cap and the landfill permanently closed. The mounds are approximately 15 meters high and covered with grass. Near-surface ground water near the site is known to be contaminated with organic and inorganic compounds, some of which are carcinogenic (Dunlap and others, 1976). This site is not on the EPA Superfund list.

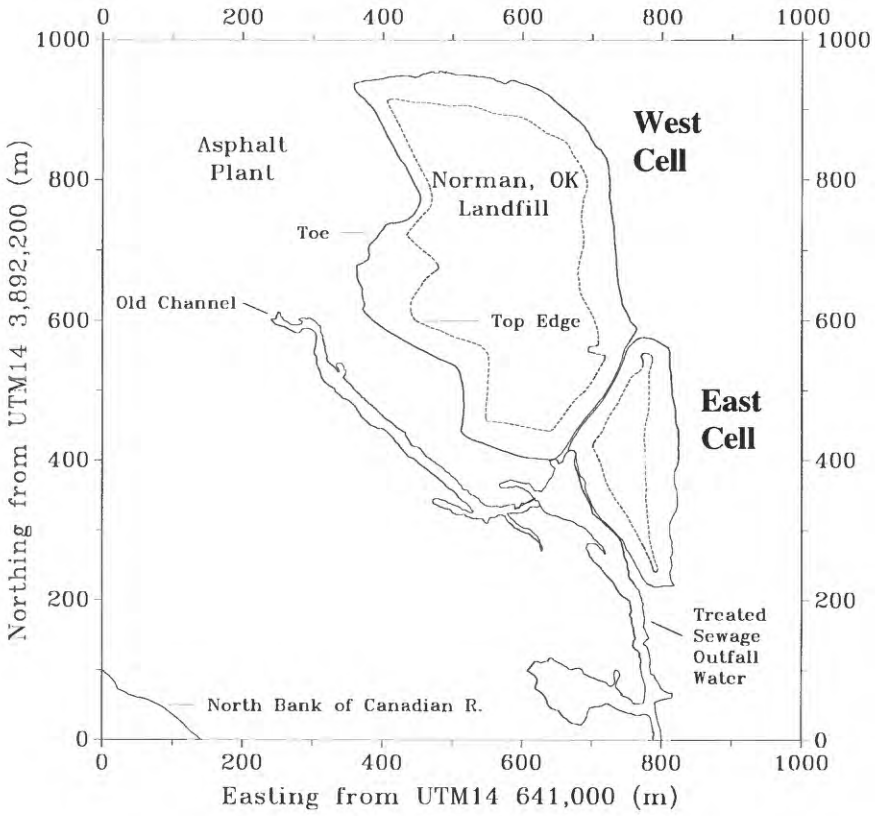

Figure 2. Site map showing outlines of the two landfill cells and surface water areas at the old channel and downstream from the treated sewage outfall. Landform outlines derived from GPS data processed by Scott Christenson and James Greer, USGS, WRD.

Geologic Setting

The alluvium, upon which the landfill is located, has been continually eroded, transported, and deposited by the Canadian River, and so it is Quaternary in age and the youngest geologic unit in the area. It consists of unconsolidated sand, silt, gravel, and clay and is from 10 to 15 meters thick (Callender and others, 1993). The water table is very shallow, ranging in depth from less than a meter, near the borrow areas for the Norman

Asphalt Plant, to as much as 3 or 4 meters, near the landfill and on the alluvial dunes (Callender and others, 1993). Immediately below the alluvium is the Hennessey Group consisting of reddish-brown shales and mudstones with a few thin beds of fine-grained sandstone (Parkhurst and others, 1993). Beneath the landfill, the Permian-age Hennessey Group is about 60 meters thick (Wood and Burton, 1968). Hydraulic transmissivity is low in the Hennessey Group and so it acts as a confining unit. Below the Hennessey Group is the Garber Sandstone, a major aquifer in central Oklahoma. The Garber Sandstone is also Permian in age and consists of lenticular beds of fine-grained, massive-appearing, cross-bedded sandstone irregularly interbedded with shale, siltstone, and mudstone (Wood and Burton, 1968; Parkhurst and others, 1993). The contact between the Garber sandstone and the overlying Hennessey Group has been described as apparently conformable and in places there may be a zone up to 10 m thick where the two formations interfinger (Wood and Burton, 1968).

Geophysical Data Acquisition, Processing, and Interpretation

The next sections in this report will present the theory and methodology of the geophysical techniques used at the Norman, Oklahoma site in January and February of 1995. They will also discuss how the data were processed, manipulated, and organized for analysis, presentation, and interpretation. The purpose of geophysical data interpretation is to determine the data's geological significance. Interpretation is greatly helped by having geological and hydrological information from the area where the geophysical data were acquired. Some ambiguity will always be involved in interpretation of geophysical data because, generally, a unique cause or source of a measurement cannot be determined. For this reason, multiple geophysical techniques were employed at Norman, each technique measuring different properties of the subsurface. By integrating the data from different geophysical techniques, ambiguity in the data can often be lessened.

EM INDUCTION

Principle of Operation and Instrumentation

Electrical conductivity is the property of a material that facilitates the flow of electrical current. Electromagnetic induction instruments, models EM31-D and EM34-3, manufactured by Geonics Limited (Mississauga, Ontario, Canada) were used to measure the electrical conductivity of the ground using magnetically induced currents at low frequencies (McNeill, 1980). The Geonics instruments operate by energizing a transmitter coil, on or near the earth, with an alternating current. A receiver coil is located a small distance (3.66 m to 40 m) away and is aligned to be coplanar with the transmitting coil. Secondary alternating electric currents are generated in the earth by the time-varying primary magnetic field arising from the alternating current in the transmitter coil. The induced alternating electric currents in the earth generate a secondary magnetic field which is sensed, together with the primary magnetic field, by the receiver coil. The indicated apparent conductivity is a function of intercoil spacing, operating frequency, ratio of the secondary to primary magnetic fields, and coil orientation. The apparent conductivity is equivalent to true conductivity only when conductivity is uniform throughout the subsurface. The conductivity of the alluvium and bedrock is controlled by the matrix (sediment or rock), porosity, pore space saturation, and conductivity of pore solutions (water or leachate). See McNeill (1980) for a more detailed discussion of Geonics instruments. Keller and Frischknecht (1966) and Nabighian (1987) provide further explanations of electromagnetic inductive methods.

Site Surveys

Four groups of EM conductivity measurements were made: two test lines, the perimeter stations, and the grid (figures 3, 4). Test line 1 extended from the base of the west (larger) landfill mound south 40^{o} west to the Canadian River. Test line 2 was oriented perpendicular to test line 1 approximately 170 meters from the landfill. The perimeter stations were along the toe (or base) of both mounds. The grid was aligned with the test lines, southwest of the larger mound. All conductivity meter readings (in mS/m) were recorded in field notebooks and are presented in the Appendix.

The test lines were designed to evaluate the feasibility of using the EM method to detect the conductive part of the leachate plume and to measure representative subsurface conductivity away from the landfill ("background"). Test line 1 consisted of 67 stations spaced 10 m apart. Both EM31-D and EM34-3 instruments were used with the following combinations of coil spacings and orientations - 3.66 m, 10m, 20m, and 40m spacings, horizontal coplanar coils (vertical magnetic dipoles, VMD) and vertical coplanar coils (horizontal magnetic dipoles, HMD). Measurements were assigned to stations located midway between the two coils which were on the test line. The EM31-D was held at hip height (approximately 1 meter above the ground). EM34-3 coils were placed on the ground.

Test line 2 was placed perpendicular to test line 1, about 170 meters from the landfill mounds, and extended 100 m northwest of test line 1 and 500 m southeast. There were 31

stations spaced 20 m apart. Both coil orientations were used with the EM31-D at hip height and with the EM34-3 using the 10m and 20m coil separations. No measurements were made with the coils 40 m apart. Measurements were assigned to stations located midway between the coils which were on the test line.

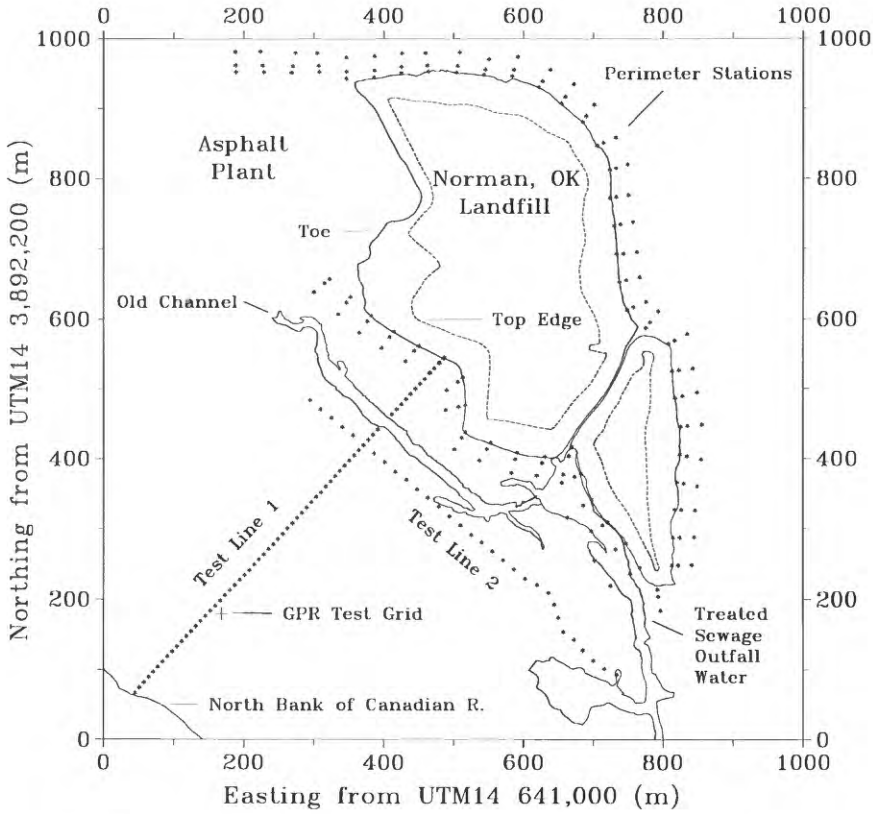

Figure 3. Locations of EM stations along test lines 1 and 2, and perimeter.

The perimeter stations were placed around the base of both landfill mounds to determine which direction (or directions) the leachate plume was flowing away from the landfill (fig. A4 in Appendix). No measurements were made on the west side of the larger mound because the asphalt plant occupied that area. There were 51 sets of three stations spaced about 40 meters apart. Each set of stations consisted of one near the toe of a mound, one about 10 m out from the toe, and one about 30 m out. The EM31-D was used in VMD mode only, at hip height. Two readings were taken at each station, one parallel to the landfill toe and one perpendicular to it.

The grid of stations consisted of 21 profiles, parallel to test line 1, spaced about 20 meters apart. There were 10 m between stations along the profiles. No stations were occupied where there was standing water, so the grid has some "holes" in it. There were a total of 405 stations on the grid. Both coil orientations were used with the EM31-D at hip height and with the EM34-3 using the 10m and 20m coil separations. No measurements were

made with the coils 40 m apart. Measurements were assigned to stations located midway between the coils, which were on the profiles.

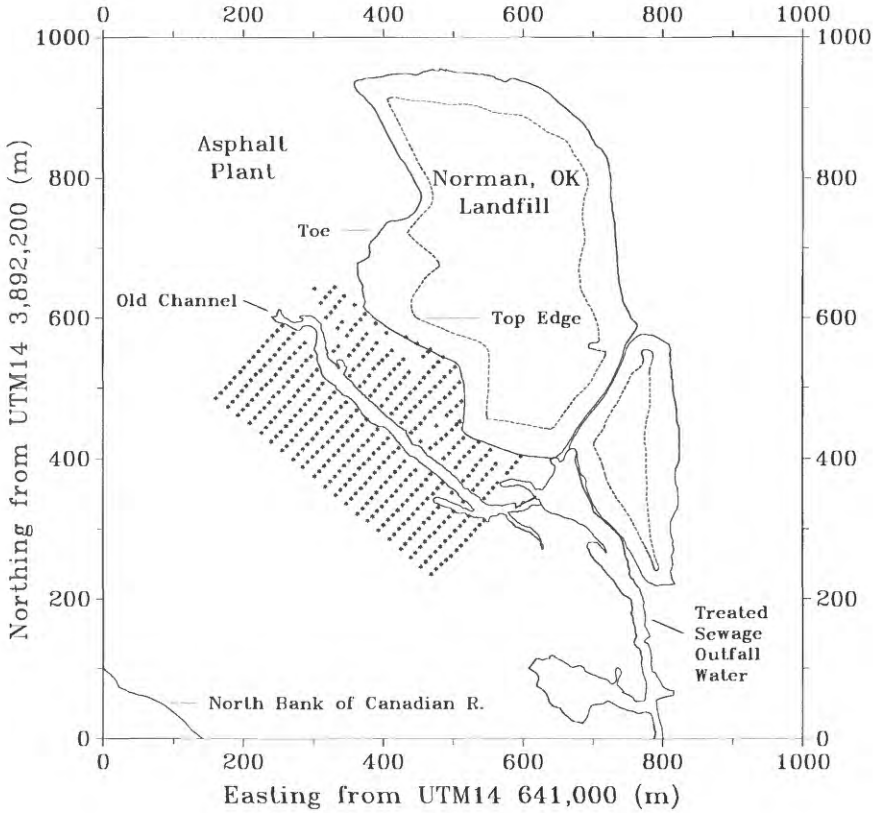

Figure 4. Locations of EM stations on the grid.

Data Processing

Data from the Geonics terrain conductivity meters did not require processing before being used for display, analysis, and interpretation. This section briefly describes peculiarities about the instruments and reasons for not manipulating the data.

For the Geonics EM conductivity meters to accurately measure terrain conductivity the induction number B must be low. The induction number is the intercoil spacing divided by the electrical skin depth, which is defined as the distance in a homogenous half-space that a propagating plane wave has traveled when its amplitude has been attenuated to $1/e$ (or ≈ 0.368) of the amplitude (McNeill, 1980). The low induction number approximation breaks down as terrain conductivity increases. Figure 5 shows a plot from McNeill (1980) of the indicated conductivity for the EM31-D versus true conductivity for a homogenous half-space. The conductivity indicated by the meter is increasingly less than the true terrain conductivity when the meter reads above 50 mS/m (mmho/m). The HMD orientation is linear to greater values of conductivity than is theVMD orientation. The EM34-3 conductivity meter exhibits

even greater non-linearity (see McNeill, 1983, fig. 1) than the EM31-D. The EM conductivity meter readings were not corrected for non-linearity. The main utility of the conductivity meters is to map relative changes in terrain conductivity rather than to determine the actual values of conductivity. Programs that model the data to determine subsurface horizontal stratification automatically correct for the non-linearity.

The EM34-3 conductivity readings are affected by misalignment of the coils (coil geometry is fixed in the EM31-D). The VMD (horizontal coplanar coil) mode is most sensitive to misalignment. Because of heavy brush and dense growth of trees, the operators of the two EM34-3 coils sometimes could not see each other, and coil misalignment was inevitable. No correction can be applied for these errors in the data, but it must be recognized that significant inaccuracy in meter readings can be present in the 20 m and 40 m coil separations, especially for VMD orientations.

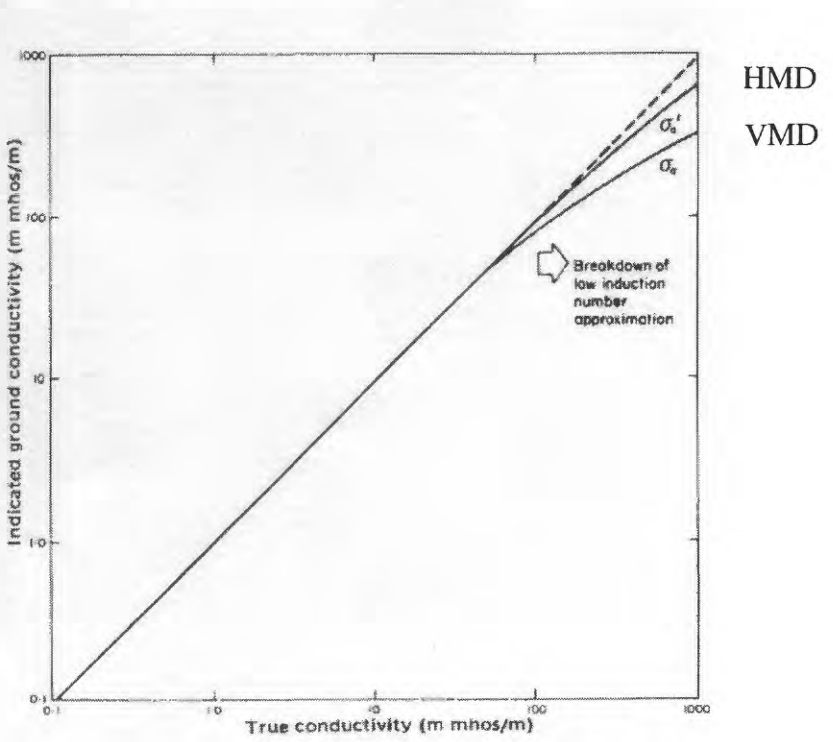

Figure 5. Plot of indicated conductivity for EM31 versus true (homogenous half-space) conductivity for both vertical (VMD) and horizontal (HMD) magnetic dipoles (modified from McNeill, 1980).

Changes in conductivity in the saturated zone exert a major influence on the conductivity meter readings, especially as the distance between the instrument and the water table varies. Therefore, a "reduction to water table" correction is often applied to the data when a conductivity value and thickness can be assumed for the unsaturated zone. Because most of the survey area was relatively flat and the water table was very near the surface (from 0 to 3 meters), this correction was not performed on the data.

The EM measurements, at the different coil spacings and orientations for each station, were collated into computer text files and associated with the GPS-derived station locations (see the Appendix). These files were used as input for unpublished USGS software and for a commercial EM modeling program, EMIX 34™ (Interpex Ltd., 1989). To generate map views of the terrain apparent conductivity, the data for each coil separation and orientation was submitted to a minimum-curvature gridding algorithm (Briggs, 1974). Ten-meter-cell grids were calculated for the site with grid nodes greater than 20 meters from an EM station "blanked" out.

Analysis and Interpretation

Apparent conductivity values are normally displayed in plan view, as either a contour map or gray-scale image showing the spatial distribution of measurements, or as a graph showing measurements along one or more profiles. In either case, the measurements indicate an *apparent* conductivity for the ground that weighs together conductivity at various depths and does not indicate a *true* conductivity. If the ground is horizontally stratified into 2 or 3 layers or is homogeneous, a computer model can be designed to account for the measurements. Often, however, the conductivity measurements are more simply treated as relative (as opposed to absolute) values of conductivity from an "effective" depth dependent on coil orientation and spacing.

Depths of investigation (75% of instrument response is from the surface to this depth) and depths of maximum sensitivity for the Geonics instruments depend on coil orientation and spacing and are summarized in table 1.

Table 1. Depth of investigation and depth of maximum sensitivity for coil spacings and orientations of the Geonics EM induction instruments, derived from McNeill (1980)

Instrument	Coil Spacing (m)	Coplanar Coil Orientation	Depth of Investigation (m)	Depth of Maximum Sensitivity (m)
EM31-D	3.66	Vertical	3.5	near surface
EM31-D	3.66	Horizontal	7.3	1.5
EM34-3	10.00	Vertical	9.5	near surface
EM34-3	10.00	Horizontal	20	4
EM34-3	20.00	Vertical	19	near surface
EM34-3	20.00	Horizontal	40	8
EM34-3	40.00	Vertical	38	near surface
EM34-3	40.00	Horizontal	80	16

Coil orientation determines the manner in which the instrument responds to the subsurface. The magnetic field dipole (the axis of the field) generated by a coil is perpendicular to the plane of the coil. When the magnetic dipoles of the two coplanar coils are vertical (VMD; dipoles perpendicular to the ground; coils horizontal or lying flat on the ground), the instrument is relatively insensitive to the near-surface conductivity and objects.

When the magnetic dipoles are horizontal (HMD) the instrument is most sensitive to near-surface conductivity and objects. The relative and cumulative response (that is, the relative and cumulative influence of current flow) can be calculated for a homogeneous or horizontally-stratified earth (McNeill, 1980, p. 15). Figure 6 shows the relative response versus coil spacing (normalized depth) of the Geonics instruments for the two coil orientations. Figure 7 shows the cumulative response of the instruments versus coil spacing (normalized depth). The horizontal dashed lines at 0.5 (50% of cumulative response) and at 0.25 (75% of cumulative response), and corrsponding vertical dashed lines, where the horizontal lines intersect the curves, show what depth the response percentage has accumulated from. It should be noted that the instruments in VMD orientation average the subsurface conductivity to about twice the depth that they would in HMD orientation. In other words, the VMD mode measures twice as deep as the HMD mode. Figures 8 and 9 are similar to figure 6, except that they show the relative responses for HMD and VMD modes, respectively, as a function of true depth for particular instruments.

EM data collected on the grid is shown in figures 10 and 11 as gray-scale image maps of relative conductivity. Darker shades indicate higher conductivity. Horizontal magnetic dipole (vertical coplanar coils) measurements are grouped together in figure 10 and vertical magnetic dipole measurements are presented in figure 11. To aid interpretation, a graph accompanies each image map showing the relative response of the instrument, for that coil separation and orientation, versus depth. The dashed line in each graph indicates the depth at which 75% of the total, or cumulative, response of the instrument has occurred. In other words, the ground conductivity from the surface to this depth contributed 75% to the instrument's response. The shallowest measurements are at the top of each figure.

Figures 10 and 11 show that the highest conductivities occur within 200 meters of the landfill mounds, suggesting that the *measurable* conductive part of the leachate plume probably does not extend beyond this limit. Variations in intensity near the landfill also suggests that the leachate distribution is not equal over the area. Away from the landfill, there appears to be little variation in the ground conductivity, except for increases with depth. As mentioned earlier, the EM34-3 is very sensitive to coil misalignment when used in the vertical magnetic dipole (horizontal coplanar coils) mode. Inaccurate readings due to coil misalignment are probably the main cause of the "blotchy" appearance of image maps in figure 11, especially 11(c).

According to Callender and others (1993), the alluvium is about 10 to 14 meters thick. Using the "75%" line in the graphs, the conductivity values in all the image maps in figure 10 and the top two in figure 11, are dominantly derived from the saturated and unsaturated alluvium. Only in figure 11(c) do electric currents in the Hennessey shale below the alluvium contribute substantially to the measurements. The somewhat more uniform appearance of the data in figure 11(c) then suggests that the leachate has not substantially penetrated into the shale below the alluvium.

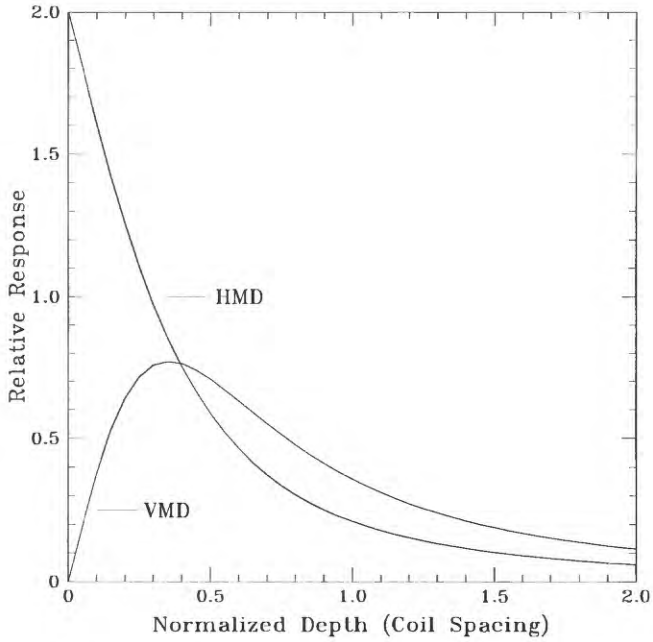

Figure 6. Comparison of relative responses versus coil spacing for vertical (VMD) and horizontal (HMD) magnetic dipoles for Geonics EM induction instruments (from McNeill 1980).

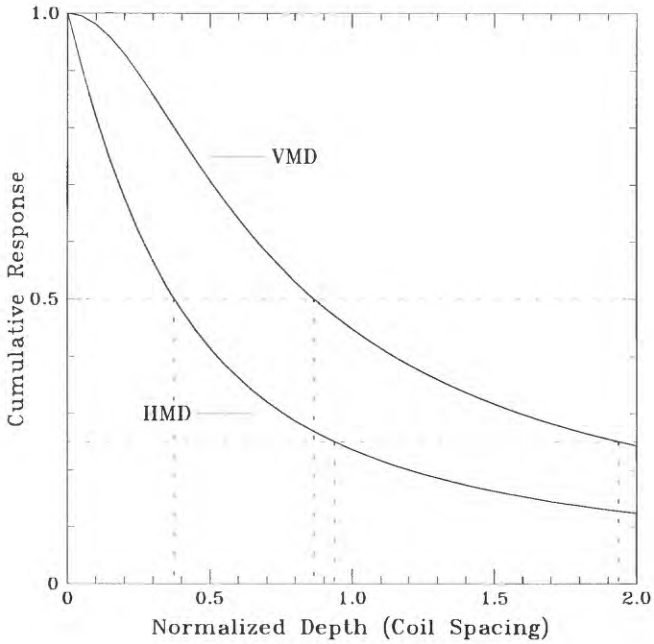

Figure 7. Comparison of cumulative response versus coil spacing for vertical (VMD) and horizontal (HMD) magnetic dipoles for Geonics EM induction instruments (from McNeill 1980).

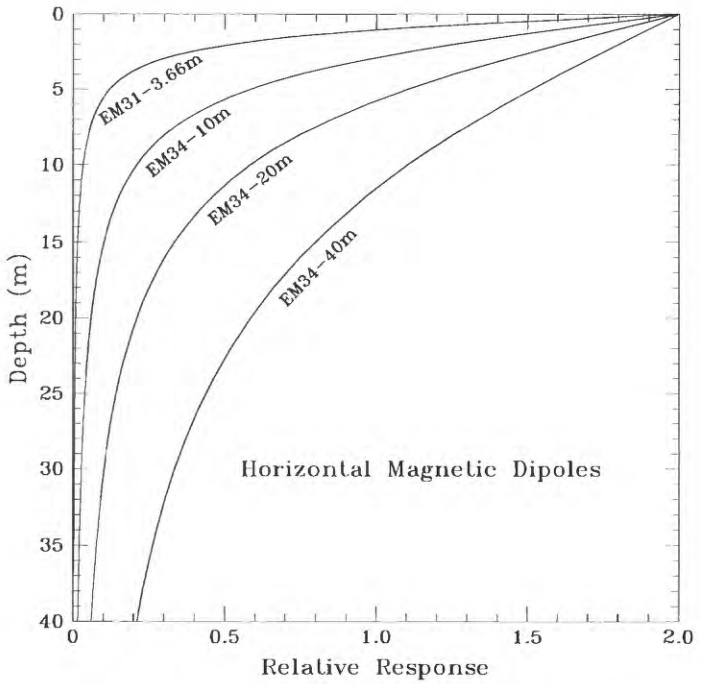

Figure 8. Comparison of relative responses versus depth for horizontal magnetic dipoles for various coil spacings for Geonics EM induction instruments (from McNeill 1980).

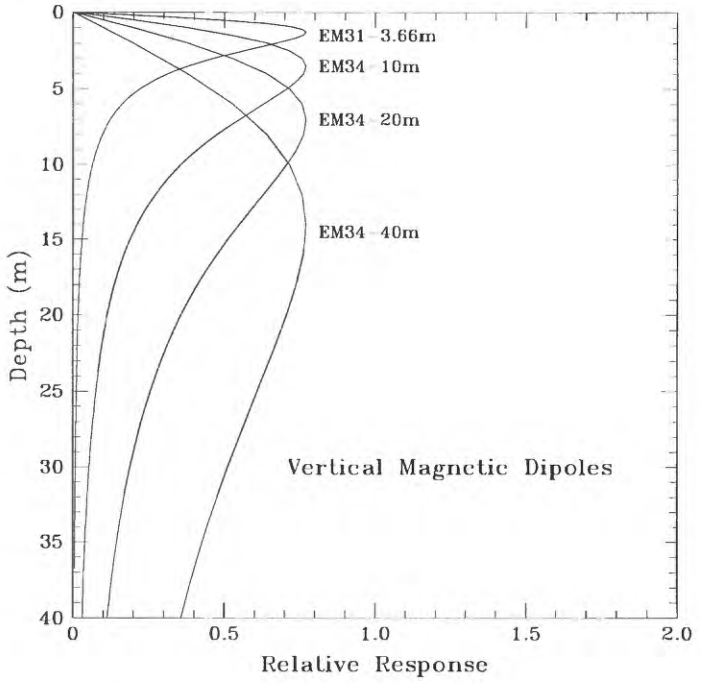

Figure 9. Comparison of relative responses versus depth for vertical magnetic dipoles for various coil spacings for Geonics EM induction instruments (from McNeill 1980).

Presenting the EM conductivity data in graphic form as a profile allows better inspection of the actual values. Figures 12 and 13 show the HMD and VMD measurements, respectively, taken along test line 1 (fig. 3). The HMD measurements in fig. 12 show an increase in conductivity with depth probably due to the small increase in current flow in the conductive shale below the alluvium as coil separation increased (fig. 10). The apparent conductivity is much higher within 200 m of the landfill presumably due to conductive leachate from the landfill in the ground water. No measurements were taken in the old channel which was about 20 m wide and 1 m deep, but measurements were relatively higher near the channel. Measurements were nearly uniform for each coil separation on the alluvium away from the landfill, suggesting lateral homogeneity in the near subsurface at the horizontal scales that the EM31-D and EM34-3 were measuring. The small conductivity variations at 3.66 m and 10m coil separations between 300 m and 450m can be correlated to topographic changes due to alluvial dunes. The slight increase in conductivity at the left side of fig. 12 is due the influence of the Canadian River, which may be more conductive than the ground water. Similar conclusions can be drawn for VMD data in fig. 13, noting that greater variation in measurement accuracy is more likely due to coil misalignment than subsurface heterogeneity. Greater non-linearity in instrument response is also a factor in VMD mode.

The EM induction technique using the Geonics EM31-D and EM34-3 is very good at quickly and easily detecting lateral changes in terrain conductivity, but poorer at defining layers in the subsurface. The number of measurements obtained from limited coil spacing and orientation are insufficient to uniquely solve a system of equations relating conductivity and thickness for multiple layers. The inherent ambiguity in the data leads to equivalence of different combinations of thickness and conductivity and the number of layers. Still, the data were input into a commercial modeling program, EMIX 34 Plus (Interpex Ltd., 1989), in an attempt to find reasonable models that fit the data. In general, the three-layer models that best fit the data near the landfill had a conductive (100-200 mS/m) layer about 2 m thick at the surface, a second layer 7-13 m thick that thins toward the landfill with conductivity of 25 to 200 mS/m, and a bottom layer with conductivity of 150 to greater than 200 mS/m. Since the unsaturated, sandy alluvium near the surface should have low conductivity, these models suggest that the conductive layer of the plume is relatively thin and shallow and that most of the saturated alluvium is not contaminated with conductive leachate. This scenario is highly speculative and conclusions regarding vertical stratification of the conductive leachate in the ground water will have to wait for well samples and measurements that are not yet available.

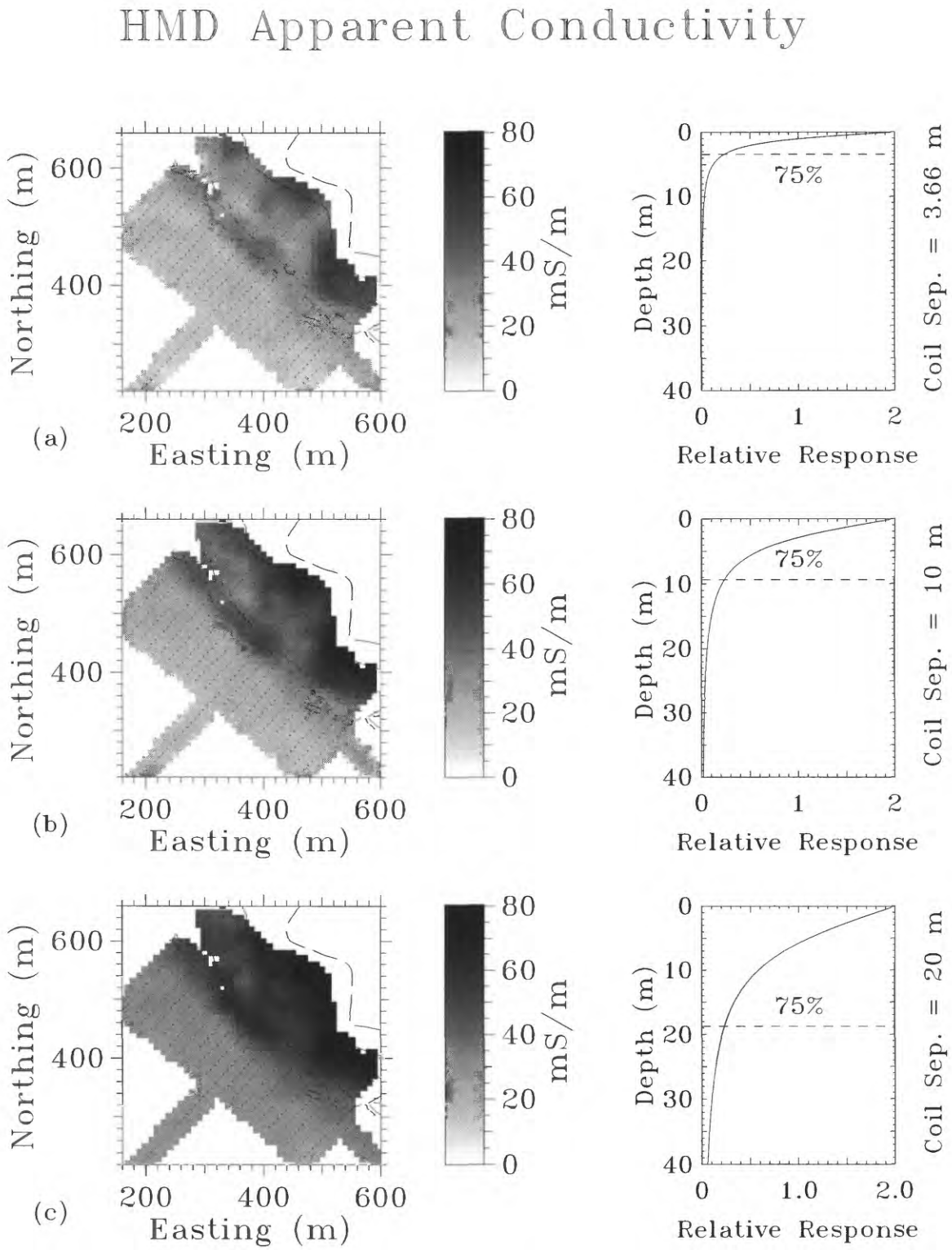

Figure 10. Image maps of apparent conductivity values for horizontal magnetic dipole modes for the EM31-D, (a), and EM34-3, (b) and (c), for stations near the grid next to the Norman landfill west cell. The small dots in each image are the station locations.

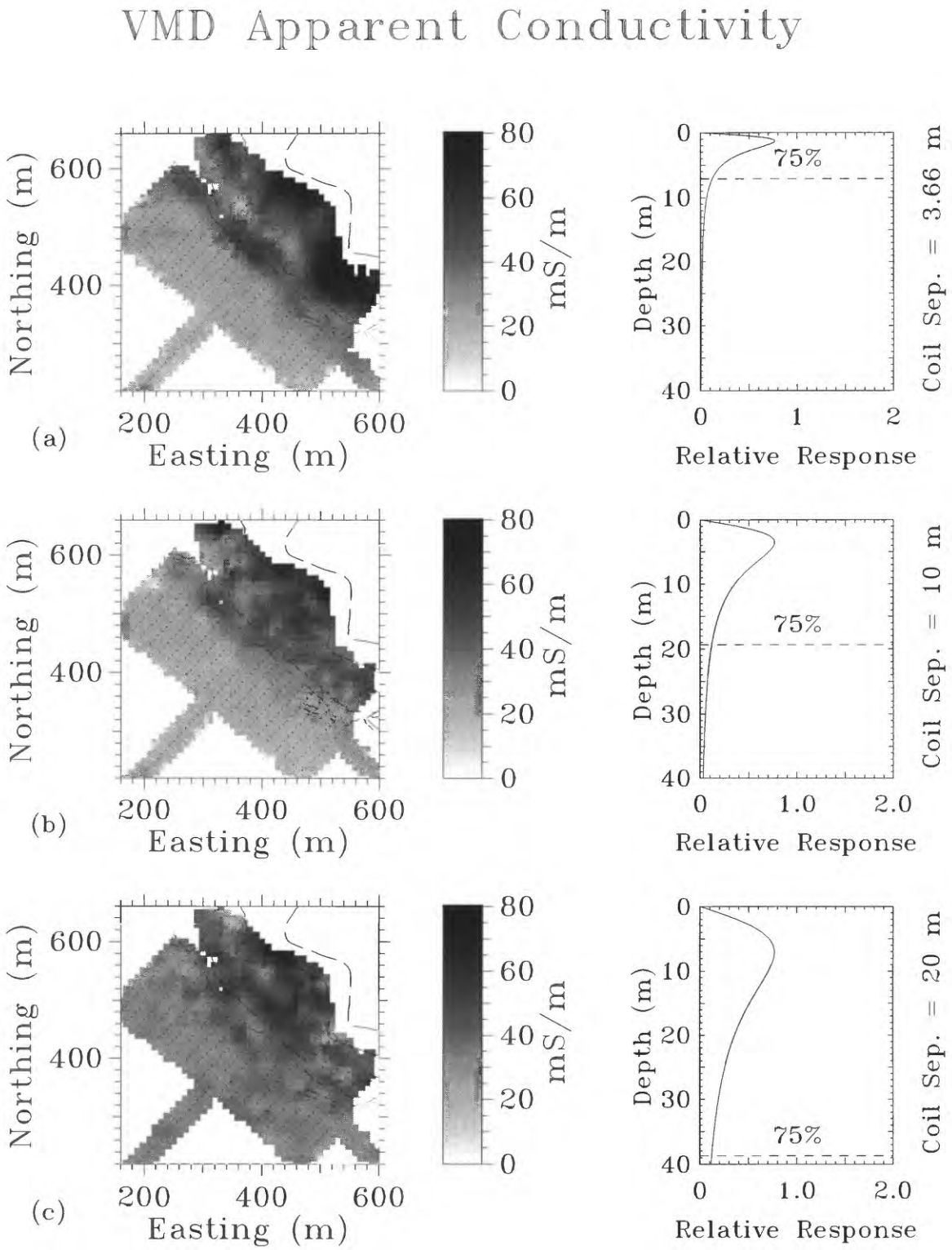

Figure 11. Image maps of apparent conductivity values for vertical magnetic dipole modes for the EM31-D, (a), and EM34-3, (b) and (c), for stations near the grid next to the Norman landfill west cell. The small dots in each image are the station locations.

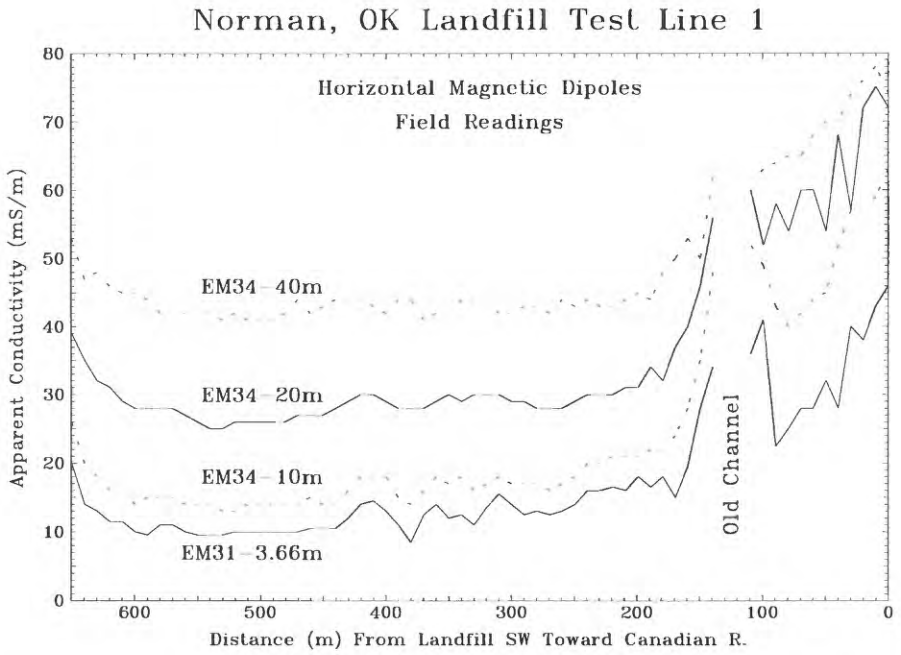

Figure 12. Graph of apparent conductivity along test line 1 for EM31-D and EM34-3 in horizontal magnetic dipole mode near the Norman landfill.

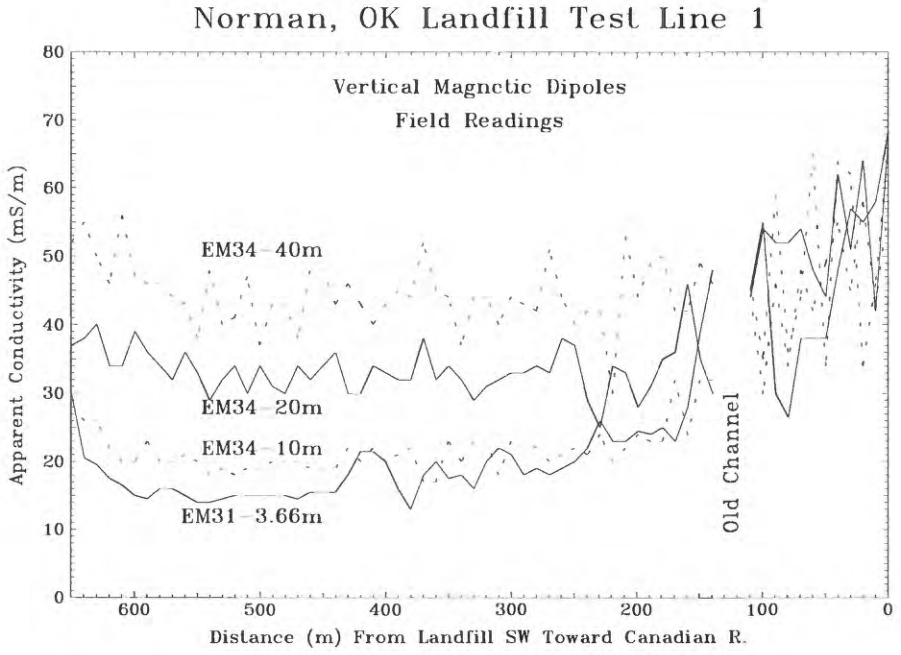

Figure 13. Graph of apparent conductivity along test line 1 for EM31-D and EM34-3 in vertical magnetic dipole mode near the Norman landfill.

DC RESISTIVITY

Principle of Operation and Instrumentation

DC resistivity is a fundamental rock property that remains constant for a homogeneous isotropic material, irrespective of the sample size or measuring geometry. The resistivity of a material is equal to the resistance of a unit cube of that material to the flow of electrical current (Zohdy and others, 1974), and is normally expressed in ohm-meters (ohm-m). The direct current (DC) resistivity system we used at Norman was built by the U.S. Geological Survey. A commutated direct electric current or very low frequency (< 1 hertz, Hz) current, I, is introduced into the ground using two metal electrodes (A and B in fig. 14). Potential difference, ΔV, is concurrently measured at two other metal electrodes (M and N in fig. 14). The DC resistivity sounding surveys at Norman employed a Schlumberger arrangement of the electrodes. In this method, all the electrodes are placed in a straight line, current electrodes are positioned at the ends, and potential electrodes are located symmetrically about the center at various distances. The distance between the potential electrodes, MN, is no more than one fifth that between the current electrodes, AB. A sounding is obtained by making measurements at increasing current electrode separations.

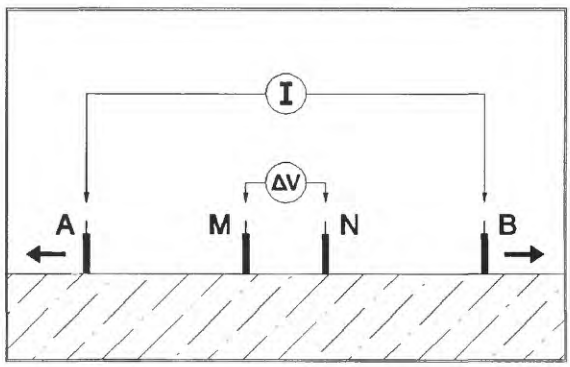

Figure 14. The Schlumberger array in cross section.

For the Schlumberger method, the apparent resistivity, ρ_a, is calculated using equation 1 below.

$$\rho_a = K \Delta V / I, \quad (1)$$

where the geometric factor $K = \pi ((AB/2)^2 - (MN/2)^2) / MN$.

The apparent resistivity is equivalent to true resistivity only when the resistivity is uniform throughout the subsurface. For more detailed discussions of DC resistivity methods, see Zohdy and others (1974), Dobrin (1976), and Koefoed (1979).

Site Surveys

Each DC resistivity sounding consists of a series of measurements made by varying the current and potential electrode separations about a central point. The apparent resistivity, ρ_a, is

calculated for each measurement using equation 1. The current, I, is read from a milliammeter on the electrical current pulser; the potential voltage difference, ΔV, is measured off a potentiometric chart recorder; and the electrode separations, MN and AB, are set at predetermined distances.

Seventeen DC resistivity soundings were measured on and near the landfill (fig. 15). Seven soundings were located near test line 1, with one sounding located on top of the west cell on an extension of test line 1. Five soundings were located along test line 2. The remaining soundings were placed near the toe of the west cell. Sounding measurements started with AB/2 and MN/2 spacings of 3 feet (ft) and 0.6 ft, respectively. MN/2 spacings were increased to 2 ft and 20 ft, with associated AB/2 spacings as shown in table 2. The sounding spreads were generally aligned in a northwest-southeast direction. The DC resistivity sounding curves and automatic computer interpretations are presented in the Appendix.

Table 2. Listing of DC resistivity sounding MN/2 spacings and associated AB/2 values

MN/2 = 0.6 ft	MN/2 = 2 ft	MN/2 = 20 ft
3	10	100
4	14	140
6	20	200
8	30	300
10	40	400
14	60	600
	80	800
	100	1000
	140	

Data Processing

The set of apparent resistivities for a sounding are normally automatically interpreted using computer programs that calculate the thickness and resistivity for a sequence of layers that fit the observed data (Zohdy and Bisdorf, 1989). Computer files of AB/2 and apparent resistivities are constructed for each sounding. The data may undergo some processing before being submitted to the interpretation program. For instance, the field data may be smoothed before the inversion is performed, corrections may be made for non-linear electrode geometry (Zohdy and Bisdorf, 1990), or the sounding's S-line (Zohdy and others, 1974, p. 36) may be manually extended. The last, or bottom, layer resistivity can be fixed at some value as part of the automatic processing. Only sounding Norman 8 was smoothed prior to interpretation.

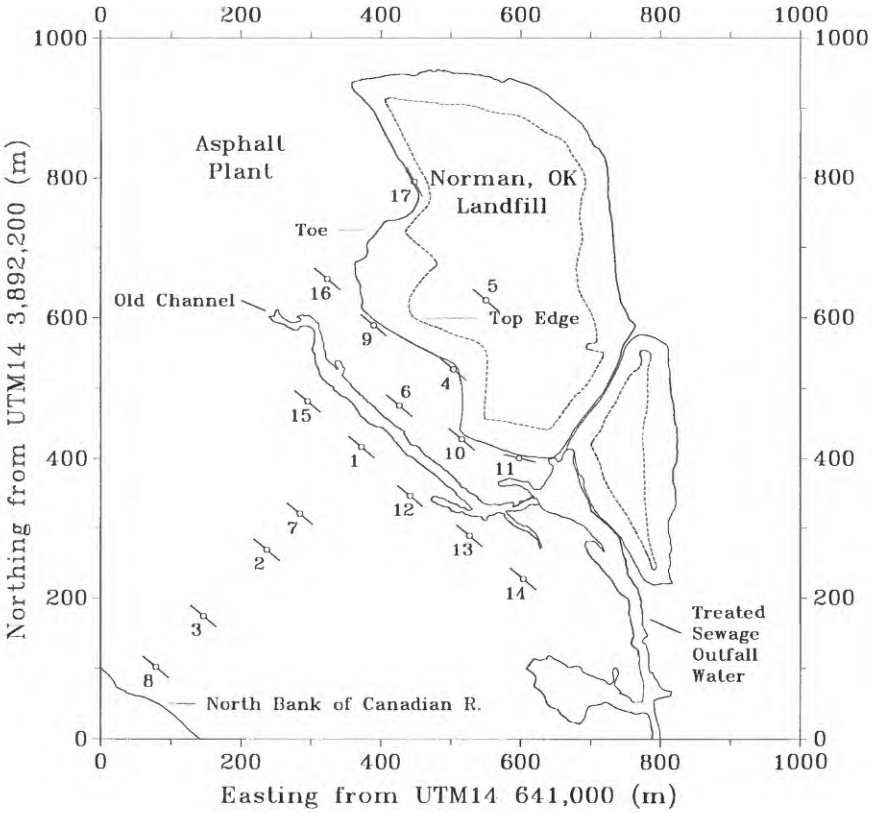

Figure 15. Location of DC resistivity soundings. The bars on either side of the circle indicate the electrode directions of expansion.

Analysis and Interpretation

Three cross sections were generated from the individual sounding interpretations. Each sounding interpretation was sampled in a manner that approximates a continuous vertical distribution of resistivity with depth (Bisdorf, 1982). The vertical data were then horizontally interpolated to create a grid. Color values, or shades of gray, are assigned based on the interpolated resistivity values and the desired contour levels. For resistivity data, it is generally best to use logarithmic contour values. Each figure shows two cross sections, one of the upper 50 m vertically exaggerated four times and another of the complete cross section with no vertical exaggeration. Triangles show the location of the center of each sounding. Soundings were expanded perpendicular to the cross section of figure 16 and parallel to the cross sections of figures 17 and 18.

The interpretation of resistivity data can be ambiguous and generally requires a knowledge of the local geology so that the number of choices for a particular resistivity range can be limited. The gray scale on the side of figures 16, 17 and 18 ranges from light shades, representing high resistivities, through medium shades, representing intermediate resistivities, to dark shades, representing low resistivities, or high conductivities. For the Norman landfill

area, the white shades probably represent dry alluvial sand. Lighter gray shades probably represent clean sand (limited amount of clay) saturated with uncontaminated water. The intermediate shades can be ambiguous, either reflecting the water quality or clay content. In the intermediate shades, darkening represents either an increase in the quantity of clay or a decrease in the quality of the ground water. The lowest (<10 ohm-m) resistivities, darkest shades, almost certainly represent the mudstones and siltstones of the Hennessey Group at depth or, if near the surface, relatively conductive ground water.

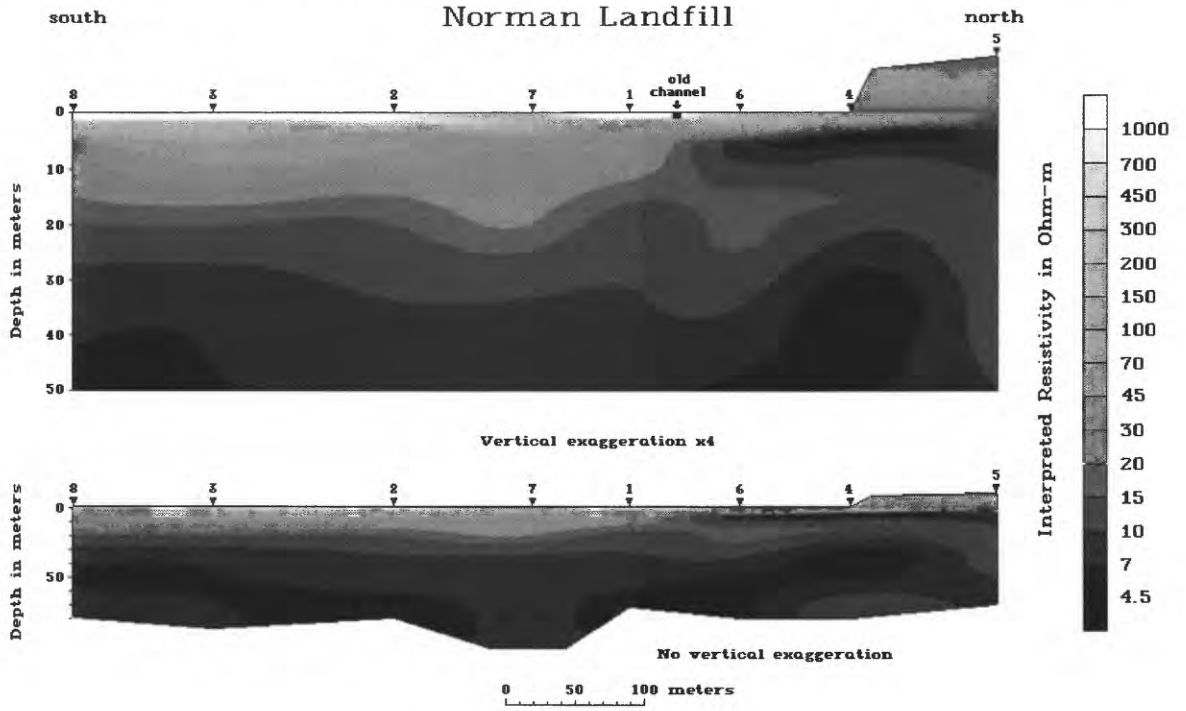

Figure 16. Interpreted DC resistivity sounding cross section along Norman Landfill test line 1.

Figure 16 shows a cross section that extends from sounding 5 to sounding 8 (see fig. 15 for locations). This cross section runs from the top of the landfill toward the Canadian River. Except for sounding 5 on the landfill, the cross section shows a near-surface, greater than 300 ohm-m, high-resistivity layer (light-gray on the cross section) 1 to 2 meters thick that probably represents dry sand. Under soundings 1, 7, 2, 3, and 8 the high resistivities grade smoothly into lower resistivities down to a thick zone characterized by resistivities of less than 10 ohm-m. This low resistivity zone is thought to represent the mudstones and siltstones of the Hennessey Group. The top of the Hennessey is interpreted to be 20 m to 25 m deep. As discussed above, the lighter the shades the higher the sand content. There appears to be a thicker zone of cleaner sand as the Canadian River is approached.

Under soundings 5, 4 and 6 a shallow, less than 10 ohm-m, low-resistivity layer is present. This layer is too shallow to represent the Hennessey Group and is interpreted to represent contaminated ground water. It is assumed that the source of the contamination is the

landfill. The layer is characterized by a sharp upper contact at a depth of about 2m and a gradational lower contact. The upper contact should represent the water table, while the lower contact is indicative of possible lower porosity sediments and less contaminated ground water in the alluvium.

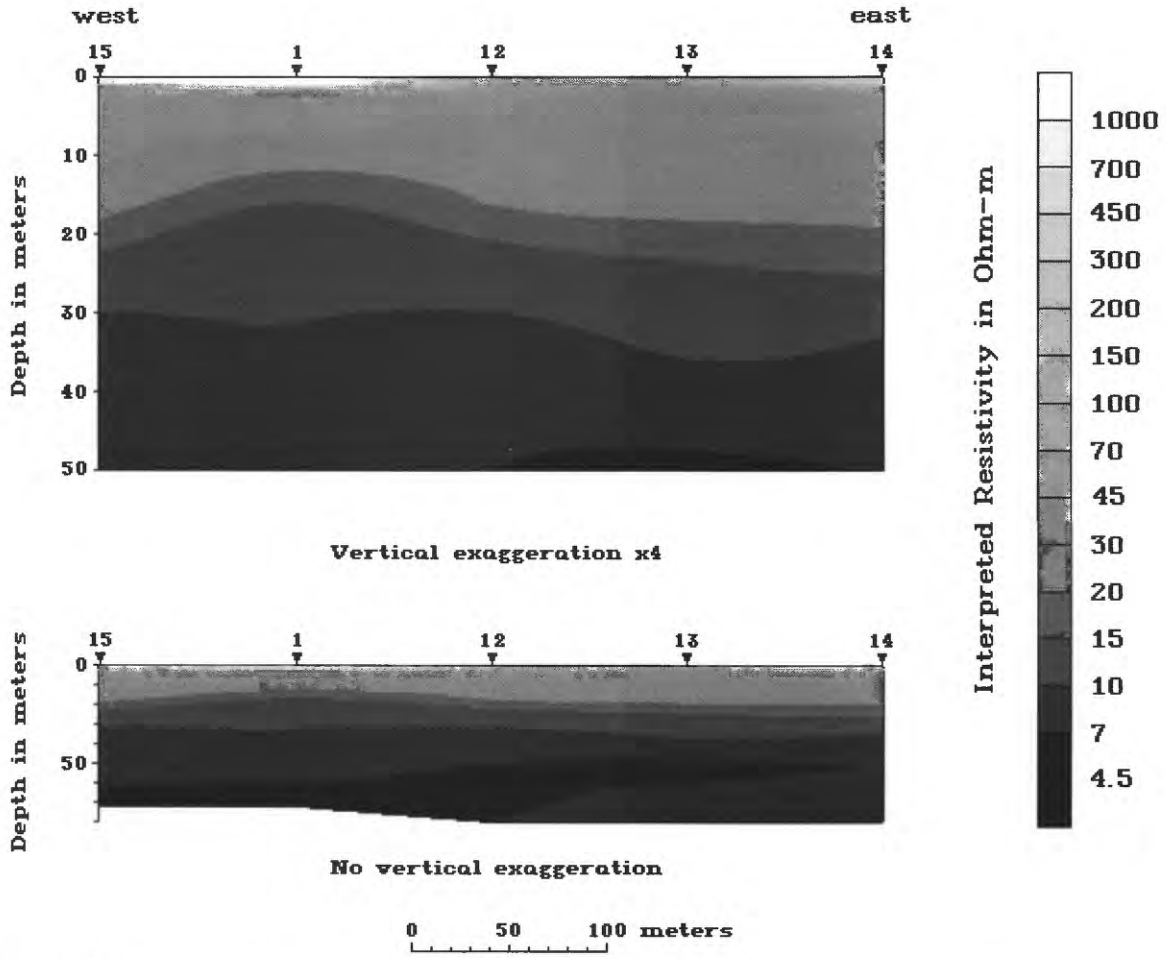

Figure 17. Interpreted DC resistivity sounding cross section along Norman Landfill test line 2.

Figure 17 shows a cross section perpendicular to the cross section shown in figure 16, with sounding 1 common to both cross sections (see fig. 15 for locations). Soundings 15, 1 and 14 show a high resistivity layer in the upper 1 to 2 m which we interpret to represent dry sand. Interpretations of soundings 12 and 13 do not indicate the presence of sand in the upper 1 to 2 m, but indicate higher clay content materials. At sounding 1 a lower resistivity layer is present. This layer might represent a thin zone of contamination caused by a nearby stagnant canal. This low resistivity layer is present under soundings 12 and 13 as well. The top of the Hennessey group is interpreted to be about 22 to 30 m deep and may dip slightly to the southeast.

Figure 18 shows a cross section perpendicular to the cross section shown in figure 16 but near the base of the landfill west cell (see fig. 15 for locations). The cross sections have sounding 4 in common. A low resistivity layer is present under all the soundings, generally at a depth of 1 to 2 m. This layer is thinner and somewhat shallower under sounding 16, and is

about 7 m deep under sounding 11. The layer may appear deeper because the sewage outflow may be adding uncontaminated water just southeast of sounding 11.

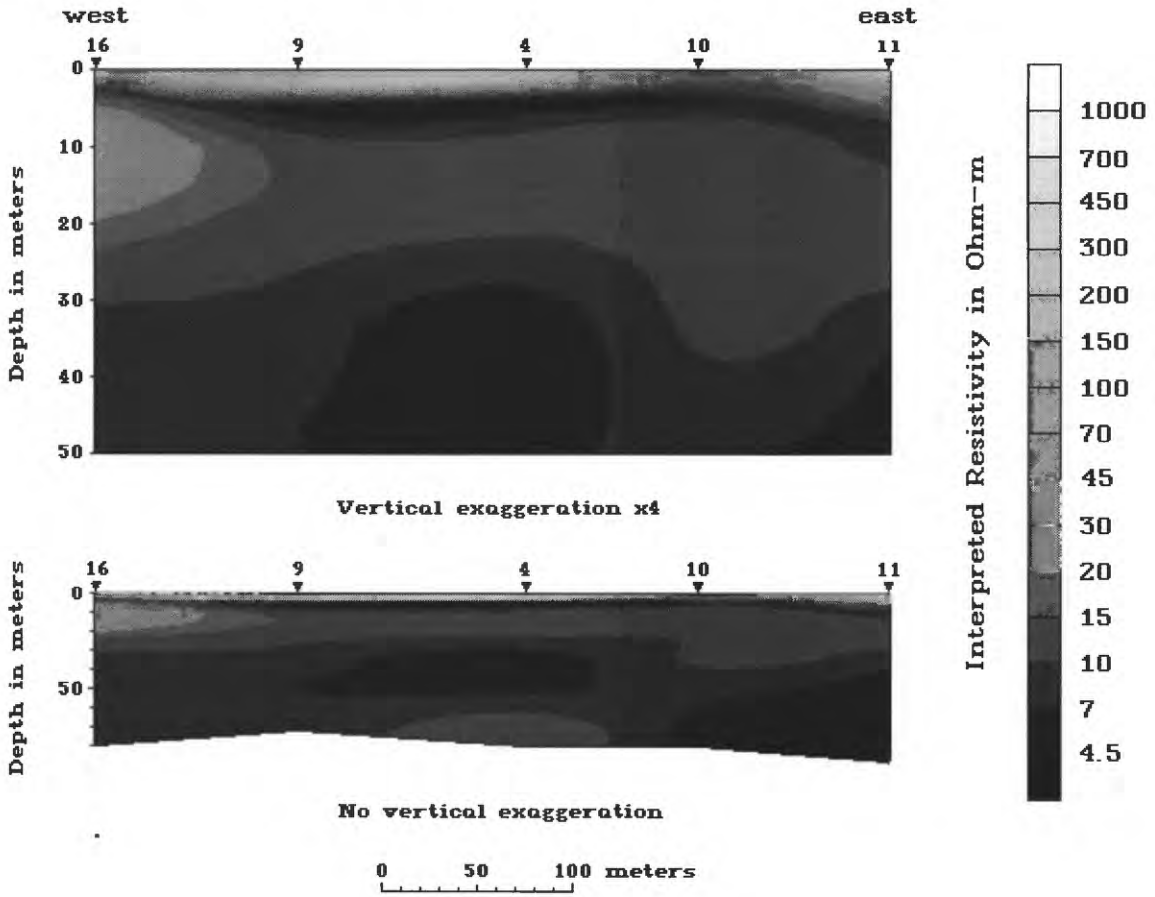

Figure 18. Interpreted DC resistivity sounding cross section along base of Norman Landfill west cell.

GROUND PENETRATING RADAR

Principle of Operation and Instrumentation

The GPR system used was a Subsurface Interface Radar (SIR^{TM}) System 10A+ manufactured by Geophysical Survey Systems, Inc. (GSSI), North Salem, NH, USA, running version 5.1 beta software. The radar system periodically transmitted radio-frequency electromagnetic pulses into the ground. The pulses propagated through the earth and were partially reflected back to a GPR antenna when they encountered changes in relative dielectric permittivity (RDP), electrical conductivity, or magnetic permeability. Dielectric permittivity is a measure of the capacity of a material to store charge (polarize) under an applied electric field. RDP is the dimensionless ratio of a medium's dielectric permittivity to that of free space ($\approx 8.8542 \times 10^{-12}$ farads/m). Electrical conductivity is the ability of a substance to transmit electric current. Magnetic permeability is the ability of a substance to become magnetized in an externally-applied magnetic field. Changes in electromagnetic properties in the earth are dominantly controlled by water content, lithology, bulk density, and porosity. The propagation velocity of the radar waves is controlled mostly by the relative dielectric permittivity of the medium. Attenuation of the radar wave is dominantly affected by the electrical conductivity of the medium (but magnetic permeability can significantly affect attenuation if ferrous minerals are present).

GPR antennas are broad-band transducers, usually covering at least two octaves of frequencies, with center frequencies ranging from 10 megahertz (MHz) to several thousand MHz. Depth of penetration of the EM pulses into the earth generally decreases with increasing antenna frequency. However, resolution of subsurface features is approximately proportional to antenna frequency (in other words, higher frequencies see smaller buried features, but gernerally don't see as deep). Surveys were performed by slowly pulling a pair of antennas (one transmitter and one receiver at constant, near-zero offset) across the ground surface along linear paths called profiles or traverses. Reflected radar waves created voltage changes on the receiver antenna, which were sent back to the control unit along copper cables, then digitized and stored on computer disk using the GSSI binary storage format. See Olhoeft (1984), Daniels (1989), Davis and Annan (1989), Lucius and others (1990), Annan and Cosway (1992), Finnish Geotechnical Society (1992), and Waterloo Centre for Groundwater Research and Canadian Geotechnical Society (1994) for more complete discussions of the GPR method and applications.

Site Surveys

If the conductivity of the subsurface is high, as it is near the Norman landfill, radar energy is rapidly attenuated and cannot propagate very far into the subsurface. Therefore, the GPR technique would not be effective near the landfill and an area was selected away from the landfill on the alluvium (fig. 3). The purpose of the measurements was to test the performance of the GPR system and not to image any particular aspect of the subsurface. The performance was judged, in this case, by how far the radar waves propagated into the subsurface for a particular antenna and if recognizable alluvial features could be detected.

A small area was selected on the alluvium next to test line 1 approximately 470 m away from the landfill to evaluate the performance of the GPR system in this environment. GPR data were collected along 21 profiles that formed a grid 10 m wide by 20 m long. Profiles were spaced 1 m apart parallel to the test line (long dimension of the grid) and 2 m apart perpendicular to the test line (fig. 19). Radar antennas having center frequencies of 300 MHz, 500 MHz, and 900 MHz were used. Using metal or plastic pin flags, stations were placed at the intersections of the profiles. When a GPR antenna passed a station, a "mark" was placed in the radar data (bytes were changed in the trace group header) so that the location of the antenna along a profile could be calculated. The location of each station was topographically surveyed (using an electronic total station) and relative orthogonal coordinates (x, y, and z) were calculated (see Appendix).

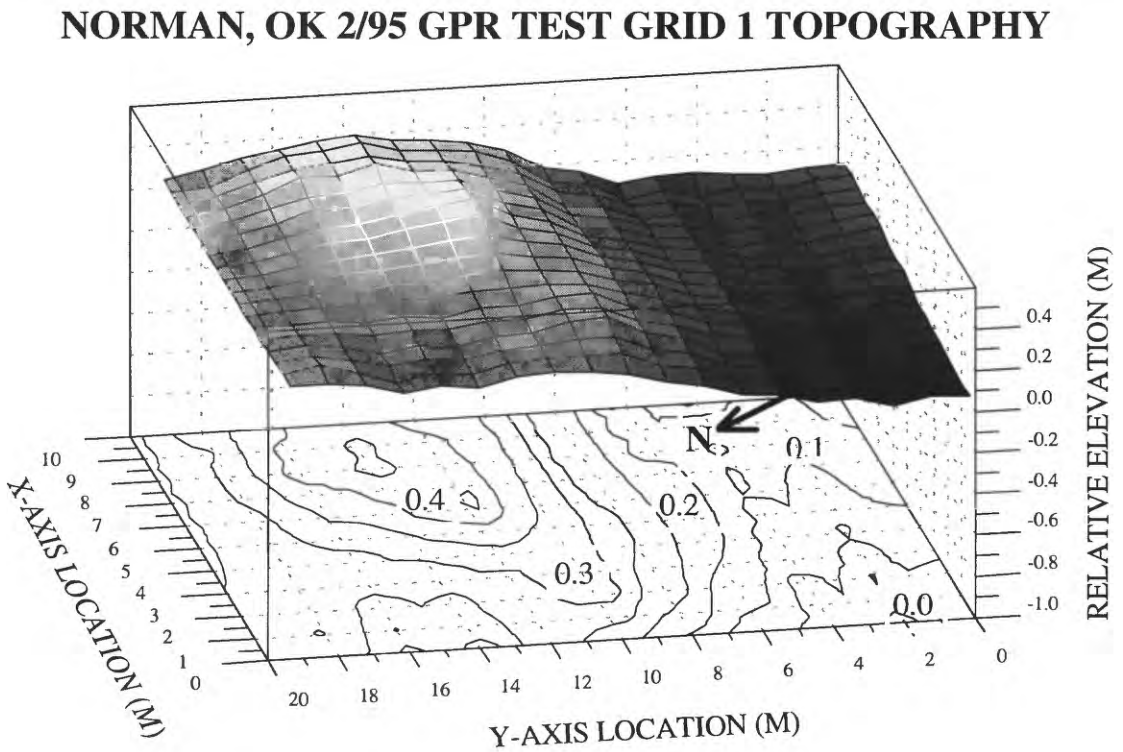

Figure 19. 3D surface plot with contours of relative elevation at the 2/95 GPR test grid 1. Contour interval = 0.05 m. GPR profiles are projected along the dashed lines on and at the edge of the bottom plane.

Data Processing

Surface ground penetrating radar data are sequences of time series (called traces or scans) that record the relative amplitude changes and arrival times of radar waves detected by the receiver antenna as its position changes on the ground surface. The GSSI SIR™ System 10A+ stores the radar data digitally on computer disc or tape using a binary storage format that includes a fixed-length file header followed by the data.

GPR processing attempts to improve the imaging and interpretation of the data. It involves operations that are performed by the SIR™ System 10A+ operating software, as the data are digitized and recorded, and operations that manipulate the stored data after acquisition. The operations and processes typically performed by the SIR™ System 10A+control unit (Geophysical Survey Systems, Inc., 1993) on GPR data follow.

1. Select a time window (or time range) appropriate for the maximum target depth. Because the performance of the GPR system was being evaluated, a time window was selected that exceeded the effective penetration range of each antenna. The length of the time window is given in nanoseconds (ns), 10^{-9} seconds.

2. Select the number of samples to digitize per trace and the number of bits to use for each sample. The number of bits used per sample was 16 (2 bytes, unsigned), the maximum allowed by the SIR™ System 10A+. This permits 96 decibels of dynamic range in the data. The number of samples per trace for all antennas and time windows was 512, a value that eliminated aliasing of the radar signal that could be caused by an inadequate sampling rate of the frequencies within the transmitter antenna's range. The sample rate is determined by the length of the time window divided by the number samples per trace minus 1, and is often given in picoseconds (ps), 10^{-12} seconds.

3. Position the radar signal within the time window so that the first response of the receiver antenna to the transmitter antenna is clearly discernible.

4. Apply a bandpass filter (called a vertical filter by the SIR™ System 10A+) to the digitized radar signal. A broad, bandpass, Infinite Impulse Response (IIR) filter was used to remove radar signals whose frequencies were outside of the broadcast limits of each transmitter antenna. These type of signals may be caused by radio or television transmissions or "noise" caused by the radar system itself or its power source. It should be noted that IIR filters slightly distort the phase of the signal they are filtering.

5. Select a static stacking rate (called a horizontal filter by the SIR™ System 10A+) to remove random high-frequency signals (noise). Stacking involves adding successive digitized and filtered radar traces together sample by sample then dividing the resultant trace by the number of traces stacked. Spurious noise was not a serious problem at the Norman site, so a stacking value of 16 was used during acquisition, resulting in a 12 dB improvement ($10 \log_{10} 16$) in the signal to noise ratio.

6. Apply an appropriate time-varying gain (also called range gain) to the digitized and filtered radar traces. The range gain normally increases the amplitude of later arriving signals in the time window to enhance their recognition. The amplitude of received radar signals decreases fairly rapidly in time and, though preserved within the dynamic range of the sample size (16-bits), can be too small to detect on the monitoring screen without amplification. Range gain has the unfortunate drawback of possibly distorting the apparent shape and phase of the radar signal. The range gain applied to the data varies

depending on the antenna used and the subsurface conditions. The values are stored in the file header so that the range gain can be removed by later processing if required.

7. Select a recording rate in traces per second. Usually the maximum rate permitted by the SIR™ System 10A+ system is used. For the Norman data, this value was 96 traces per second for all antennas. The number and type of filters and the number of software recording channels used (up to four in the SIR™ System 10A+) determine the rate at which the system can digitize, process, and store radar data. The recording rate in conjunction with the towing speed is related to the horizontal sampling rate, that is, the number of traces recorded per meter of radar profile.

All of the above values and settings, as well as others, are recorded in the file header for each radar profile. The table below summarizes the relevant parameters for each antenna used.

GSSI Antenna Model Number	Center Frequency (MHz)	Time Window (ns)	Sample Rate (ps)	Traces Recorded Per Second	IIR Bandpass Filter Low (MHz)	IIR Bandpass Filter High
3105	300	154	301	96	39	831
3102	500	102	200	96	59	255
3101	900	32	62	96	187	4000

Unpublished USGS computer software was used to process the stored (post-acquisition) GPR data for display and interpretation. The operations performed on the data were as follows.

1. Prepare support files so that a static topographic correction can be applied when displaying the data. As explained in the preceding section, marks were placed in the GPR data so that the location of the antenna along a profile could be calculated. It was determined that there were extra marks or missing marks in some GPR profiles. Computer text files were created that contained the trace numbers associated with the location markers for each GPR profile. Other text files were created for each profile that contained the topographic location (relative orthogonal coordinate system) of each location marker. Using the information in these files, the computer software corrected for changes in towing speed and topography, and display the radar traces in an approximately-correct geometrical relationship.

2. Calculate the time the GPR transmitter fired (time-zero) for each trace and update the file headers. Time-zero was calculated by knowing the spatial relationship of the transmitter and receiver antennas and observing in the data the first response of the receiver antenna to the transmitter. The "position" field in the GSSI file header records the offset from time-zero to the start of each recorded trace. The header in each data file was modified to record the calculated time-zero value. It is necessary to know time-zero so that accurate travel times to and from radar reflectors can be calculated.

3. Calculate and remove system noise not removed by the SIR™ System 10A+ operating software. The residual radar system noise appears as horizontal bands when the data are displayed as amplitude-modulated gray-scale images (see Appendix). These bands were removed by adding all traces in a profile together to calculate an average trace, then subtracting this average trace from each trace in the profile. The average or "background" trace represents that part of the recorded signal that is generally invariant with time. Given a sufficient number of traces (usually at least several hundred) and the lack of persistent "horizontal" subsurface features, geohydrological causes of reflections will tend to "stack out", that is, disappear due their "random" variations, from the background trace. Background noise removal was performed when the data were displayed; the original data files were not modified.

4. Select an average radar wave velocity so that a simple transformation can be made from travel time to depth and so that the geometric correction mentioned in step 1 above can be applied. The velocity of the radar wave in any media is determined primarily by the relative dielectric permittivity of the media. If the velocity (and therefore RDP) is known, then travel time (as the radar data are recorded in) can be converted to distance or depth. Usually, the radar wave velocity structure of the subsurface is not well known, and simplifications or estimates are made. An estimate for the Norman GPR test grid was made that approximated the velocity above the water table. Velocities in the saturated zone, therefore, were overestimated and the geometry of reflections from below the water table may have been distorted.

5. Generate images of the radar data and print. Radar data are typically displayed in one of two formats, wiggle trace (Sherrif, 1984) or gray scale. The gray-scale display was chosen for the Norman GPR data. A gray-scale display shows traces as a single vertical line where each sample value is assigned a shade of gray (from black to white) according to its relative amplitude. The top of the line is early time; the bottom is later time. The traces are placed next to each other to form an image (raster or bit-mapped display). Line widths may vary and traces may be skipped to fit the image into the display area.

Analysis and Interpretation

Figures 20 through 22 show representative images of GPR data collected along one traverse on the GPR test grid using 300 MHz, 500 MHz, and 900 MHz center-frequency antennas. (Images from all traverses on the test grid appear in the Appendix both in raw and processed pseudo-section forms.) The upper image in each figure shows the raw data as recorded to disk. The lower image in figures 20 and 21 and the lower two images in figure 22 show the processed data. The strong horizontal banding (present in the 300 MHz and 500 MHz raw data) has been removed, a static geometric correction has been applied to the traces placing the start (top) of each trace correctly in space, and a nominal velocity transformation (from travel time to distance or depth) has been applied using an average RDP of 6 (0.123 m/ns) for the sections. For the 900 MHz data in fig. 22 an additional image is presented with vertical exaggeration of 2.

To transform the two-way travel time of radar waves (from the transmitter to a reflector and back to the receiver) to an approximate distance or depth, the propagation velocity of the radar waves must be known. In a low-loss medium, radar wave velocity can be determined from the following formula (Powers, 1995, p. 33):

$V_r = V_c / \sqrt{\varepsilon}$,

where V_r is the velocity of the radar wave in the medium (in m/ns),

V_c is the velocity of EM waves in a vacuum (0.2998 m/ns), and

$\sqrt{\varepsilon}$ is the square root of the medium's RDP.

Or, by rearrangement, if the velocity is known, the RDP, ε, can be determined.

Usually it is difficult to know precisely the velocity of radar waves in the subsurface, so estimates or averages are calculated. The propagation velocity for alluvium near the ground surface was determined by pulling a receiver antenna slowly away from a transmitting antenna and marking their separation periodically. This was performed on the higher (dryer) and lower (wetter) areas of the GPR test grid. Propagation velocity was determined by observing the first arrivals (the waves traveling very near the surface) at various separations. For the dryer sand, velocity was 0.154 m/ns (RDP $\approx$ 3.8). In the moister sand, velocity was 0.133 m/ns (RDP $\approx$ 5.1). A slightly slower velocity (higher RDP) was used to generate the images shown in figures 20 to 22 and in the Appendix to account for increasing water content with depth. The radar wave velocity below the water table undoubtedly is slower yet, as the RDP of water is about 81 (0.033 m/ns), causing some distortion in the radar images.

The transmitting radar antenna illuminates an elongated, elliptical, cone-shaped volume of the subsurface, so that radar waves reflect off objects to the front and rear of the antenna, as well as slightly off to the sides. This causes hyperbolic-shaped high-angle reflections to sometimes appear in the radar data as the antennas approach, pass over, and move away from buried objects (point-source reflectors) whose sizes are of the same order of magnitude as the radar wavelength in the ground. Median radar wavelengths for the 300 MHz, 500 MHz, and 900 MHz antennas were approximately 0.4 m, 0.25 m, and 0.15 m, respectively. Point-source reflectors can be seen in the 300 MHz and 500 MHz data at a "depth" of about 1 m and may be caused by rocks, debris such as tree trunks, or trash like automobile parts (which we saw scattered about the surface). Features or interfaces in the subsurface that are sub-parallel to the ground surface appear as sub-horizontal reflections in the radar data. A small alluvial dune was deliberately selected for the test grid, so many of these features most likely reflect periodic erosion and accretion events as the Canadian River meandered within the floodplain. The bright or strong reflections between -1.5 and -2.5 m relative elevation are probably due to strong water-content changes in the alluvial sand near the top of the saturated zone.

Though it is best to have only those radar waves reflected from subsurface interfaces and objects of interest present in the recorded data, often there are also unwanted signals in the data, such as from radio or television broadcasts, systematic noise, or reflections from objects above ground. For example, the vertical "bars" seen in fig. 20 in the 300 MHz data at 2 m intervals are from reflections off of the metal pin flags used to mark intersections of the

profiles. The 300 MHz GSSI radar antenna is not shielded as well as the 500 MHz and 900 MHz antennas and some EM energy is transmitted into the air as well as into the ground.

The three images (fig. 20 to 22) illustrate the change in resolution and penetration for different radar antenna frequencies. Lower frequency antennas typically penetrate, or propagate, farther into the ground, while higher frequency antennas have better resolution of subsurface features. The 300 MHz and 500 MHz antennas propagated energy for about 100 ns (two-way travel time), or about 5 m into the alluvium, before the radar signal dropped below the environment noise level and system dynamic range. The 900 MHz antennas performed at about one quarter of this level, penetrating only about 1 m into the alluvium. However, the 900 MHz antennas resolved features in the top 1 m that the lower-frequency antennas could not.

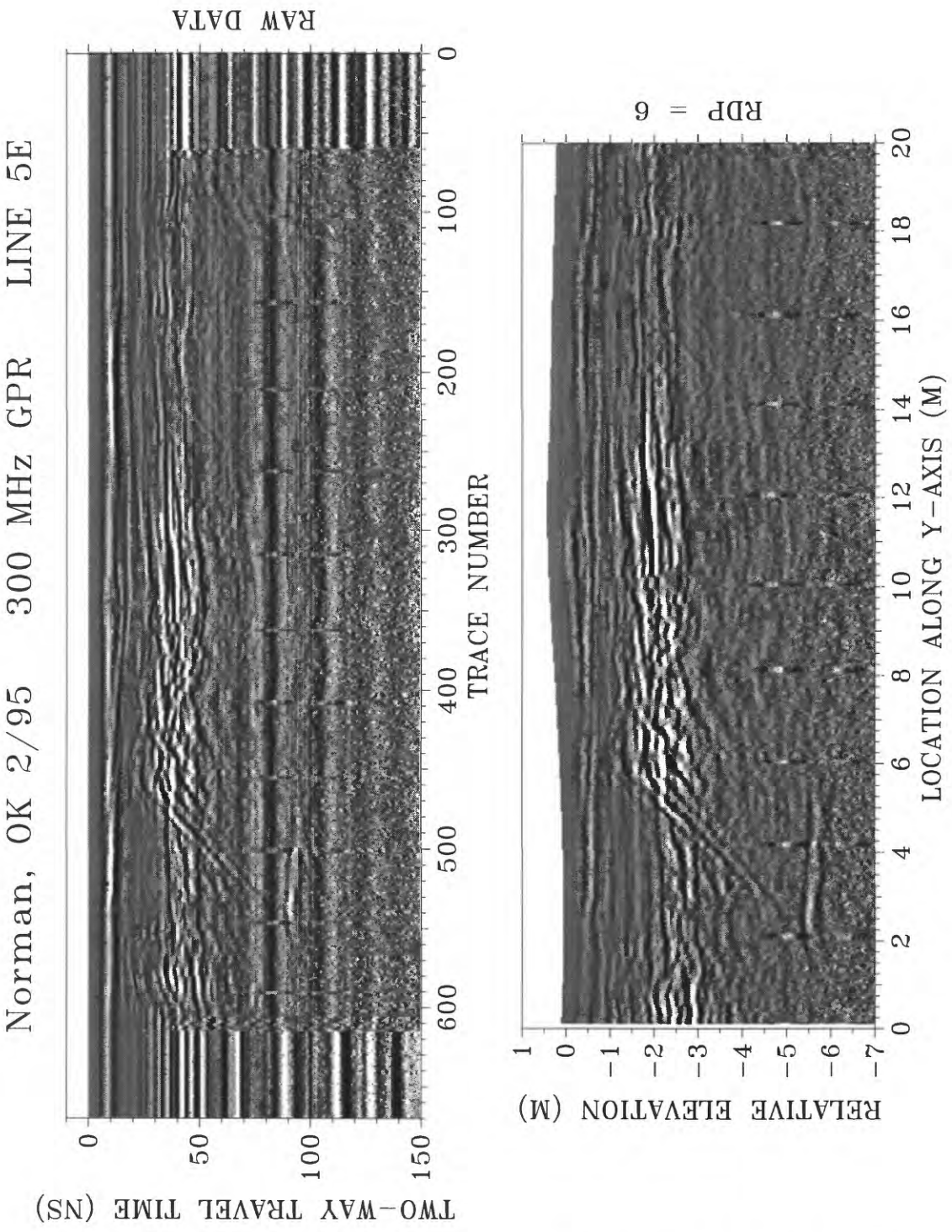

Figure 20. GPR images from 300 MHz antennas along line 5 of Norman Landfill GPR test grid.

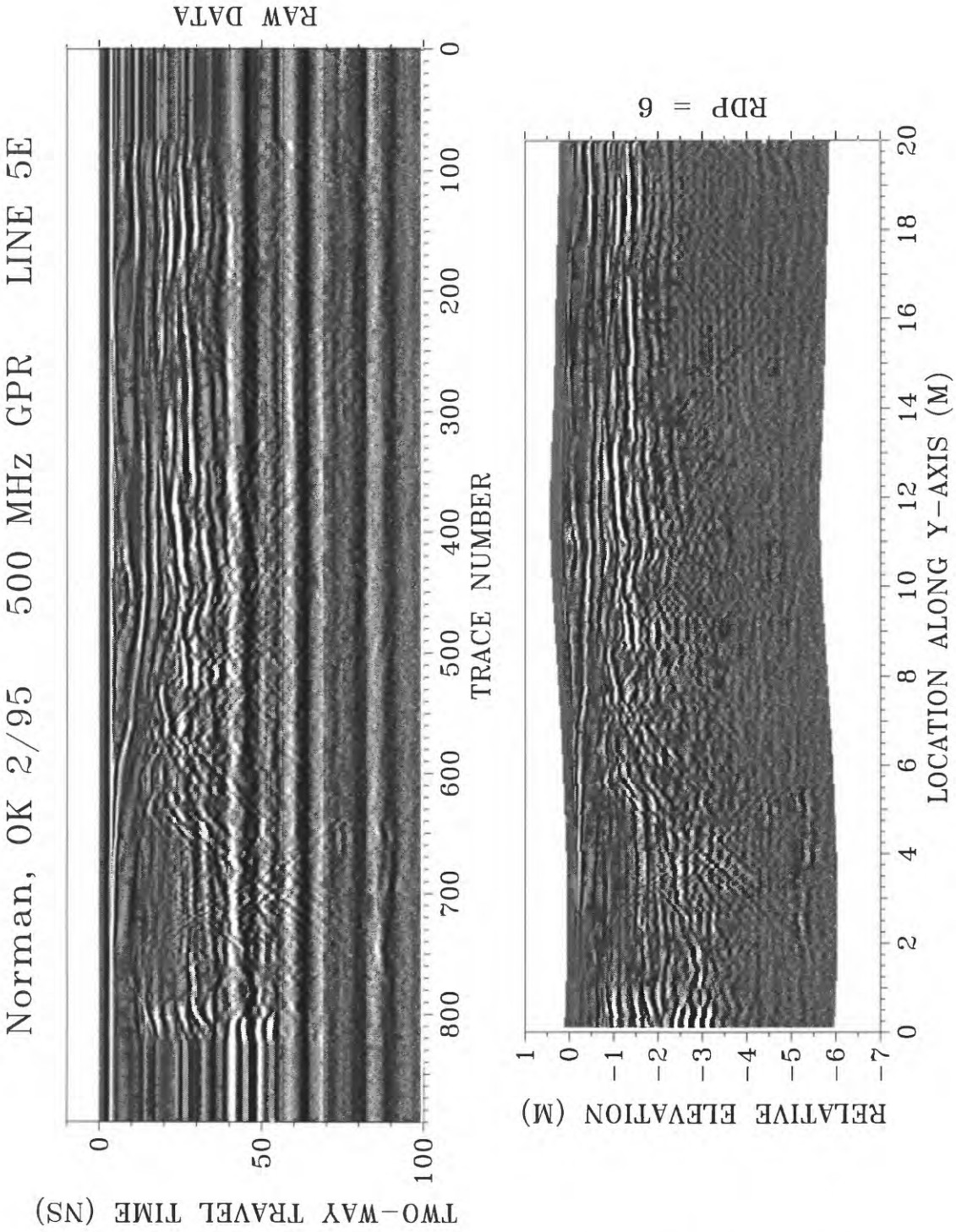

Figure 21. GPR images from 500 MHz antennas along line 5 of Norman Landfill GPR test grid.

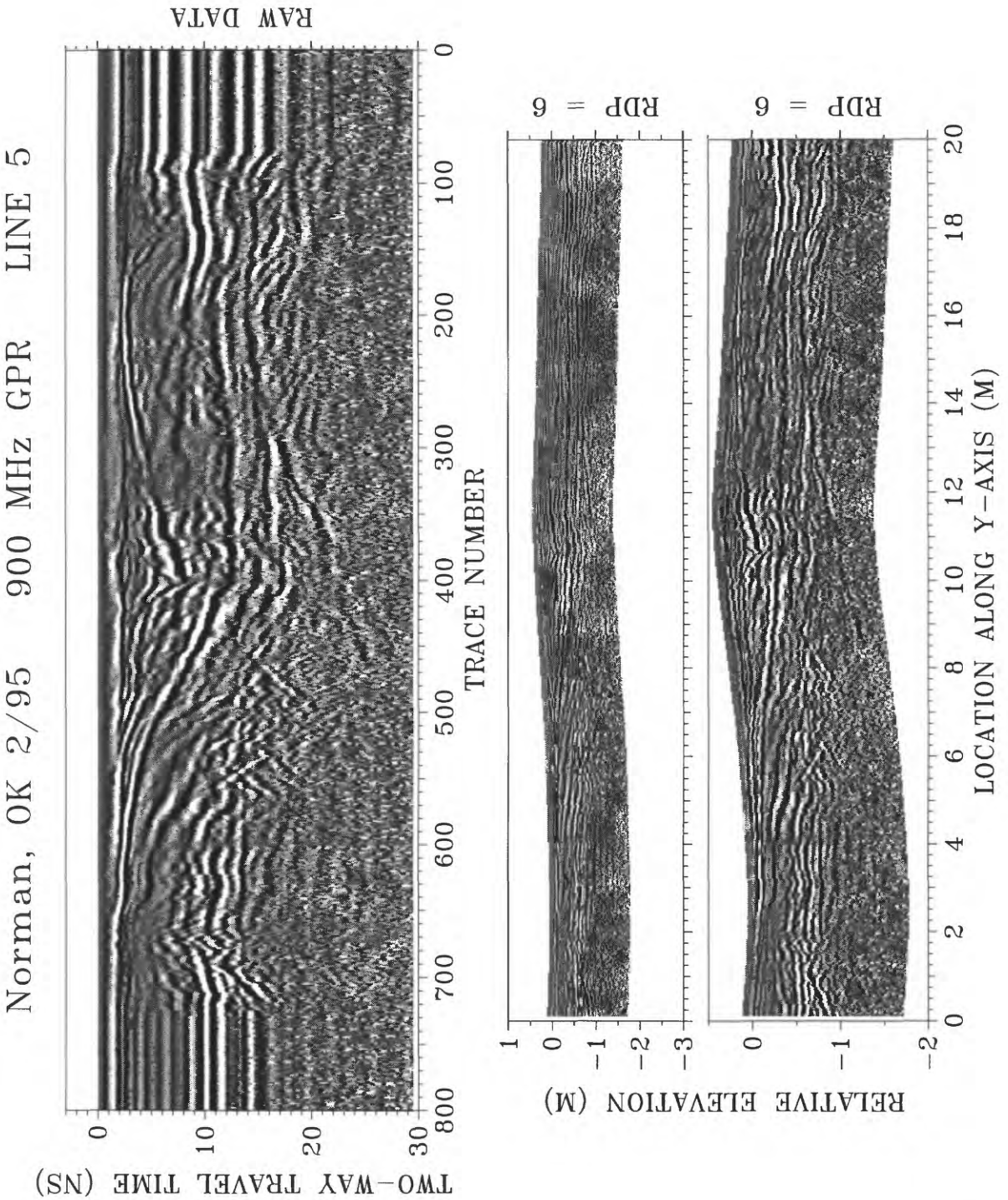

Figure 22. GPR images from 900 MHz antennas along line 5 of Norman Landfill GPR test grid.

CONCLUSION AND DISCUSSION

The major concern of the WRD at the Norman, Oklahoma Landfill site for the 1995 geophysical investigations was the lateral distribution of leachate emanating from under the landfill. The EM conductivity and DC resistivity methods determined that the electrically conductive part of the leachate plume appears to be confined to within 200 m on the southerly sides of the two landfill cells and unevenly distributed within that area. However, these two geophysical techniques used at the site mapped only electrical conductivity (or resistivity) and it is difficult to determine if observed variations are caused only by changes in pore-fluid conductivity (due to the leachate) without substantially more geologic and hydrologic information, which presently is not yet available. The geophysical data also indicate that as one moves away from the landfill toward the Canadian River the electrical conductivity of the alluvium is laterally relatively homogenous at scales of 10 to 100 m, in both horizontal directions.

Neither EM nor DC methods used could resolve the vertical distribution of conductive material with precision. But modeling of data from both methods suggests that a conductive layer, presumably contaminated ground water, is near the top of the saturated zone and may not extend into the Hennessey Formation beneath the alluvium.

Other problems remain to be examined at the Norman site; in particular, aquifer geometry and structure, distribution of hydraulic properties, identification of geochemical interactions, and possible mixing of landfill leachate with treated sewage at the surface in the ground water. Geophysical techniques can be applied to all of these problems. The WRD has requested that the next problem addressed, in 1996, be alluvial aquifer thickness, structure, and lithology both down-gradient and up-gradient from the landfill. The GPR tests conducted near the site demonstrated that GPR is a feasible method for providing information concerning structure and lithology. Geophysical methods proposed for 1996 work include surface seismic (P-wave) refraction, more DC resistivity soundings, GPR surface reflection, and more frequency-domain or time-domain EM.

The geophysical methods used in 1995 were successful in quickly and efficiently outlining areas with high conductivity that can be interpreted as being caused by leachate flowing from the landfill and mixing down-gradient with the ground water in the alluvium. The results of this study should help other investigators in siting monitoring wells near the landfill. As additional geologic and hydrologic information about this site is revealed from well data and other sampling, increased confidence can be given to the interpretation of the geophysical data.

REFERENCES

Adrian, N., Mangaokar, A., Phanapadipong, P., and Wainaina, S., 1990, Design of a Ground Water Monitoring Well System, Norman Municipal Landfill: Unpublished student paper, University of Oklahoma, Norman.

Annan, A.P. and Cosway, S.W., 1992, Ground Penetrating Radar Survey Design: *in* Proceedings, Symposium on the Application of Geophysics to Engineering and Environmental Problems, Society of Engineering and Mineral Exploration Geophysicists, Oakbrook, IL, USA, April 26-29, 1992, p.329-351.

Bisdorf, R.J., 1982, Schlumberger Sounding Investigations in the Date Creek Basin, Arizona: U.S. Geological Survey Open-File Report, 82-953, 55 p.

Briggs, I.C., 1974, Machine Contouring Using Minimum Curvature: Geophysics, v. 39, p. 39-48.

Callender, E.C., Christenson, S.C., Cozzarelli, I.M., Eganhouse, R.P., Reilly, T.E., and Suflita, J.M., 1993, Toxic Substances Hydrology Program Research Site Nomination, Norman Landfill, Norman, Oklahoma: Unpublished report, 22 p.

Daniels, J.J., 1989, Fundamentals of Ground Penetrating Radar: *in* Proceedings, Symposium on the Application of Geophysics to Engineering and Environmental Problems, Society of Engineering and Mineral Exploration Geophysicists, Golden, CO, USA, March 13-16, 1989, p. 62-142.

Davis, J.L. and Annan, A.P., 1989, Ground penetrating radar for high resolution mapping of soil and rock stratigraphy: Geophysical Prospecting, v. 37, p. 531-551.

Dobrin, M.B., 1976, Introduction to Geophysical Prospecting, 3rd ed.: New York, NY, McGraw-Hill, 630 p.

Dunlap. W.J., Shew, D.C., Robertson, J.M., and Toussaint, C.R., 1976, Organic pollutants contributed to groundwater by a landfill: *in* Proceedings, Symposium on gas and leachate from landfills, Rutgers University - Cooks College, New Brunswick, New Jersey, March 24-26, 1975, U.S. Environmental Protection Agency 600/9-76-004, p. 96-110.

Finnish Geotechnical Society, 1992, Ground Penetrating Radar: Geophysical Research Methods no. 102, The Finnish Building Centre (Rakennustieto Oy), Rovaniemi, Finland, 64 p.

Geophysical Survey Systems, Inc., 1993, SIR™ System-10A User's Manual #MN90-305: North Salem, NH, USA, Geophysical Survey Systems, Inc., various pagination.

Interpex, Ltd., 1989, EMIX 34 PLUS User's Manual: Golden, CO, Interpex, Ltd, various pagination.

Keller, G.V. and Frischknecht, F.C., 1966, Electrical Methods in Geophysical Prospecting: London, England, Pergamon Press, 517 p.

Koefoed, Otto, 1979, Geosounding Principles, 1. Resistivity Sounding Measurements: New York, NY, Elsevier Scientific Pub. Co., 276 p.

Lucius, J.E., Olhoeft, G.R., and Duke, S.K., eds., 1990, Third International Conference on Ground Penetrating Radar, Abstracts of the technical meeting, Lakewood, CO, USA, May 14-18, 1990: U.S. Geological Survey Open-File Report 90-414, 94 p.

McNeill, J.D., 1980, Electromagnetic Terrain Conductivity Measurements at Low Induction Numbers: Mississauga, Ontario, Canada, Geonics Ltd. Technical Note TN-6, 15 p.

McNeill, J.D., 1983, EM-34 Survey Interpretation Techniques: Mississauga, Ontario, Canada, Geonics Ltd. Technical Note TN-8 (revised from 1980), 16 p.

Nabighian, M.N., 1987, Electromagnetic Methods in Applied Geophysics -- Theory, V.1: Tulsa, OK, Soc. Exploration Geophysicists, 513 p.

Olhoeft, G.R., 1984, Applications and Limitations of Ground Penetrating Radar: *in* Expanded Abstracts, Society of Exploration Geophysicists 54th Annual International Meeting and Exposition, Atlanta, GA, Dec. 2-6, 1984, p. 147-148.

Parkhurst, D.L., Christenson, S., and Breit, G.N., 1993, Ground-Water-Quality Assessment of the Central Oklahoma Aquifer, Oklahoma -- Geochemical and Geohydrologic Investigations: U.S. Geological Survey Open-File Report 92-642, 113 p.

Powers, M.H., 1995, Dispersive Ground Penetrating Radar Modeling in 2D: PhD Thesis T-4820, Colorado School of Mines, Golden, CO, 157 p.

U.S. Geological Survey, 1983, Norman Quadrangle., Oklahoma, 7.5 Minute Series (Topographic), 1965, photorevised 1983: U.S. Geological Survey, 1 sheet.

Waterloo Centre for Groundwater Research and Canadian Geotechnical Society, 1994, Proceedings of the Fifth International Conference on Ground Penetrating Radar, June 12-16, 1994, Kitchener, Ontario, Canada: Waterloo, Ontario, Canada, University of Waterloo, 3. Vols., 1294 p.

Wood, P.R. and Burton, L.C., 1968, Ground-Water Resources, Cleveland and Oklahoma Counties: Oklahoma Geological Survey Circular 71, 75 p.

Zohdy, A.A.R. and Bisdorf, R.J., 1989, Programs for the Automatic Processing and Interpretation of Schlumberger Sounding Curves in QuikBASIC 4.0: U.S. Geological Survey Open-File Report 89-137 A&B, 64 p. plus 1 diskette.

Zohdy, A.A.R. and Bisdorf, R.J., 1990, Schlumberger Soundings Near Medicine Lake, California: Geophysics, v. 55, p. 956-964.

Zohdy, A.A.R., Eaton, G.P., and Mabey, D.R., 1974, Application of Surface Geophysics to Ground-Water Investigations: Techniques of Water-Resources Investigations of the U.S. Geological Survey, Book 2, Chapter D1, 116 p.

APPENDIX - GEOPHYSICAL DATA

Summary of Geonics EM Instruments Specifications

Instrument (model)	Coil spacing (m)	Frequency (Hz)
EM31-D	3.66	39,200
EM34-3	10.0	6,400
EM34-3	20.0	1,600
EM34-3	40.0	400

EM Conductivity Readings and Station Locations for Norman, OK 1995

STATION ID:

Wxxx_Nxxx or Exxx_Nxxx are stations on grid or test lines.
W000_N000 is 170 m south from landfill on Test Line 1 at cross line.
N is north of the cross line.
S is south of the cross line.
W is west of Test Line 1.
E is east of Test Line 1.
TL_Exxxx are stations along toe of landfill.

COORDINATES:

GPS coordinates are given as UTM 14 coordinates with a constant value subtracted.
X is less 641,000.
Y is less 3,892,200.
Z coordinates are not given because the GPS elevation data was accurate to only +/- 3 meters.

CONDUCTIVITY MEASUREMENTS

HC indicates Horizontal coplanar coils; vertical magnetic dipoles.
VC indicates Vertical coplanar coils; horizontal magnetic dipoles.
Measurements are in millisiemens per m (mS/m).
Station locations are defined as midway between the two coils.
NR indicates "No Reading".

STATION ID Orientation	X	Y	EM31-D 3.66 m HC	EM31-D 3.66 m VC	EM34-3 10 m HC	EM34-3 10 m VC	EM34-3 20 m HC	EM34-3 20 m VC	- Instrument - Coil Spacing - Coil
W200_N120	301.992	639.900	35	30	39	36	41	47	
W200_N060	256.176	586.296	42	30	30	38	34	48	

W200_N050	249.229	579.524	42	29	31	35	28	44	
W200_N040	242.291	572.269	31	20	31	29	30	41	
W200_N030	235.147	564.648	32	22	27	26	43	38	
W200_N020	228.668	556.876	33	19.5	16	24	24	35	
W200_N010	222.379	549.508	33	19.5	4	27	27	34	
W200_N000	215.569	541.413	26	16	20	21	30	33	
W200_N-10	209.201	534.907	20	14.5	22	20	36	32	
W200_N-20	201.911	527.055	22	14.5	18	20	29	30	
W200_N-30	196.550	519.667	19	12	23	17	34	30	
W200_N-40	188.396	512.328	22.5	15	19	17	34	29	
W200_N-50	181.905	505.365	22.5	15.5	23	20	32	29	
W200_N-60	175.226	498.214	23.5	17	22	21	34	32	
W200_N-70	168.246	490.775	24.5	17	23	21	34	32	
W200_N-80	161.516	483.433	24.5	17	22	21	30	32	
W180_N140	330.841	641.389	66	40	70	52	-4	46	
W180_N130	324.151	633.991	44	29	44	42	40	53	
W180_N120	317.421	626.637	42	30	38	35	42	47	
W180_N110	310.952	619.294	31	24	28	40	41	57	
W180_N060	271.940	575.873	46	30	28	42	30	52	
W180_N050	265.243	567.673	42	28	38	34	30	44	
W180_N040	258.495	560.399	30	22	31	27	33	40	
W180_N030	252.011	552.675	25.5	17	24	23	38	36	
W180_N020	245.756	544.274	24	17.5	23	21	36	33	
W180_N010	239.174	537.311	21	15	24	19	36	32	
W180_N000	231.391	529.213	19.5	13	27	18	36	32	
W180_N-10	225.602	522.196	22	16	18	20	36	31	
W180_N-20	218.507	516.198	25	17.5	26	22	30	32	
W180_N-30	211.471	508.929	25	17.5	17	22	29	32	
W180_N-40	204.509	500.891	24.5	16	19	20	32	32	
W180_N-50	198.595	493.540	27	18.5	21	22	31	32	
W180_N-60	192.027	485.895	24	16.5	22	22	28	33	
W180_N-70	185.345	478.176	25.5	17.5	19	20	35	30	
W180_N-80	178.644	470.790	21.5	15	20	19	32	29	
W160_N140	344.717	628.319	54	47	24	42	15	46	
W160_N130	338.095	620.555	44	40	12	40	36	52	
W160_N120	331.431	613.061	20	35	35	39	43	52	
W160_N110	325.438	605.219	22	25	27	32	36	49	
W160_N100	318.392	597.606	34	24	35	39	52	49	
W160_N060	287.989	561.695	48	34	34	44	37	50	
W160_N050	281.369	555.370	42	29	26	40	26	50	
W160_N040	273.906	547.132	34	22	24	30	18	44	

W160_N030	266.884	539.931	23.5	16	25	24	43	38	
W160_N020	259.833	532.894	22	15	22	19	32	34	
W160_N010	253.463	524.606	22	13.5	23	19	36	34	
W160_N000	246.865	516.176	24	16	15	20	29	32	
W160_N-10	240.078	508.660	25.5	17	22	22	33	33	
W160_N-20	232.895	502.558	25.5	17.5	23	22	34	33	
W160_N-30	226.458	496.493	27	19	23	23	26	32	
W160_N-40	220.150	488.404	25	16.5	24	21	36	32	
W160_N-50	213.345	480.997	22	15.5	23	21	34	31	
W160_N-60	206.738	473.745	21	14	22	19	34	31	
W160_N-70	199.777	466.950	22.5	16	20	18	30	28	
W160_N-80	193.046	459.238	17	12	19	17	32	29	
W140_N140	359.498	615.465	51	32	46	50	38	60	
W140_N110	341.353	591.173	44	30	40	36	36	52	
W140_N100	335.504	582.703	32	24	24	40	60	50	
W140_N050	297.179	542.657	35	23	47	36	45	50	
W140_N040	290.246	536.721	33	21	33	33	32	42	
W140_N030	284.261	529.132	24	16	33	27	35	40	
W140_N020	277.348	521.481	20	13	24	21	37	37	
W140_N010	271.030	514.213	18.5	13.5	19	19	43	34	
W140_N000	264.086	506.734	21	13.5	24	19	30	32	
W140_N-10	257.723	499.416	28	19	19	19	24	31	
W140_N-20	250.785	492.104	26	17.5	21	22	28	32	
W140_N-30	243.365	485.329	26.5	19	25	22	28	32	
W140_N-40	237.652	477.198	22.5	15.5	25	20	35	32	
W140_N-50	230.677	470.070	22.5	15	20	20	34	31	
W140_N-60	223.875	463.090	20.5	15	21	19	28	30	
W140_N-70	216.855	455.727	19	13	22	17	32	28	
W140_N-80	209.983	448.659	18	12	22	16	35	27	
W120_N140	374.193	602.549	42	29	42	44	62	62	
W120_N130	367.908	595.102	27	30	27	36	40	52	
W120_N120	361.313	587.673	40	26	28	35	43	48	
W120_N110	354.976	579.855	38	31	9	30	30	48	
W120_N100	348.970	571.609	32	25	60	37	45	45	
W120_N080	336.092	556.516	35	26	34	32	41	44	
W120_N070	329.689	549.207	36	25	36	39	40	58	
W120_N040	305.670	523.246	34	22	50	36	44	46	
W120_N030	298.839	515.807	26.5	18	33	28	33	38	
W120_N020	292.372	508.725	21.5	14	30	22	44	36	
W120_N010	285.630	501.478	23	16	23	21	34	33	
W120_N000	278.601	494.456	24.5	16	23	20	31	32	

W120_N-10	272.839	486.402	26	18	20	22	32	30
W120_N-20	265.899	478.821	27	18.5	20	21	35	30
W120_N-30	259.449	471.443	24	16	24	19	34	30
W120_N-40	252.902	464.656	21	15.5	21	20	32	30
W120_N-50	246.138	457.310	21	14.5	22	19	32	30
W120_N-60	239.572	449.791	18.5	13.5	21	17	34	29
W120_N-70	232.979	442.182	19	13.5	20	17	34	28
W120_N-80	226.456	434.842	21	14	20	18	28	28
W100_N140	389.491	589.540	44	30	48	49	51	64
W100_N120	376.817	574.140	41	27	44	37	50	54
W100_N110	371.074	567.074	44	27	43	33	40	49
W100_N100	364.743	558.272	30	22	32	34	42	50
W100_N090	358.654	550.996	15.5	18	35	32	39	48
W100_N080	352.346	543.027	23	19	38	29	50	50
W100_N030	313.310	504.161	32	20	34	30	42	39
W100_N020	307.598	496.592	25	16	31	24	30	40
W100_N010	300.811	488.495	25.5	17	16	23	29	34
W100_N000	294.902	481.556	22	16	21	21	38	32
W100_N-10	288.212	474.360	22	16.5	23	20	36	31
W100_N-20	281.587	466.618	23	16.5	21	20	30	31
W100_N-30	274.216	459.299	22.5	15	23	20	35	31
W100_N-40	268.132	451.682	20.5	16	19	19	29	30
W100_N-50	261.268	444.424	21	14.5	21	19	30	29
W100_N-60	254.501	437.154	19	13.5	19	17	30	29
W100_N-70	247.488	429.827	20	14.5	19	17	31	28
W100_N-80	240.598	422.678	20	14.5	17	18	33	28
W080_N140	404.885	575.709	55	36	50	53	63	65
W080_N120	391.197	561.123	37	30	55	40	35	59
W080_N110	384.939	551.972	31	30	33	37	42	49
W080_N100	378.360	545.469	35	23	26	32	50	45
W080_N090	372.529	537.214	10	14	35	25	60	40
W080_N080	366.385	529.373	13	15.5	25	24	47	38
W080_N070	358.293	522.857	30	24	30	31	52	43
W080_N060	352.776	514.277	42	34	42	42	56	56
W080_N030	329.893	491.180	42	27.5	38	42	38	58
W080_N020	323.787	484.382	22	17	28	27	42	41
W080_N010	316.798	476.237	20	15	28	22	44	33
W080_N000	310.363	468.645	23.5	17	21	20	36	32
W080_N-10	303.691	461.177	21	15	23	20	35	31
W080_N-20	297.169	453.300	22	15.5	22	19	34	30
W080_N-30	289.638	447.489	22	16	22	19	29	29

W080_N-40	283.004	439.291	21	14	22	18	30	29
W080_N-50	276.087	431.591	20	14	21	18	31	29
W080_N-60	269.438	424.297	20	14	19	18	31	29
W080_N-70	262.573	417.056	20	14.5	18	18	31	28
W080_N-80	255.967	409.879	20.5	15	20	18	30	29
W060_N150	432.736	569.906	69	47	62	60	66	64
W060_N130	412.872	550.499	57	40	38	55	30	64
W060_N120	406.059	543.352	49	40	30	50	30	63
W060_N110	399.629	536.632	51	44	33	50	32	58
W060_N100	394.225	531.252	50	34	36	43	41	57
W060_N090	387.102	524.142	23	18	43	30	60	51
W060_N080	380.722	514.791	20	23.5	38	30	54	46
W060_N070	373.393	505.962	58	37	34	41	34	54
W060_N060	366.448	499.629	45	29	32	42	34	52
W060_N030	347.285	477.078	48	34	38	41	40	52
W060_N020	339.909	470.801	27	18.5	34	24	44	40
W060_N010	332.708	462.880	19	13	28	19	42	35
W060_N000	325.653	456.057	20	14	20	18	33	30
W060_N-10	319.229	449.027	23	15	23	19	34	30
W060_N-20	312.370	441.486	22	15	23	20	30	30
W060_N-30	305.378	433.931	21.5	15.5	23	19	31	29
W060_N-40	299.164	426.662	21	14.5	22	18	33	29
W060_N-50	292.004	419.070	20	15	20	18	30	28
W060_N-60	285.571	411.921	19	14	18	17	34	28
W060_N-70	278.530	404.403	18.5	13.5	19	17	32	28
W060_N-80	271.647	397.055	21	14.5	19	17	32	28
W040_N160	449.019	560.849	68	49	53	64	66	69
W040_N130	429.864	538.736	48	33	40	51	52	61
W040_N120	423.253	531.119	42	32	50	42	43	58
W040_N110	416.548	524.018	44	36	36	44	54	51
W040_N100	410.124	516.771	40	34	39	49	46	59
W040_N090	403.117	510.076	45	29	46	46	50	59
W040_N080	394.714	501.782	42	30	38	43	42	54
W040_N070	388.257	493.850	40	28	44	41	42	54
W040_N060	382.131	486.673	42	31	38	46	40	58
W040_N030	362.343	465.785	50	38	34	48	38	61
W040_N020	354.738	458.097	28.5	20	35	31	38	45
W040_N010	348.141	450.084	20.5	15	22	22	42	38
W040_N000	341.458	442.938	22.5	16	18	20	36	33
W040_N-10	334.830	436.440	23	15	19	18	31	31
W040_N-20	328.113	428.078	23	16	21	18	36	30

W040_N-30	321.353	421.545	24	17.5	19	19	29	28		
W040_N-40	313.612	415.098	21.5	16	19	19	28	30		
W040_N-50	306.049	407.675	22	17	16	19	27	29		
W040_N-60	299.103	400.729	20.5	15.5	20	18	33	29		
W040_N-70	292.092	393.708	19	14	20	18	33	29		
W040_N-80	284.934	386.139	20	14	19	17	30	28		
W020_N170	467.930	552.763	73	54	54	68	44	74		
W020_N160	465.047	548.865	63	48	49	70	48	78		
W020_N150	457.944	541.866	55	38	41	59	54	73		
W020_N120	437.550	519.466	45	37	29	52	46	56		
W020_N110	431.121	512.437	40	30	NR	NR	NR	NR		
W020_N100	424.386	504.601	42	28	NR	NR	NR	NR		
W020_N090	417.544	497.404	38	30	53	31	34	58		
W020_N080	411.372	489.663	30	28	50	38	64	58		
W020_N070	405.649	482.001	49	40	48	47	48	58		
W020_N060	398.020	472.311	54	40	45	50	40	59		
W020_N030	376.607	453.202	51	37	42	48	32	57		
W020_N020	370.512	445.346	34	23	37	32	50	45		
W020_N010	363.616	437.888	26	19	25	25	34	39		
W020_N000	356.647	430.803	24	15	29	22	43	36		
W020_N-10	349.889	423.625	24.5	17.5	18	21	32	32		
W020_N-20	343.227	416.882	26.5	18	23	21	30	31		
W020_N-30	336.540	409.554	25.5	18	21	20	28	30		
W020_N-40	329.651	402.577	22	15.5	21	20	32	30		
W020_N-50	322.524	395.051	21.5	15.5	24	19	35	30		
W020_N-60	315.694	387.577	21	15	19	19	31	30		
W020_N-70	308.932	380.322	20	14	23	18	32	29		
W020_N-80	301.925	373.375	18	13.5	19	17	34	28	EM34-3	
									40 m	
									HC	VC
W000_N170	486.070	541.472	68	46	57	63	67	72	67	74
W000_N160	479.347	534.167	58	43	43	59	42	75	46	78
W000_N150	472.624	526.861	55	38	58	57	64	72	34	76
W000_N140	465.902	519.556	57	40	45	57	51	57	62	74
W000_N130	459.179	512.250	48	28	55	52	62	68	64	70
W000_N120	452.456	504.945	38	32	49	45	44	54	34	70
W000_N110	445.733	497.639	38	28	42	44	48	60	65	68
W000_N100	439.010	490.333	38	28	48	42	54	60	44	65
W000_N090	432.288	483.028	26.5	25	34	40	52	54	36	65
W000_N080	425.565	475.722	30	22.5	46	43	52	58	59	64
W000_N070	418.842	468.417	55	41	30	49	54	52	35	63
W000_N060	412.113	461.068	45	36	44	52	44	60	46	61

W000_N030	391.926	439.023	48	34	32	48	30	56	46	62
W000_N020	385.197	431.674	39	28	32	35	35	46	49	50
W000_N010	378.468	424.326	28	19.5	24	28	46	40	42	53
W000_N000	371.738	416.977	23	15	32	24	36	37	42	50
W000_N-010	365.009	409.628	25	18	23	22	35	32	50	48
W000_N-020	358.280	402.280	24	16.5	23	22	31	34	49	44
W000_N-030	351.551	394.931	24.5	18	24	21	28	31	44	45
W000_N-040	344.737	387.462	23	16	22	21	33	31	53	44
W000_N-050	337.924	379.993	23	16.5	20	21	34	30	30	43
W000_N-060	331.110	372.523	26	16	24	20	25	30	42	43
W000_N-070	324.296	365.054	22	16	21	20	29	30	42	44
W000_N-080	317.482	357.584	20	14	22	18	37	29	40	43
W000_N-090	310.668	350.115	19	13	21	17	38	28	44	44
W000_N-100	303.854	342.646	18	12.5	20	16	33	28	51	42
W000_N-110	297.041	335.176	19	13	22	17	34	28	42	43
W000_N-120	290.227	327.707	18	12.5	23	17	33	29	43	43
W000_N-130	283.413	320.237	21	14	23	17	33	29	44	42
W000_N-140	276.638	312.859	22	15.5	18	18	32	30	40	42
W000_N-150	269.863	305.481	20	13.5	23	17	31	30	44	44
W000_N-160	263.089	298.103	16	11	23	16	29	30	44	44
W000_N-170	256.314	290.724	18	12.5	20	18	32	29	37	44
W000_N-180	249.539	283.346	17.5	12	23	17	34	30	44	42
W000_N-190	242.764	275.968	20	14	17	18	32	29	45	42
W000_N-200	235.990	268.590	18	12.5	17	16	38	28	52	41
W000_N-210	229.215	261.212	13	8.5	22	14	32	28	44	44
W000_N-220	222.440	253.833	16	11	21	15	32	28	45	44
W000_N-230	215.665	246.455	20	13	20	18	33	29	43	42
W000_N-240	208.711	239.235	21.5	14.5	22	18	34	30	40	43
W000_N-250	201.757	232.014	21.5	14	20	18	30	30	43	44
W000_N-260	194.803	224.794	18	12	22	16	30	29	46	44
W000_N-270	187.848	217.574	15.5	10.5	19	14	36	28	43	44
W000_N-280	180.894	210.353	15.5	10.5	19	14	34	27	48	43
W000_N-290	173.940	203.133	15.5	10.5	19	15	32	27	48	42
W000_N-300	166.985	195.912	14.5	10	20	14	34	27	38	44
W000_N-310	160.031	188.692	15	10	20	14	30	26	43	42
W000_N-320	153.077	181.471	15	10	20	14	31	26	43	41
W000_N-330	146.122	174.251	15	10	19	14	34	26	37	41
W000_N-340	139.286	167.027	15	10	19	14	30	26	47	41
W000_N-350	132.449	159.803	15	10	18	13	34	26	41	42
W000_N-360	125.612	152.579	14.5	9.5	19	13	32	25	40	41
W000_N-370	118.776	145.355	14	9.5	18	14	29	25	48	42
W000_N-380	111.939	138.131	14	9.5	20	14	33	26	38	42
W000_N-390	105.102	130.907	15	10	21	14	36	27	43	42

W000_N-400	98.266	123.683	16	11	20	15	32	28	44	42	
W000_N-410	91.429	116.459	16	11	20	15	34	28	46	42	
W000_N-420	84.592	109.235	14.5	9.5	23	15	36	28	46	44	
W000_N-430	77.756	102.011	15	10	20	14	39	28	47	45	
W000_N-440	71.222	94.491	16.5	11.5	20	16	34	29	56	45	
W000_N-450	64.689	86.971	17.5	11.5	22	16	34	31	46	46	
W000_N-460	58.156	79.451	19.5	13	26	18	40	32	50	48	
W000_N-470	51.623	71.931	20.5	14	26	20	38	35	55	47	
W000_N-480	45.090	64.411	30	20	28	26	37	39	52	53	
E020_N170	503.100	527.209	49	33	68	59	32	78			
E020_N160	496.283	520.344	45	31	38	54	65	74			
E020_N150	488.407	513.190	48	34	40	52	59	70			
E020_N140	481.528	506.527	46	32	54	49	46	64			
E020_N130	474.331	499.472	43	28	55	46	53	66			
E020_N120	467.365	492.163	45	29	52	45	39	60			
E020_N110	460.301	485.352	32	26	62	39	64	58			
E020_N100	453.249	478.196	28	27	46	39	57	54			
E020_N090	446.209	471.071	22	23	46	40	51	53			
E020_N080	439.101	464.140	35	22.5	44	35	64	51			
E020_N070	432.509	456.440	50	36	41	46	50	58			
E020_N060	426.508	448.839	45	34	44	47	45	56			
E020_N030	407.081	427.023	41	30	32	42	37	53			
E020_N020	400.632	419.608	37	24.5	37	32	38	44			
E020_N010	394.076	412.166	28	19	28	27	38	40			
E020_N000	386.856	405.219	23.5	15.5	27	23	42	38			
E020_N-10	379.968	397.367	26	18	22	22	37	34			
E020_N-20	372.990	390.254	26	18.5	23	23	33	32			
E020_N-30	366.282	383.756	25	18	22	22	31	33			
E020_N-40	359.640	374.991	23.5	17	20	21	32	32			
E020_N-50	353.044	367.763	22	16.5	22	19	36	32			
E020_N-60	346.429	360.281	22	16	24	20	36	30			
E020_N-70	339.460	353.154	21	15	23	21	28	31			
E020_N-80	332.609	345.973	22.5	15.5	20	20	32	31			
E040_N160	509.076	505.492	54	37	48	60	58	76			
E040_N150	501.735	498.296	50	36	50	53	63	70			
E040_N140	495.271	490.375	53	40	57	51	55	66			
E040_N130	488.084	483.944	53	36	42	52	42	66			
E040_N120	480.971	477.010	48	32	44	53	42	66			
E040_N110	473.800	469.911	46	30	54	50	42	63			
E040_N100	467.530	463.305	42	27	49	44	48	61			
E040_N090	459.617	455.404	31	27	41	41	60	54			

E040_N080	453.485	447.950	30	23	35	36	48	52
E040_N070	446.539	441.043	40	28	44	42	41	55
E040_N060	440.393	434.947	41	29	40	39	43	50
E040_N030	422.487	413.328	39	28	32	37	38	49
E040_N020	415.537	407.084	34	24	30	31	34	42
E040_N010	408.363	399.866	24.5	16	27	25	36	38
E040_N000	401.528	392.535	23.5	16.5	25	22	32	36
E040_N-10	394.755	384.847	24	17	25	22	32	34
E040_N-20	388.075	377.800	24	17	24	22	36	32
E040_N-30	381.478	370.567	24	16.5	25	20	35	31
E040_N-40	375.409	362.567	22	15.5	23	19	36	30
E040_N-50	368.603	355.330	22	15.5	22	19	34	30
E040_N-60	361.665	348.082	21.5	15	23	20	32	30
E040_N-70	354.918	340.723	22	16	23	20	34	33
E040_N-80	347.957	333.495	25.5	17	23	20	38	33
E060_N140	512.176	478.885	67	50	46	66	44	75
E060_N130	504.988	472.139	66	54	38	63	37	69
E060_N120	496.463	464.251	61	42	38	58	40	68
E060_N110	491.161	459.104	59	42	49	51	50	61
E060_N090	476.309	444.461	39	26	35	35	45	53
E060_N060	453.797	422.663	37	26	43	38	48	52
E060_N020	430.714	394.001	35	24.5	32	32	40	43
E060_N010	424.034	386.013	27.5	18	34	28	31	39
E060_N000	417.286	378.907	25	17	23	24	35	36
E060_N-10	410.341	372.016	26	18	24	23	36	34
E060_N-20	404.076	364.173	24	16.5	22	22	37	33
E060_N-30	397.298	357.270	23.5	16	25	20	36	32
E060_N-40	390.570	349.492	23	16	24	20	37	32
E060_N-50	383.837	341.833	22	15.5	23	20	37	32
E060_N-60	377.274	334.190	22.5	15	27	19	40	32
E060_N-70	370.982	326.466	24	16	21	18	34	30
E060_N-80	363.777	319.385	20	14	21	19	34	31
E080_N120	509.770	450.646	71	58	38	66	32	73
E080_N110	505.172	446.634	71	58	36	69	37	75
E080_N100	498.320	439.005	78	63	38	65	40	68
E080_N090	490.272	432.544	65	44	42	55	32	61
E080_N080	483.150	426.630	51	36	47	48	46	58
E080_N070	475.638	419.384	44	31	49	45	48	58
E080_N060	467.984	413.118	44	31	30	46	40	56
E080_N020	446.695	382.272	40	30	32	34	33	43
E080_N010	439.258	375.167	37	26	25	30	35	40

E080_N000	432.865	367.428	30	20	30	26	38	38
E080_N-10	425.750	359.555	27	18	29	24	36	36
E080_N-20	418.995	351.865	25	17	25	23	34	34
E080_N-30	412.521	344.607	24	17	24	22	36	33
E080_N-40	405.413	337.225	23.5	16	24	21	38	34
E080_N-50	398.521	330.306	23.5	17	17	24	30	32
E080_N-60	391.879	323.396	25	16	24	18	22	30
E080_N-70	385.263	316.197	23	16	24	20	36	30
E080_N-80	378.136	309.194	25	16	20	21	36	31
E100_N100	514.858	427.904	75	57	40	68	20	75
E100_N090	507.991	420.869	79	62	48	64	50	71
E100_N080	501.518	414.007	69	50	43	62	28	68
E100_N070	494.477	406.159	65	48	33	56	49	66
E100_N060	486.860	398.325	54	39	42	51	36	60
E100_N030	468.370	376.243	37	26.5	32	34	34	46
E100_N020	461.879	368.339	42	31	30	33	37	41
E100_N010	455.387	360.084	36	26	31	34	32	41
E100_N000	448.351	353.567	33	22.5	28	28	29	39
E100_N-10	441.415	346.198	29	22	26	26	39	37
E100_N-20	434.540	338.664	28	20	22	24	36	35
E100_N-30	428.107	331.801	25	17.5	25	22	34	34
E100_N-40	421.267	324.266	24	17	23	21	32	32
E100_N-50	414.177	317.718	21	16	20	18	33	29
E100_N-60	407.459	310.668	19	23.5	21	17	40	28
E100_N-70	400.765	303.155	18.5	13.5	20	16	32	27
E100_N-80	393.969	295.915	18.5	13.5	20	16	36	28
E120_N110	536.886	422.360	78	59	54	64	55	70
E120_N100	529.656	414.870	73	56	46	68	49	72
E120_N090	523.156	407.591	66	51	48	64	48	70
E120_N080	515.942	401.430	74	55	33	64	42	68
E120_N070	509.582	393.328	70	54	30	64	25	67
E120_N060	504.081	385.201	59	46	40	58	30	64
E120_N030	484.589	363.422	35	25.5	24	33	36	44
E120_N020	477.985	355.965	36	25.5	23	32	38	43
E120_N010	471.640	348.112	43	33	18	30	29	40
E120_N000	463.756	341.542	31	22.5	28	28	47	38
E120_N-10	456.632	334.039	29	20	30	24	40	35
E120_N-20	449.684	326.435	25.5	18	26	22	33	33
E120_N-30	443.047	319.125	24	17.5	20	21	32	32
E120_N-40	436.644	311.987	23.5	17.5	20	20	29	30
E120_N-50	429.786	305.024	22	15	20	18	30	30

E120_N-60	423.120	297.748	19	14	20	17	35	30
E120_N-70	416.264	290.206	18	12.5	21	17	33	30
E120_N-80	409.596	283.262	18.5	13	20	17	32	29
E140_N110	553.400	410.544	75	54	38	72	38	78
E140_N100	547.189	402.569	70	50	47	65	43	71
E140_N090	540.114	396.266	64	46	50	59	54	68
E140_N080	533.309	388.719	67	51	40	60	38	64
E140_N070	528.706	381.484	69	51	48	58	35	62
E140_N060	522.313	373.714	50	40	30	52	35	57
E140_N050	514.337	366.498	40	28	40	35	50	49
E140_N030	498.343	349.484	34	23.5	26	30	34	41
E140_N000	479.155	328.752	29	20	28	26	31	35
E140_N-10	471.813	320.788	28	22	18	24	27	34
E140_N-20	465.511	313.106	23.5	16	23	21	28	32
E140_N-30	458.521	306.868	20.5	15.5	19	19	34	30
E140_N-40	452.224	298.924	20	14	22	17	34	30
E140_N-50	445.376	291.740	19.5	14	19	17	34	30
E140_N-60	438.766	284.022	19	14	19	17	34	29
E140_N-70	432.018	276.175	19	15	21	17	34	30
E140_N-80	425.883	269.343	21	17	17	19	28	30
E160_N100	561.619	390.917	70	49	52	64	44	70
E160_N090	556.333	383.669	68	54	44	58	43	66
E160_N080	548.148	375.506	60	47	28	56	24	63
E160_N070	542.238	368.035	57	42	32	52	20	56
E160_N060	535.307	360.883	46	32	37	42	42	51
E160_N050	529.075	353.554	35	27	28	34	40	44
E160_N030	514.439	336.610	39	26	25	30	30	40
E160_N010	500.759	323.056	35	24.5	24	29	30	39
E160_N000	494.355	315.212	31	20	29	27	38	37
E160_N-10	487.460	308.044	29.5	21	21	24	29	33
E160_N-20	480.614	300.851	24	17	20	21	34	32
E160_N-30	473.870	293.206	21	15	22	18	34	30
E160_N-40	466.996	287.053	19.5	13.5	20	16	34	30
E160_N-50	460.235	279.973	19.5	14	19	16	34	29
E160_N-60	453.685	272.161	19.5	14	20	17	33	30
E160_N-70	446.882	264.611	21	15.5	24	20	30	32
E160_N-80	440.066	257.212	21.5	15	24	21	27	32
E180_N130	597.274	400.678	67	48	49	61	54	69
E180_N120	590.697	392.834	67	48	46	69	41	77
E180_N110	584.317	385.269	74	52	54	67	37	72

E180_N100	577.956	378.359	74	53	46	68	29	71
E180_N080	563.461	363.513	53	42	40	52	50	61
E180_N070	557.750	356.996	48	36	40	43	34	52
E180_N060	550.822	349.268	39	28	22	38	42	48
E180_N050	544.212	341.620	34	26	25	34	44	43
E180_N020	523.004	316.331	36	26	22	30	29	40
E180_N010	516.235	309.494	34	23.5	26	27	38	38
E180_N000	510.064	302.420	32	22	20	27	28	36
E180_N-10	502.821	295.317	31	21.5	20	27	24	34
E180_N-20	495.780	288.104	25	17	23	23	32	32
E180_N-30	488.767	280.544	21	15	22	18	32	30
E180_N-40	482.148	272.527	19.5	14	18	17	33	28
E180_N-50	475.091	265.314	17.5	12	20	15	30	28
E180_N-60	467.917	258.194	17.5	12	19	15	38	26
E180_N-70	461.060	251.035	16	12	20	15	32	27
E180_N-80	454.542	243.674	17	12	20	16	33	28
E200_N030	544.925	310.376	38	28	28	30	34	38
E200_N020	538.343	303.840	40	31	23	29	37	38
E200_N010	531.765	296.730	32	25	30	28	32	38
E200_N000	525.811	289.062	33	23	24	26	25	34
E200_N-10	518.799	281.764	26	17	24	22	34	32
E200_N-20	511.696	274.707	23.5	16	22	19	32	30
E200_N-30	505.036	267.584	23	16	19	19	28	28
E200_N-40	497.577	259.942	21	14.5	20	17	30	28
E200_N-50	490.648	253.769	18.5	13	18	16	30	28
E200_N-60	483.461	247.407	17	12	19	15	28	25
E200_N-70	475.948	240.746	13	9	16	15	32	28
E200_N-80	469.196	233.230	16	12	15	15	34	26
E220_N000	540.682	277.698	32	20	32	29	34	36
E240_N000	556.179	265.076	36	25	29	30	32	35
E260_N000	571.676	252.453	34	23	30	30	29	35
E280_N000	587.174	239.831	28.5	19	27	28	36	35
E300_N000	602.671	227.208	27.5	18.5	29	27	34	35
E320_N000	620.098	217.812	28	17.5	28.5	27	34	35
E340_N000	636.448	206.575	31	20.5	34	28.5	36	35
E360_N000	644.924	190.324	31	24	28.5	28.5	41	34
E380_N000	650.763	171.716	28.5	18.5	30	28	30	33
E400_N000	657.709	151.885	29	20.5	29	28	34	35
E420_N000	673.351	140.700	32	22	29	28	30	34
E440_N000	685.685	125.625	30	20	30	27	36	34
E460_N000	700.679	111.776	27	19	30	26.5	35	33

E480_N000	716.135	99.676	24.5	17	25	25	35	32	
E500_N000	734.144	90.661	37	30	27	31	31	34	
TL_W0200_00	323.050	654.897	43						
TL_W0200_10	315.581	648.866	NR						
TL_W0200_30	300.643	636.804	30						
TL_W0160_00	352.863	629.427	41.5						
TL_W0160_10	347.056	621.221	56						
TL_W0160_30	335.444	604.808	51						
TL_W0120_00	382.485	602.712	47						
TL_W0120_10	376.820	594.515	39						
TL_W0120_30	365.489	578.121	40						
TL_W0080_00	415.043	580.029	58						
TL_W0080_10	409.240	572.139	56.5						
TL_W0080_30	397.633	556.360	46.5						
TL_W0040_00	450.827	559.674	64.5						
TL_W0040_10	444.418	552.335	61						
TL_W0040_30	431.600	537.657	49.5						
TL_E0000_00	486.678	542.543	68						
TL_E0000_10	480.036	535.305	60						
TL_E0000_30	466.751	520.829	58						
TL_E0040_00	513.584	513.596	62						
TL_E0040_10	505.798	507.540	48						
TL_E0040_30	490.225	495.427	51						
TL_E0080_00	516.456	474.172	72						
TL_E0080_10	507.266	471.886	70						
TL_E0080_30	488.885	467.316	60						
TL_E0120_00	516.751	435.680	78						
TL_E0120_10	511.623	427.370	70						
TL_E0120_30	501.367	410.750	74						
TL_E0160_00	553.306	419.926	85						
TL_E0160_10	547.979	411.693	74						
TL_E0160_30	537.323	395.228	67						
TL_E0200_00	590.949	406.166	60						
TL_E0200_10	588.494	396.503	68.5						
TL_E0200_30	583.584	377.177	72.5						
TL_E0240_00	631.131	400.272	75.5						
TL_E0240_10	627.357	391.349	67.5						
TL_E0240_30	619.809	373.505	61						
TL_E0280_00	669.482	414.719	28						
TL_E0280_10	665.525	401.347	NR						
TL_E0280_30	657.610	374.603	45						
TL_E0320_00	682.584	376.446	35.5						

TL_E0320_10	673.550	371.845	NR
TL_E0320_30	655.480	362.644	38
TL_E0360_00	697.767	338.645	34
TL_E0360_10	686.320	330.267	NR
TL_E0360_30	663.425	313.512	47
TL_E0400_00	721.431	306.736	35
TL_E0400_10	713.358	302.412	NR
TL_E0400_30	697.214	293.763	52
TL_E0440_00	747.427	276.245	31.5
TL_E0440_10	732.364	268.203	50
TL_E0440_30	702.238	252.118	44.5
TL_E0480_00	767.330	242.094	32
TL_E0480_10	753.364	233.643	75
TL_E0480_30	725.432	216.742	51
TL_E0520_00	792.414	211.268	17.5
TL_E0520_10	793.956	201.495	23.5
TL_E0520_30	797.039	181.950	35
TL_E0560_00	812.901	245.130	23
TL_E0560_10	822.556	245.329	23
TL_E0560_30	841.866	245.727	16.5
TL_E0600_00	814.705	284.472	22
TL_E0600_10	824.766	284.775	24.5
TL_E0600_30	844.888	285.381	27
TL_E0640_00	817.047	324.473	20.5
TL_E0640_10	826.864	324.118	22
TL_E0640_30	846.499	323.408	20.5
TL_E0680_00	820.448	363.418	25.5
TL_E0680_10	830.143	361.521	23
TL_E0680_30	849.533	357.728	22
TL_E0720_00	824.543	403.234	38
TL_E0720_10	834.717	400.977	36
TL_E0720_30	855.064	396.464	30
TL_E0760_00	825.478	443.289	36
TL_E0760_10	835.547	444.280	38
TL_E0760_30	855.684	446.261	40
TL_E0800_00	817.700	484.263	30
TL_E0800_10	828.250	487.119	37
TL_E0800_30	849.349	492.831	34
TL_E0840_00	813.070	522.882	33
TL_E0840_10	823.086	524.155	33
TL_E0840_30	843.120	526.700	24
TL_E0880_00	808.070	562.597	31
TL_E0880_10	817.117	567.132	30

TL_E0880_30	835.213	576.202	20
TL_E0920_00	776.125	585.136	27
TL_E0920_10	782.097	593.061	25
TL_E0920_30	794.042	608.910	18.5
TL_E0960_00	748.929	610.940	37
TL_E0960_10	757.963	614.710	30
TL_E0960_30	776.033	622.252	23
TL_E1000_00	737.645	650.563	43
TL_E1000_10	747.493	652.750	14
TL_E1000_30	767.191	657.123	24
TL_E1040_00	733.696	690.292	39
TL_E1040_10	743.468	691.208	9
TL_E1040_30	763.011	693.040	27
TL_E1080_00	730.170	729.938	36
TL_E1080_10	739.173	731.773	40
TL_E1080_30	757.179	735.442	29
TL_E1120_00	724.448	769.672	40
TL_E1120_10	733.090	771.037	27
TL_E1120_30	750.374	773.766	36
TL_E1160_00	724.158	809.952	37
TL_E1160_10	732.620	812.453	38
TL_E1160_30	749.545	817.456	38
TL_E1200_00	705.746	844.481	39
TL_E1200_10	714.597	848.351	32
TL_E1200_30	732.298	856.092	38
TL_E1240_00	684.503	878.458	37
TL_E1240_10	690.166	886.656	40
TL_E1240_30	701.494	903.052	32
TL_E1280_00	654.289	904.622	39
TL_E1280_10	660.410	913.789	40
TL_E1280_30	672.651	932.121	36
TL_E1320_00	622.035	927.616	39
TL_E1320_10	627.699	936.050	43
TL_E1320_30	639.028	952.919	31
TL_E1360_00	584.161	943.503	37
TL_E1360_10	587.004	952.751	38
TL_E1360_30	592.691	971.247	40
TL_E1400_00	543.556	945.612	40
TL_E1400_10	546.100	952.999	46
TL_E1400_30	551.189	967.773	44
TL_E1440_00	504.003	948.849	46
TL_E1440_10	505.643	958.631	41
TL_E1440_30	508.923	978.194	56

TL_E1480_00	**464.158**	**950.248**	**34**
TL_E1480_10	**462.768**	**959.202**	**36**
TL_E1480_30	**459.989**	**977.111**	**52**
TL_E1520_30	**426.418**	**976.766**	**34**
TL_E1520_10	**425.644**	**957.493**	**30**
TL_E1520_00	**425.258**	**947.856**	**29**
TL_E1560_00	**386.803**	**941.703**	**40**
TL_E1560_10	**386.944**	**951.987**	**42**
TL_E1560_30	**387.224**	**972.554**	**39**
TL_E1600_00	**346.994**	**939.918**	**26**
TL_E1600_10	**346.912**	**950.034**	**28.5**
TL_E1600_30	**346.749**	**970.265**	**24**
TL_E1640_00	**308.062**	**949.890**	**34**
TL_E1640_10	**307.067**	**958.978**	**27.5**
TL_E1640_30	**305.077**	**977.155**	**37**
TL_E1680_00	**268.777**	**948.411**	**44**
TL_E1680_10	**270.457**	**958.150**	**38**
TL_E1680_30	**273.818**	**977.628**	**38**
TL_E1720_00	**229.066**	**949.411**	**53**
TL_E1720_10	**227.447**	**959.362**	**48**
TL_E1720_30	**224.209**	**979.264**	**42**
TL_E1760_00	**189.232**	**949.692**	**40**
TL_E1760_10	**189.009**	**959.456**	**37**
TL_E1760_30	**188.562**	**978.982**	**37**

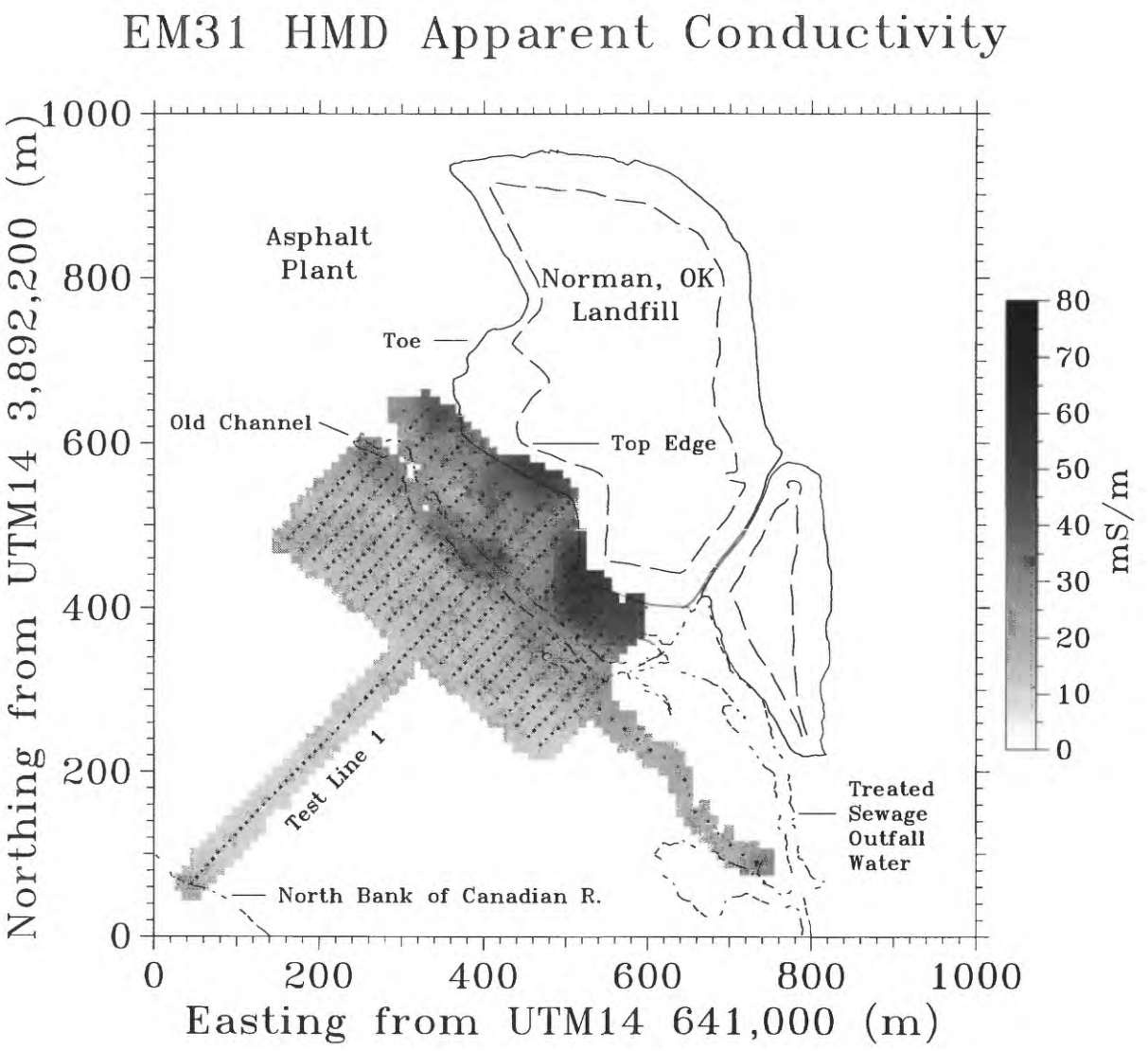

Figure A1. Image map of EM31-D HMD apparent conductivity for Norman, OK landfill area.

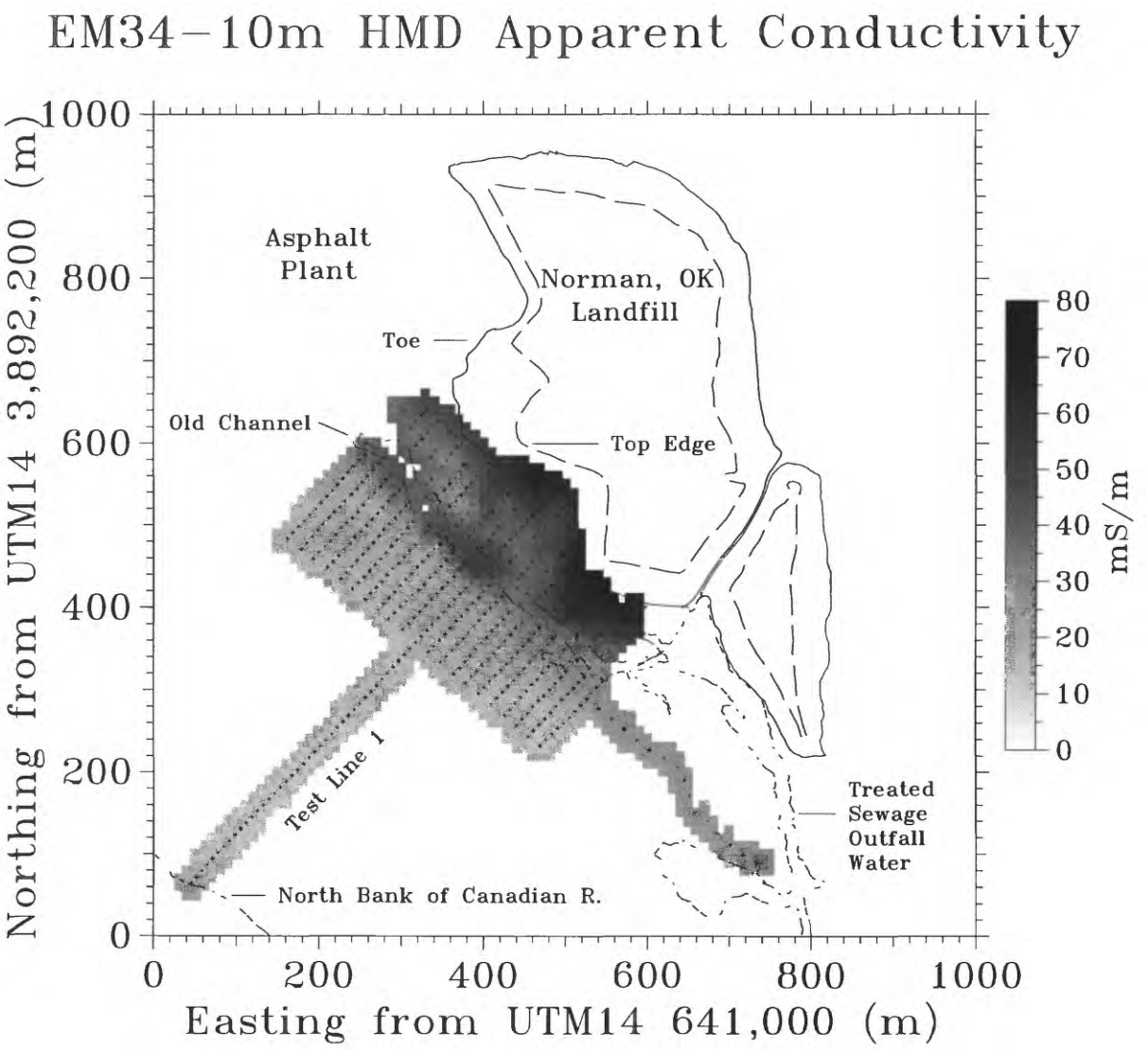

Figure A2. Image map of EM34-3 10-m HMD apparent conductivity for Norman, OK landfill area.

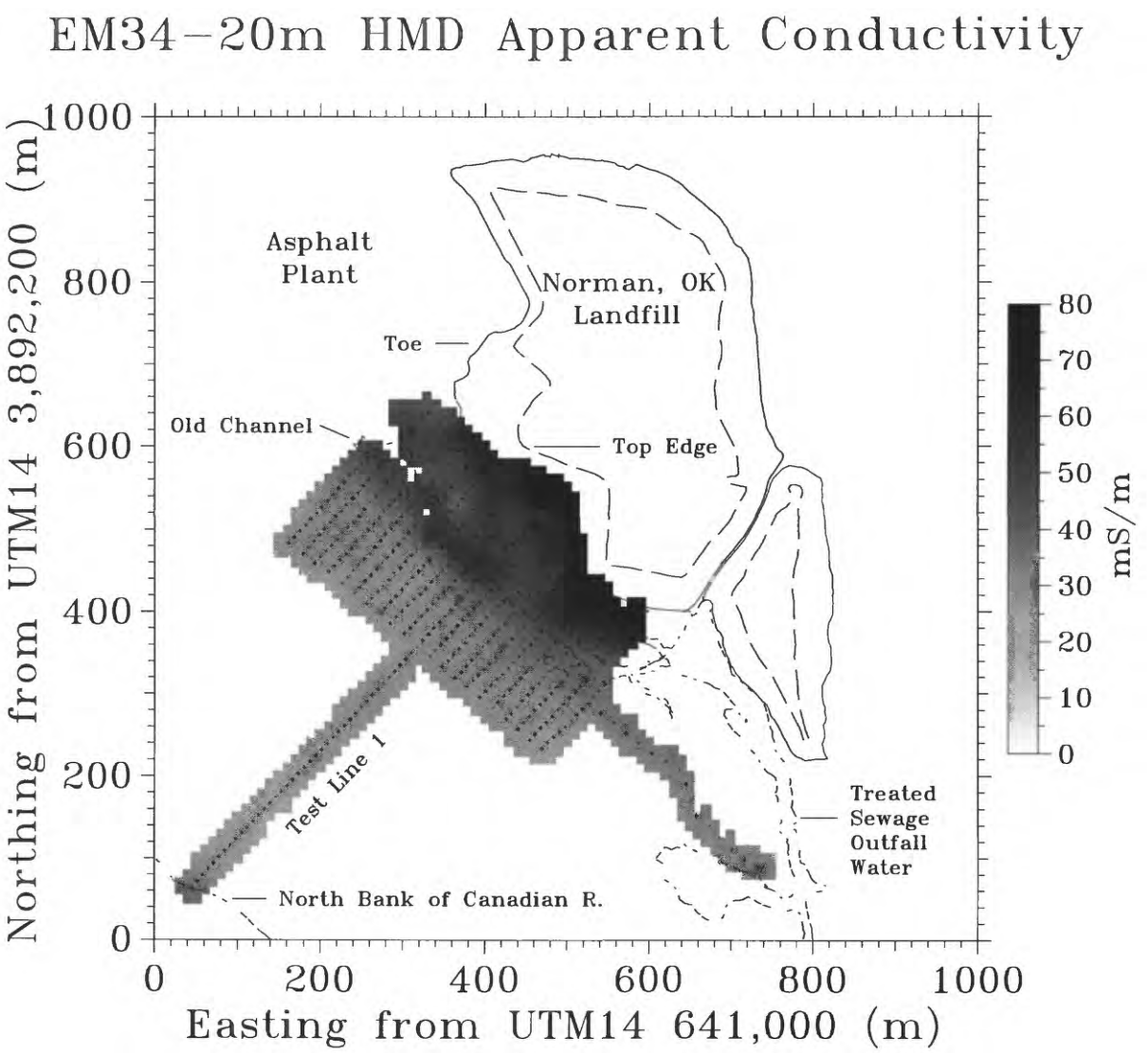

Figure A3. Image map of EM34-3 20-m HMD apparent conductivity for Norman, OK landfill area.

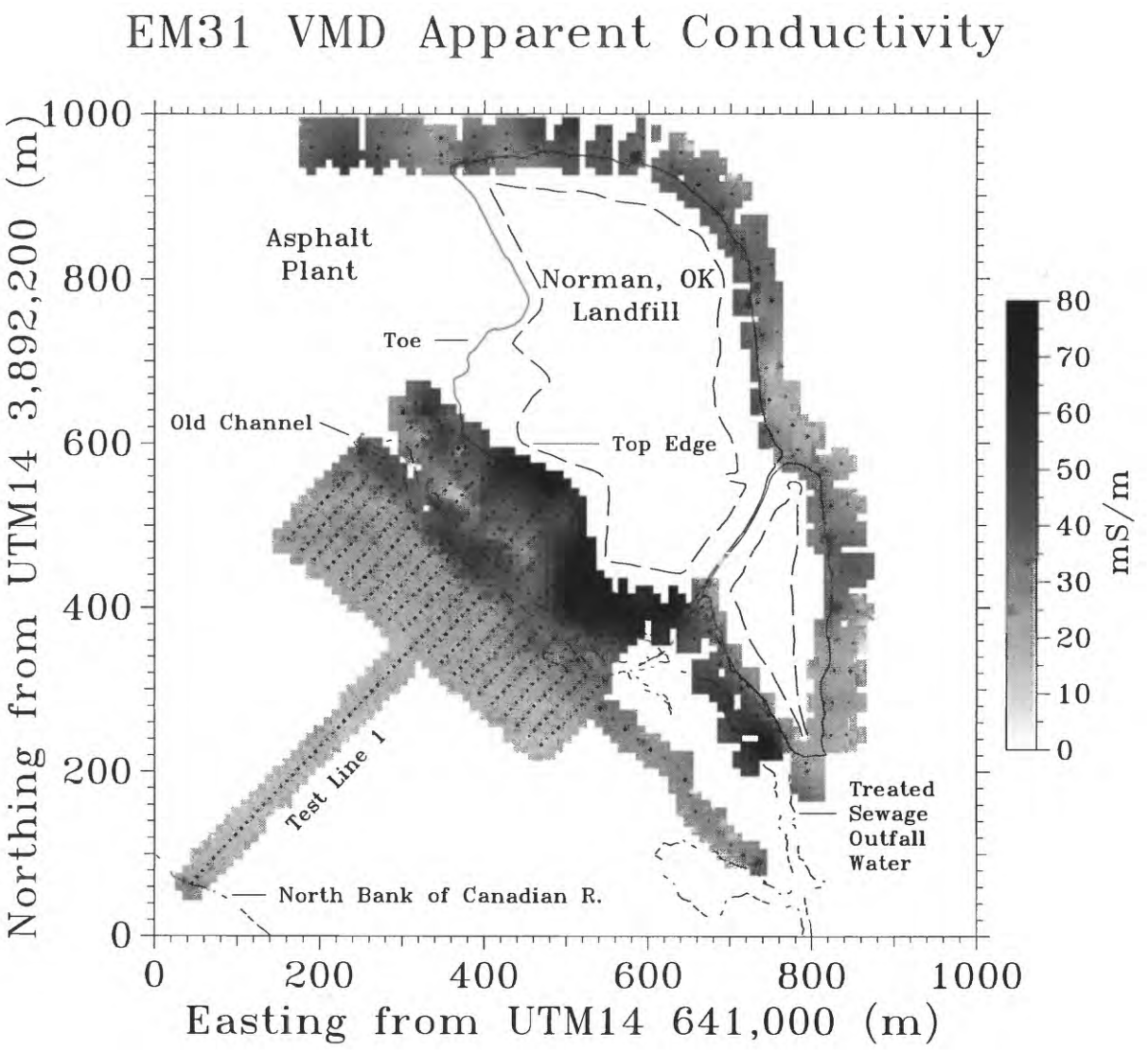

Figure A4. Image map of EM31-D VMD apparent conductivity for Norman, OK landfill area.

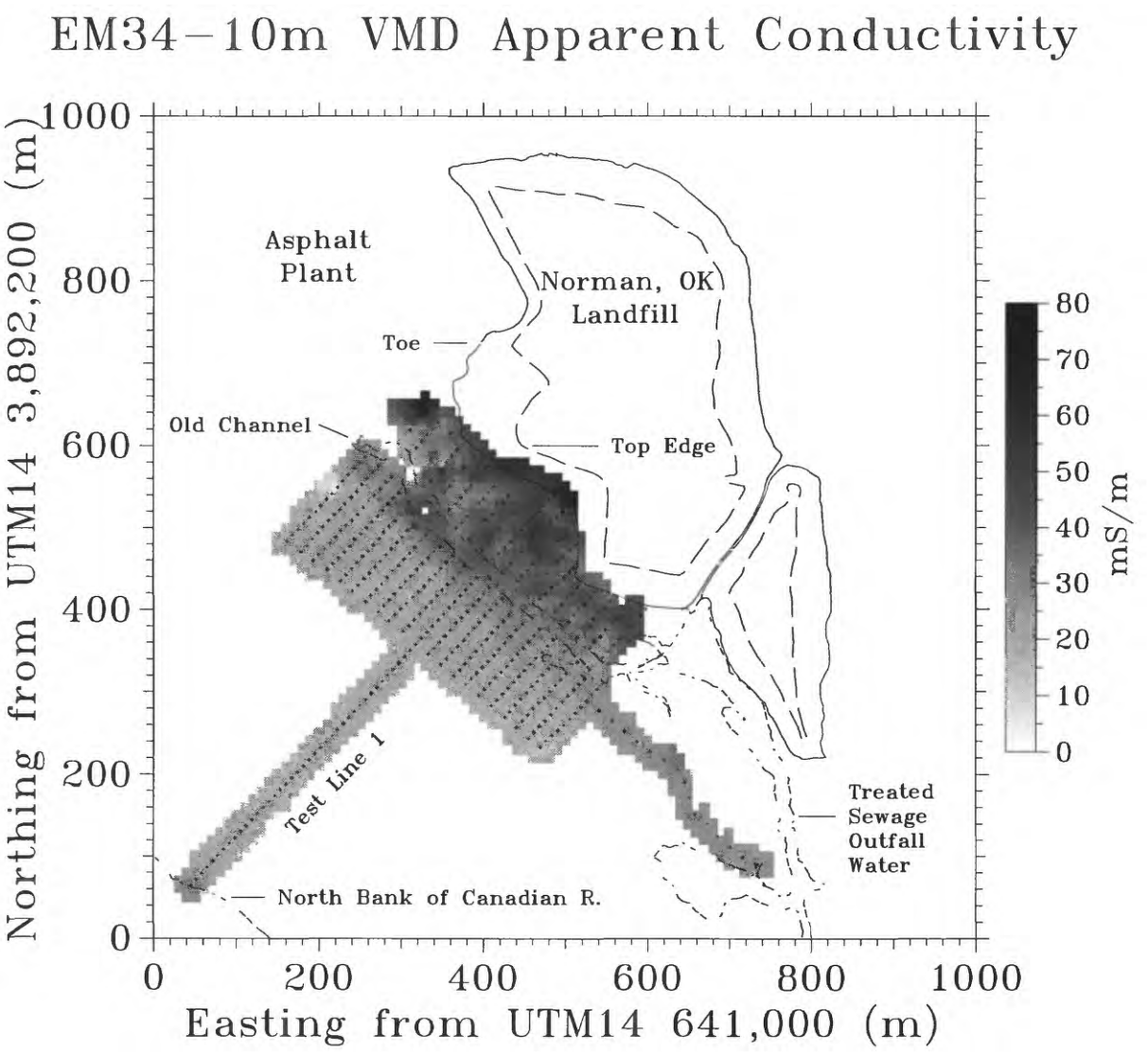

Figure A5. Image map of EM34-3 10-m VMD apparent conductivity for Norman, OK landfill area.

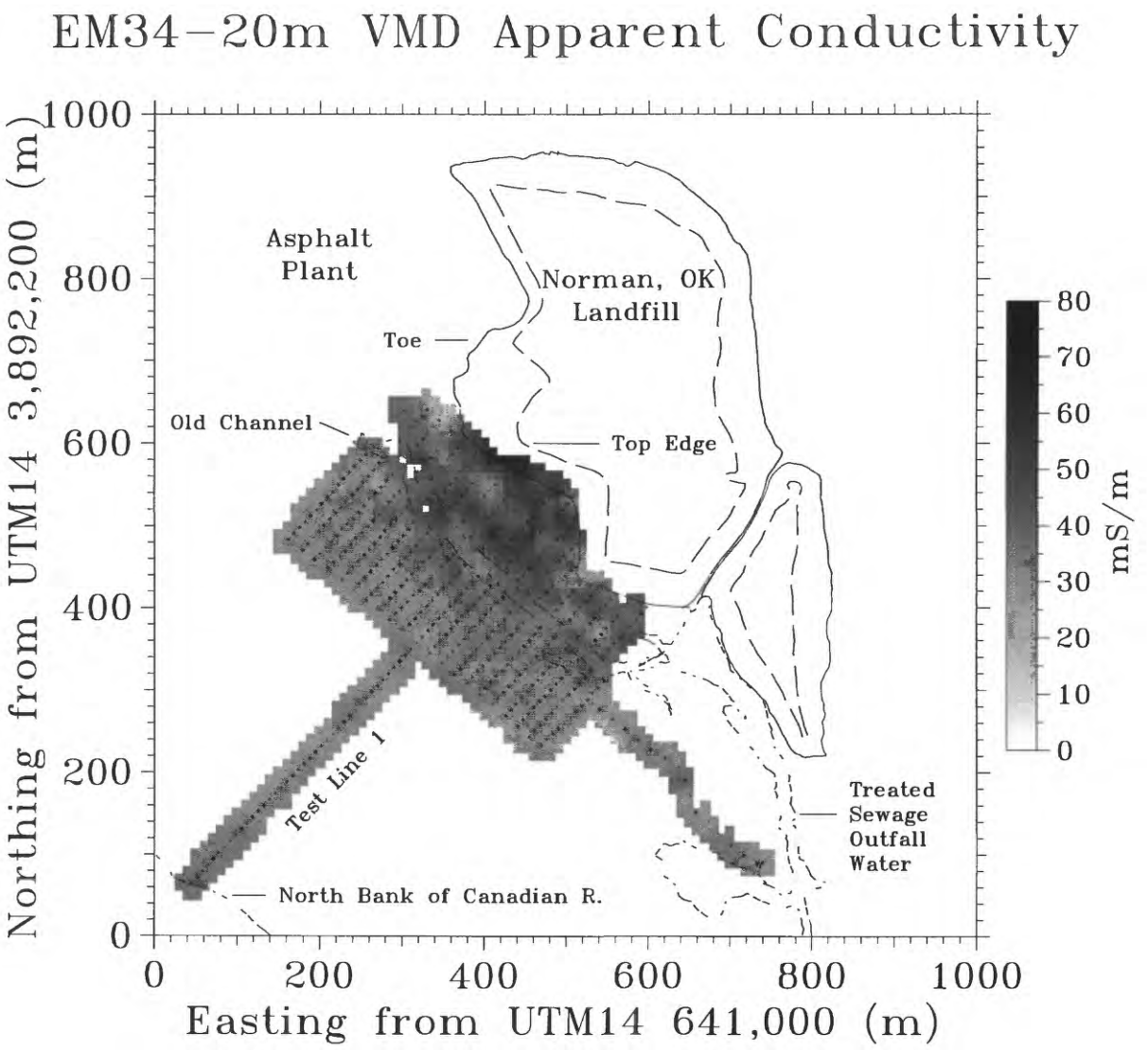

Figure A6. Image map of EM34-3 20-m VMD apparent conductivity for Norman, OK landfill area.

DC Resistivity Sounding Coordinates

GPS coordinates are given as UTM 14 coordinates with a constant value subtracted.
X is less 641,000.
Y is less 3,892,200.
Z coordinates are not given because the GPS elevation data was accurate to only +/- 3 meters.
X and Y accuracy is approximately one meter.

Sounding Number	X	Y	Sounding Number	X	Y
1	371.7	417.0	10	514.9	427.9
2	236.0	268.6	11	597.3	400.6
3	146.1	174.3	12	441.4	346.2
4	503.1	527.2	13	525.8	289.1
5	550.0	625.0	14	602.7	227.2
6	425.6	475.7	15	294.9	481.6
7	283.4	320.2	16	323.0	654.6
8	77.8	102.0	17	420.0	820.0
9	389.5	589.5			

DC Resistivity Sounding Curves

The DC resistivity data were interpreted using an automatic computerized interpretation program (Zohdy and Bisdorf, 1989) written for IBM PCs and compatible computers. The soundings are designated NORMAN 1 through NORMAN 17. For each sounding curve the figures include the following:

1) a sounding title designated by the survey area followed by the sounding number,
2) a tabulation of the AB/2 electrode spacings (in meters and feet) and corresponding apparent resistivities (in ohm-meters),
3) a log-log plot of the field data points, with each set of data points with the same potential electrode spacing (MN) connected with a solid line,
4) a tabulation of the automatically-interpreted layering with depths in meters and feet and the corresponding resistivities in ohm-meters, and
5) a log-log plot of the results of the automatic interpretation program. The circles represent the shifted digitized field data, the continuous curve represents the sounding curve calculated from the interpreted layering, and the step-function curve represents the interpreted layering.

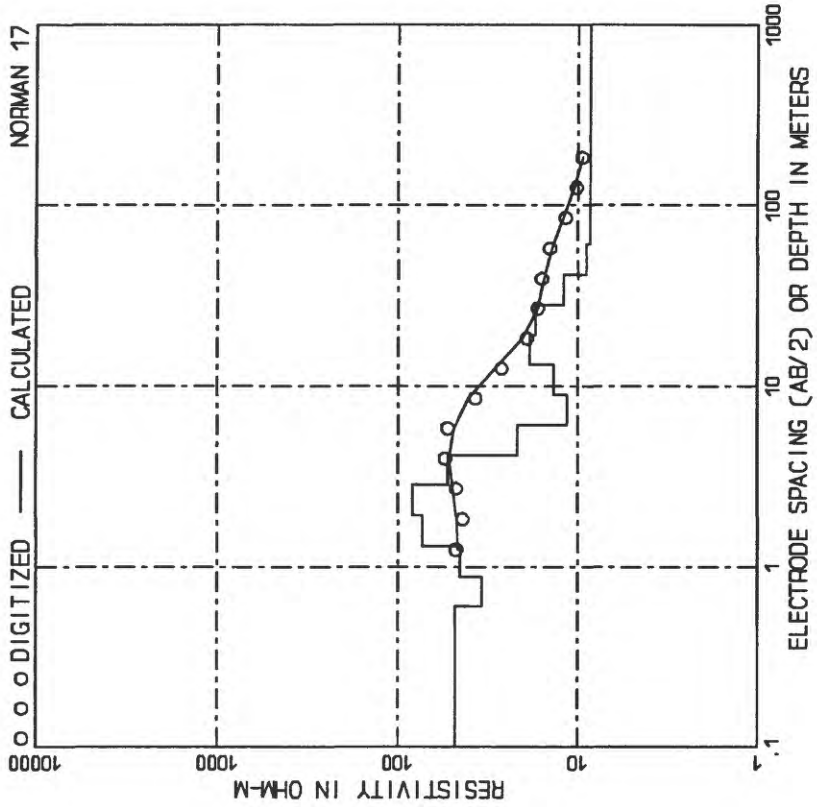

DEPTH, m (	ft)	RESIS.	DEPTH, m (	ft)	RESIS.
0.61	1.99	48.08	8.89	29.16	11.56
0.89	2.92	34.07	13.05	42.80	13.62
1.30	4.28	44.17	19.15	62.82	18.63
1.91	6.22	73.06	28.11	92.21	17.33
2.81	9.22	82.20	41.25	135.35	12.11
4.13	13.53	52.43	60.55	198.66	9.00
6.06	19.87	21.82	99999.00	(99999.00)	8.56

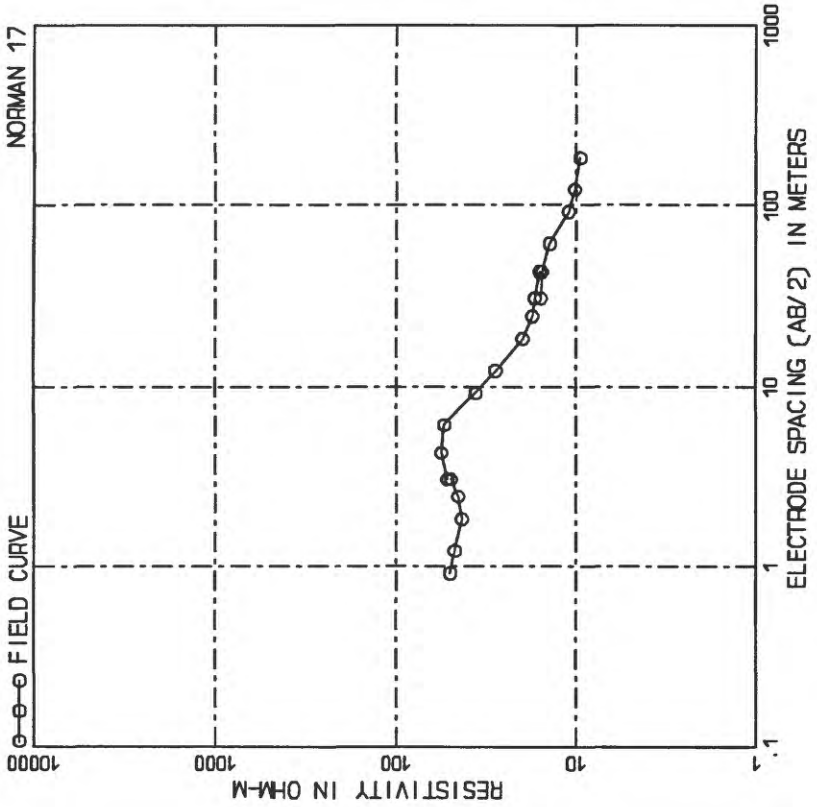

AB/2, m (	ft)	App. Res.	AB/2, m (	ft)	App. Res.
0.91	3.00	50.00	18.29	60.000	19.80
1.22	4.00	47.00	24.38	80.000	17.50
1.83	6.00	43.00	30.48	100.000	17.00
2.44	8.00	45.00	42.67	140.000	16.00
3.05	10.00	49.50	30.48	100.000	15.70
3.05	10.00	52.00	42.67	140.000	15.50
4.27	14.00	56.00	60.96	200.000	14.00
6.10	20.00	54.00	91.44	300.000	11.00
9.14	30.00	34.00	121.92	400.000	10.20
12.19	40.00	28.00	182.88	600.00)	9.50

Figure A7. DC Resistivity sounding Norman 1 and interpretation.

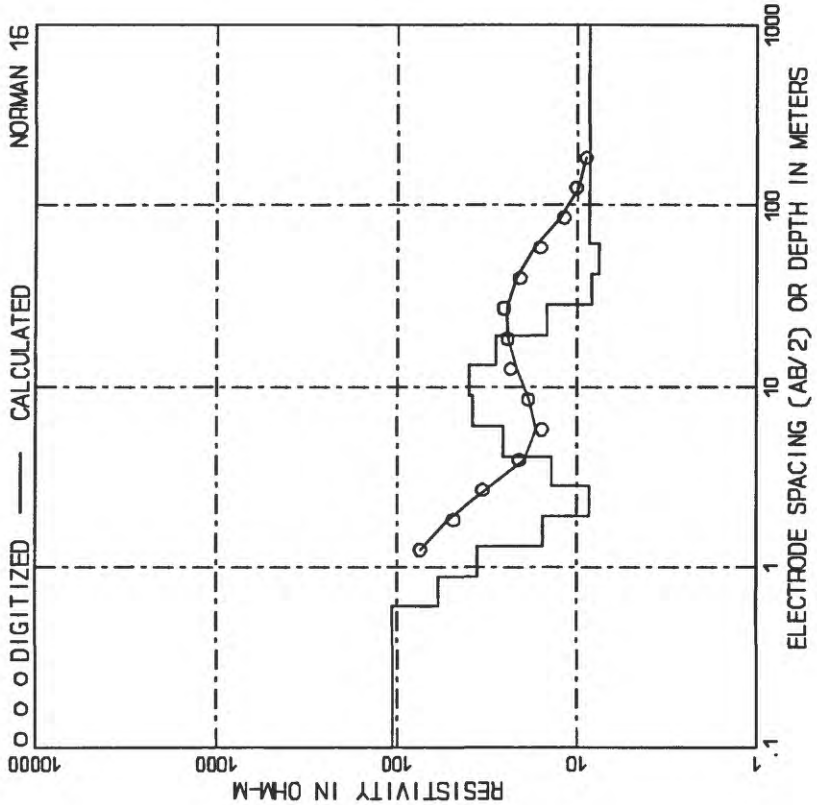

DEPTH, m (	ft)	RESIS.	DEPTH, m (	ft)	RESIS.
0.61	1.99	105.59	8.89	29.16	37.74
0.89	2.92	58.91	13.05	42.80	39.73
1.30	4.28	35.77	19.15	62.82	28.28
1.91	6.28	15.56	28.11	92.21	14.67
2.81	9.22	18.54	41.25	135.35	18.29
4.13	13.53	13.84	60.55	198.66	7.29
6.06	19.87	25.96	99999.00	(99999.00)	8.53

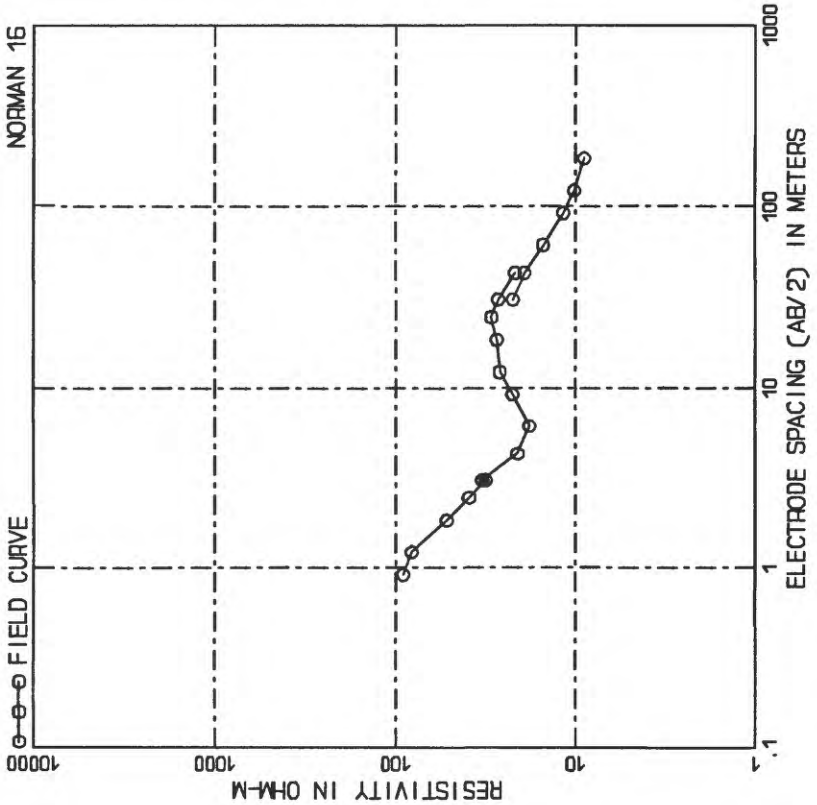

AB/2, m (	ft)	App. Res.	AB/2, m (	ft)	App. Res.
0.91	3.00	91.00	18.29	60.00	27.50
1.22	4.00	81.00	24.38	80.00	29.50
1.83	6.00	52.00	30.48	100.00	27.00
2.44	8.00	39.00	42.67	140.00	21.70
3.05	10.00	31.50	30.48	100.00	22.50
3.05	10.00	33.00	42.67	140.00	19.30
4.27	14.00	21.00	60.96	200.00	15.10
6.10	20.00	18.00	91.44	300.00	11.70
9.14	30.00	22.50	121.92	400.00	10.20
12.19	40.00	26.40	182.88	600.00	9.00

Figure A8. DC Resistivity sounding Norman 2 and interpretation.

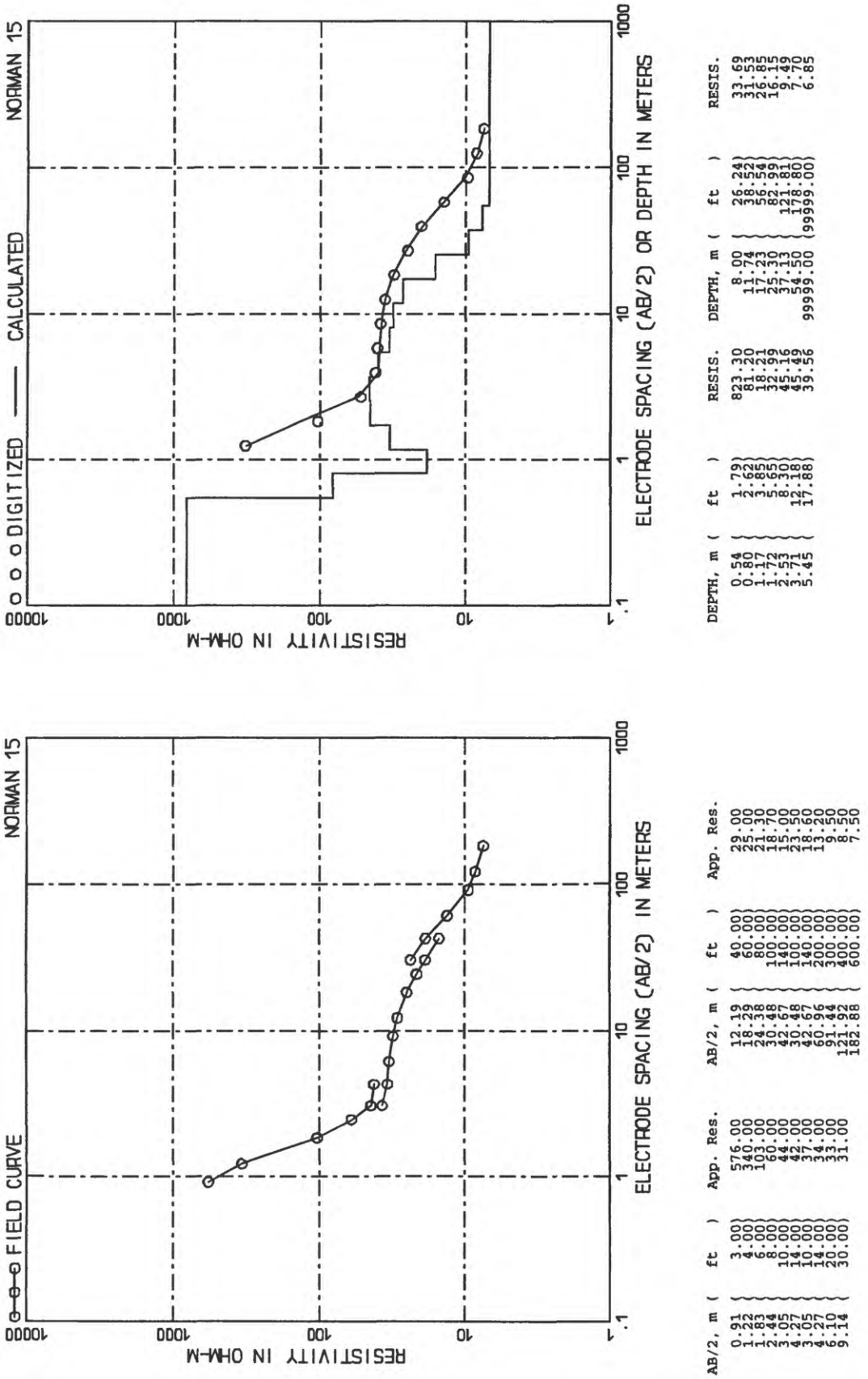

Figure A9. DC Resistivity sounding Norman 3 and interpretation.

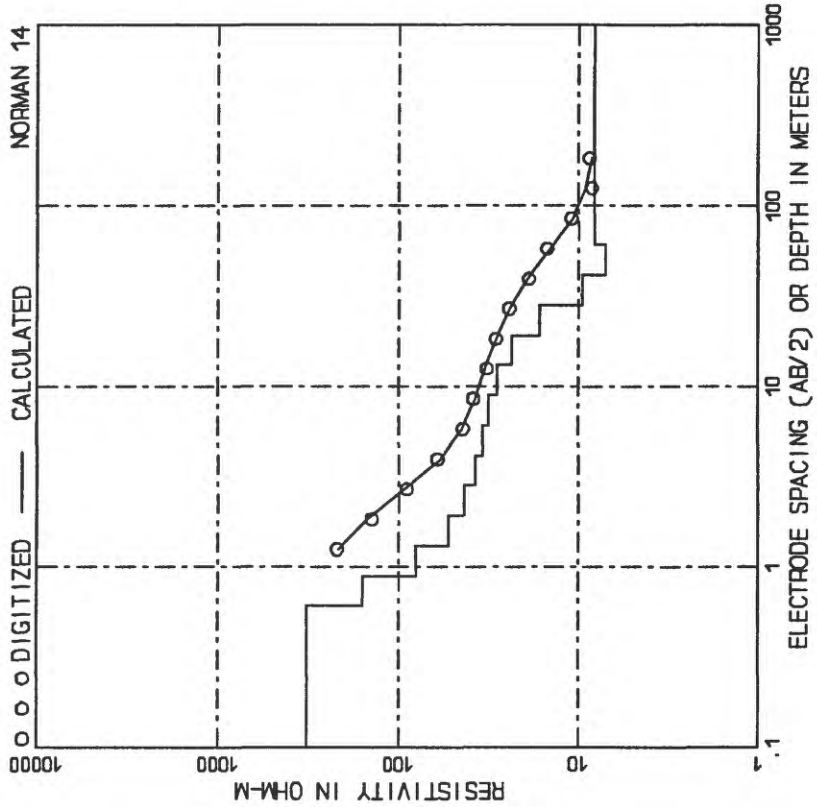

DEPTH, m	(ft)	RESIS.	DEPTH, m	(ft)	RESIS.
0.61	1.99	323.14	8.89	29.16	31.45
0.89	2.92	157.63	13.05	42.80	28.27
1.30	4.28	79.89	19.15	62.82	23.60
1.91	6.28	53.04	28.11	92.21	16.54
2.81	9.22	422.79	41.25	135.35	7.62
4.13	13.53	192.32	60.55	198.66	7.11
6.06	19.87	33.86	99999.00	(99999.00)	8.17

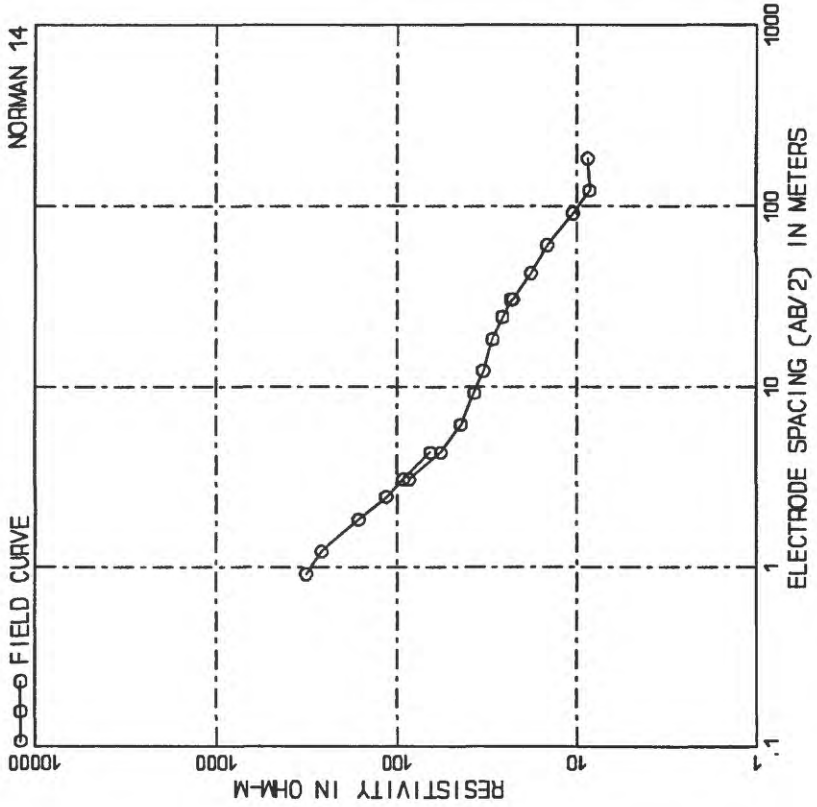

AB/2, m	(ft)	App. Res.	AB/2, m	(ft)	App. Res.
0.91	3.00	318.00	12.19	40.00	33.20
1.22	4.00	260.00	18.29	60.00	29.50
1.83	6.00	164.00	24.38	80.00	26.00
2.44	8.00	115.00	30.48	100.00	23.30
3.05	10.00	92.00	30.48	100.00	22.80
4.27	14.00	65.00	42.67	140.00	18.00
3.05	10.00	85.00	60.96	200.00	14.60
4.27	14.00	57.00	91.44	300.00	10.50
6.10	20.00	44.00	121.92	400.00	8.50
9.14	30.00	37.20	182.88	600.00	8.70

Figure A10. DC Resistivity sounding Norman 4 and interpretation.

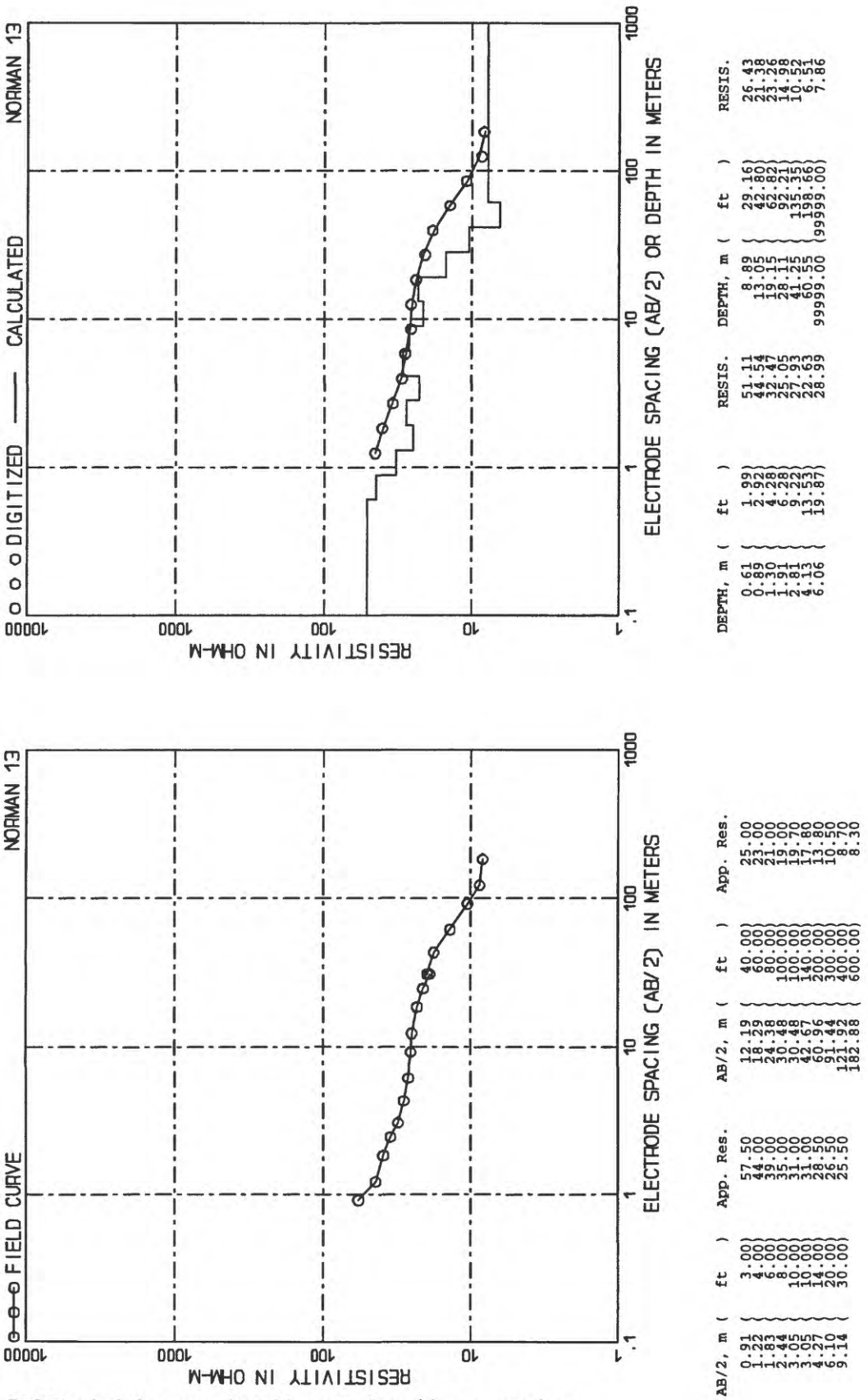

Figure A11. DC Resistivity sounding Norman 5 and interpretation.

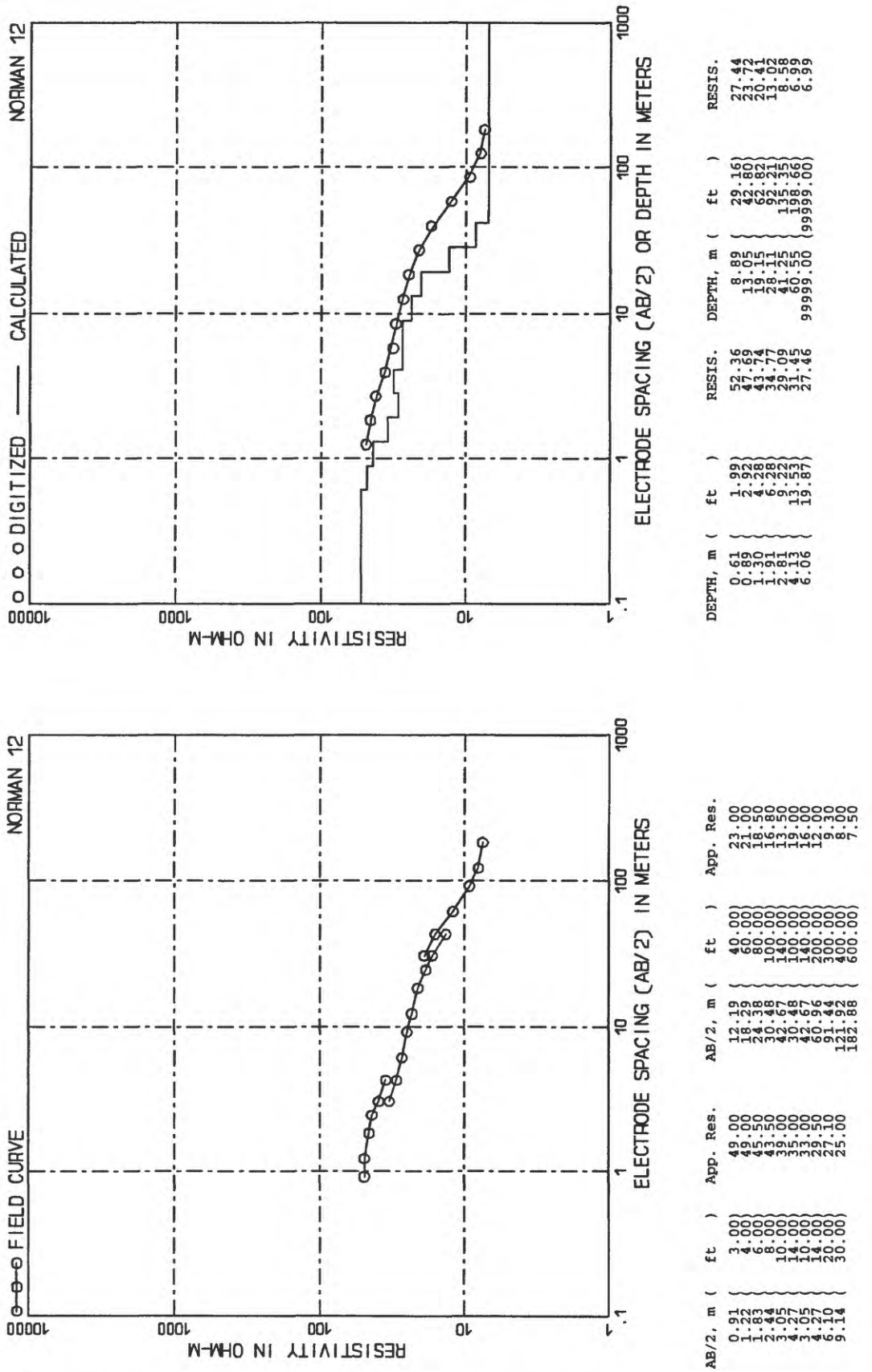

Figure A12. DC Resistivity sounding Norman 6 and interpretation.

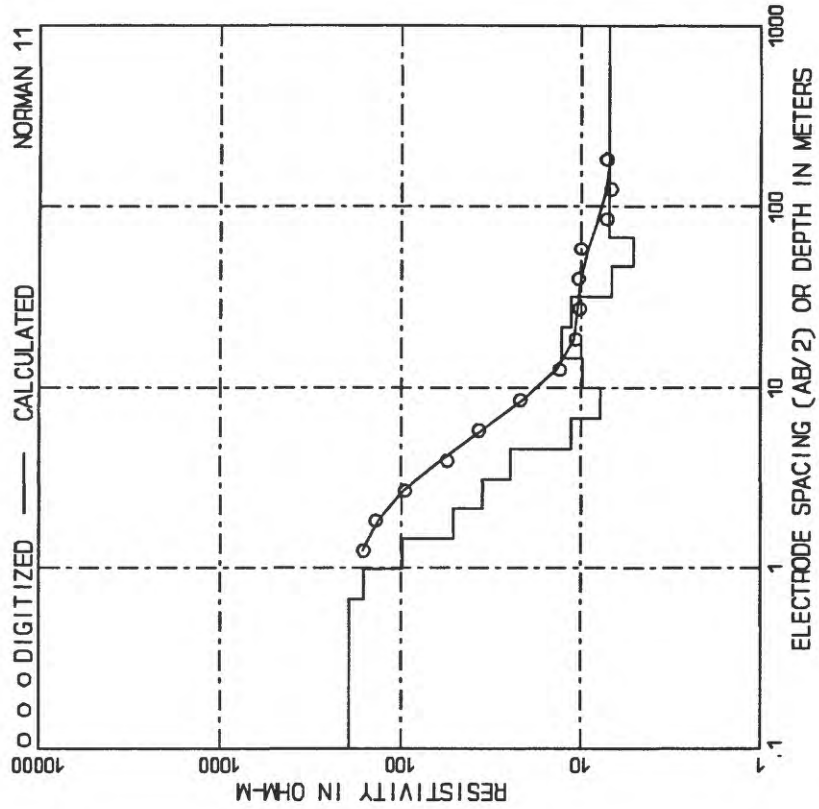

DEPTH, m (ft)	RESIS.	DEPTH, m (ft)	RESIS.
0.67 (2.21)	192.08	9.88 (32.40)	7.76
0.99 (3.24)	160.82	14.50 (47.56)	8.85
1.45 (4.76)	107.50	21.28 (69.80)	12.88
2.13 (6.98)	50.79	31.23 (102.46)	11.24
3.12 (10.25)	35.22	45.84 (150.39)	6.75
4.58 (15.04)	24.59	67.28 (220.74)	5.12
6.73 (22.07)	11.38	99999.00 (99999.00)	7.01

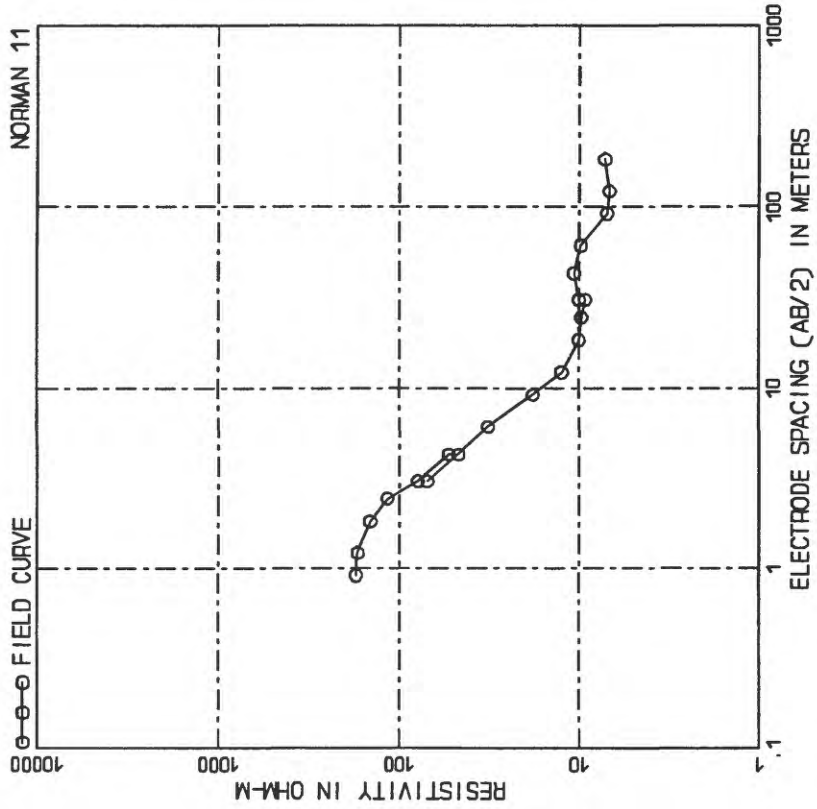

AB/2, m (ft)	App. Res.	AB/2, m (ft)	App. Res.
0.91 (3.00)	174.00	12.19 (40.00)	12.50
1.22 (4.00)	170.00	18.29 (60.00)	10.00
1.83 (6.00)	145.00	24.38 (80.00)	9.70
2.44 (8.00)	116.00	30.48 (100.00)	9.30
3.05 (10.00)	79.00	42.67 (140.00)	10.00
4.27 (14.00)	53.00	60.96 (200.00)	10.70
6.10 (20.00)	70.00	91.44 (300.00)	9.80
9.14 (30.00)	47.00	121.92 (400.00)	7.00
	32.00	182.88 (600.00)	6.80
	18.00		7.20

Figure A13. DC Resistivity sounding Norman 7 and interpretation.

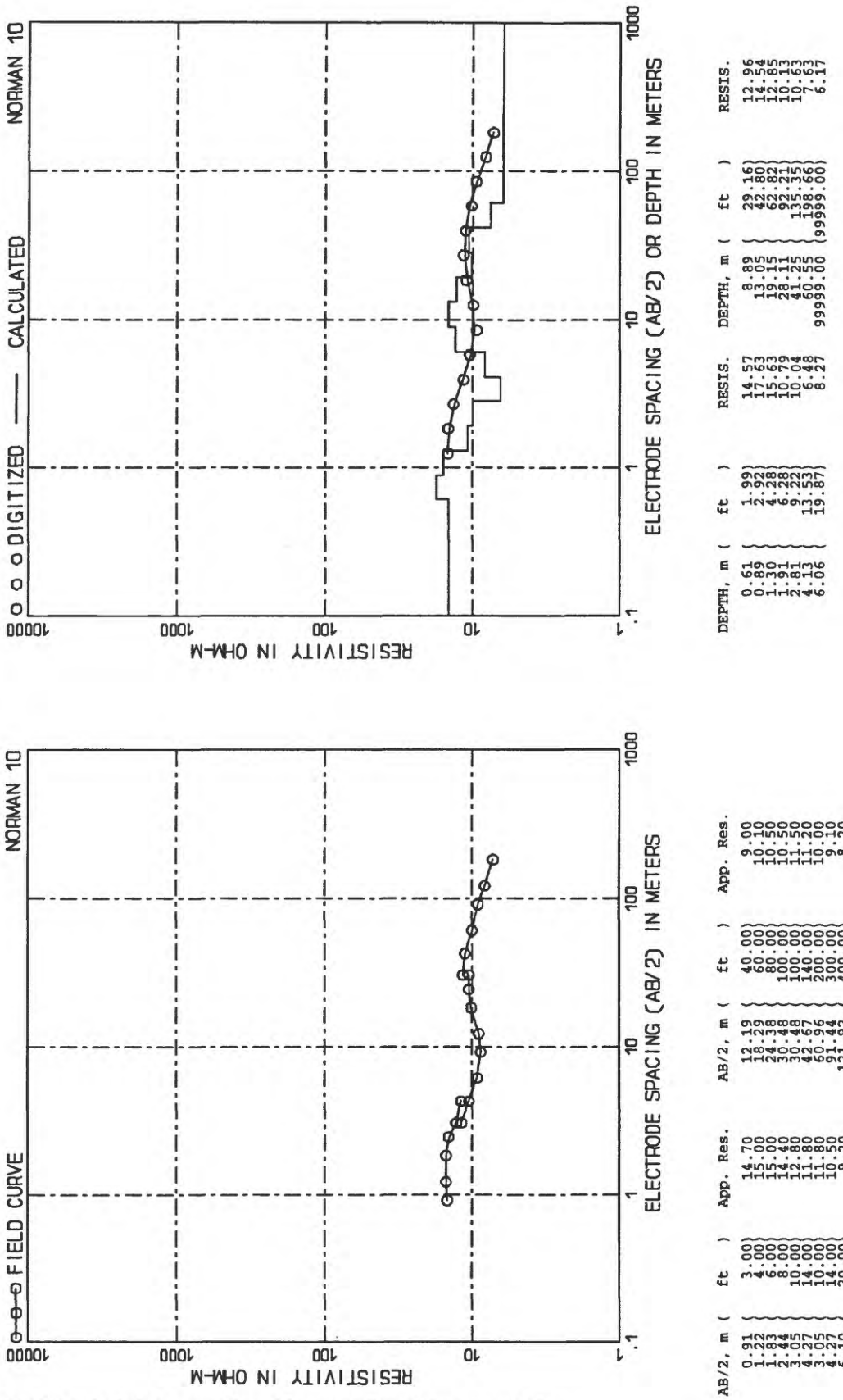

Figure A14. DC Resistivity sounding Norman 8 and interpretation.

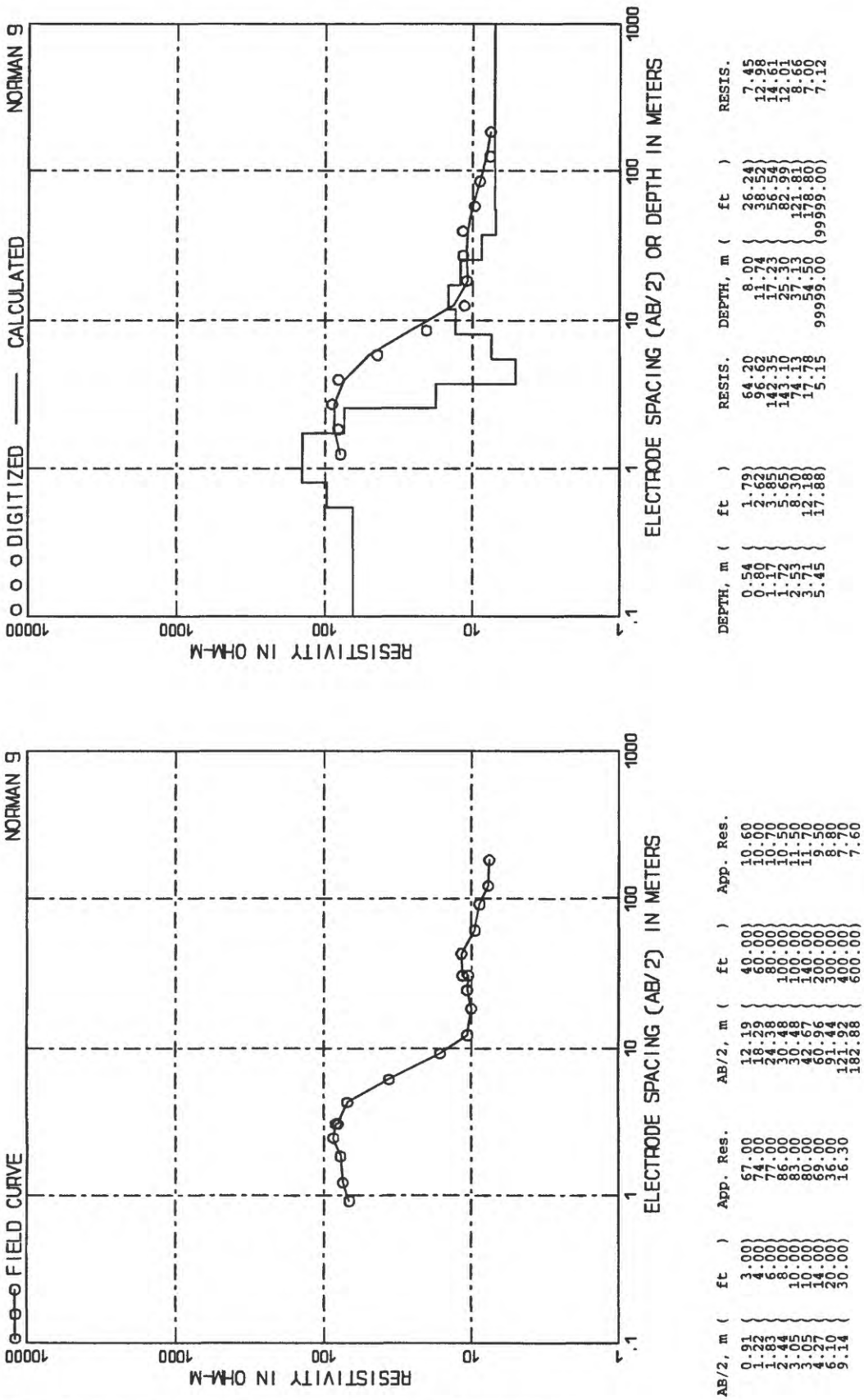

Figure A15. DC Resistivity sounding Norman 9 and interpretation.

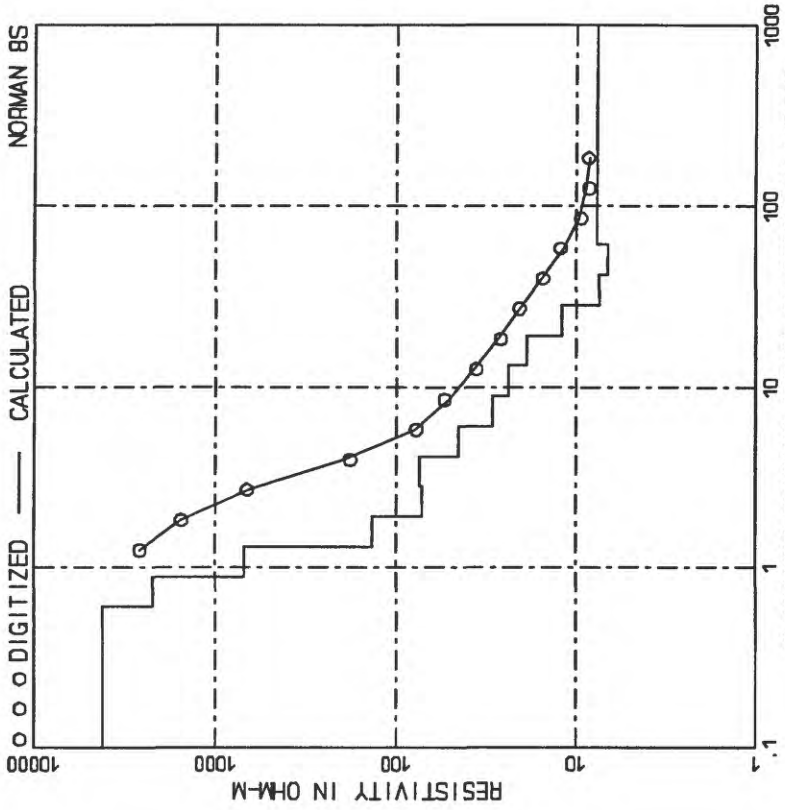

DEPTH, m (ft)	RESIS.	DEPTH, m (ft)	RESIS.
0.61 (1.99)	4194.23	8.89 (29.16)	29.24
0.89 (2.92)	2198.10	13.05 (42.80)	23.90
1.30 (4.28)	695.04	19.15 (62.82)	18.88
1.91 (6.28)	136.57	28.11 (92.21)	12.04
2.81 (9.22)	71.78	41.25 (135.35)	7.43
4.13 (13.53)	73.97	60.55 (198.66)	6.64
6.06 (19.87)	45.06	99999.00 (99999.00)	7.68

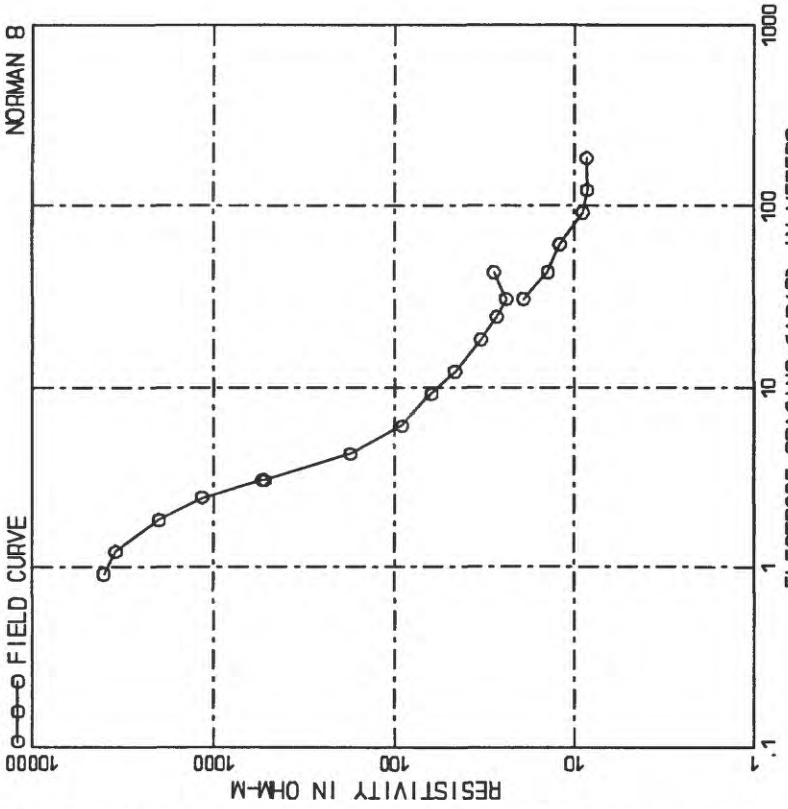

AB/2, m (ft)	App. Res.	AB/2, m (ft)	App. Res.
0.91 (3.00)	4015.00	18.29 (60.00)	33.00
1.22 (4.00)	3450.00	24.38 (80.00)	27.00
1.83 (6.00)	2000.00	30.48 (100.00)	24.00
2.44 (8.00)	1160.00	42.67 (140.00)	28.00
3.05 (10.00)	540.00	30.48 (100.00)	19.20
4.27 (14.00)	520.00	42.67 (140.00)	14.00
6.10 (20.00)	175.00	60.96 (200.00)	12.00
9.14 (30.00)	90.00	91.44 (300.00)	9.00
12.19 (40.00)	62.00	121.92 (400.00)	8.50
	46.00	182.88 (600.00)	8.55

Figure A16. DC Resistivity sounding Norman 10 and interpretation.

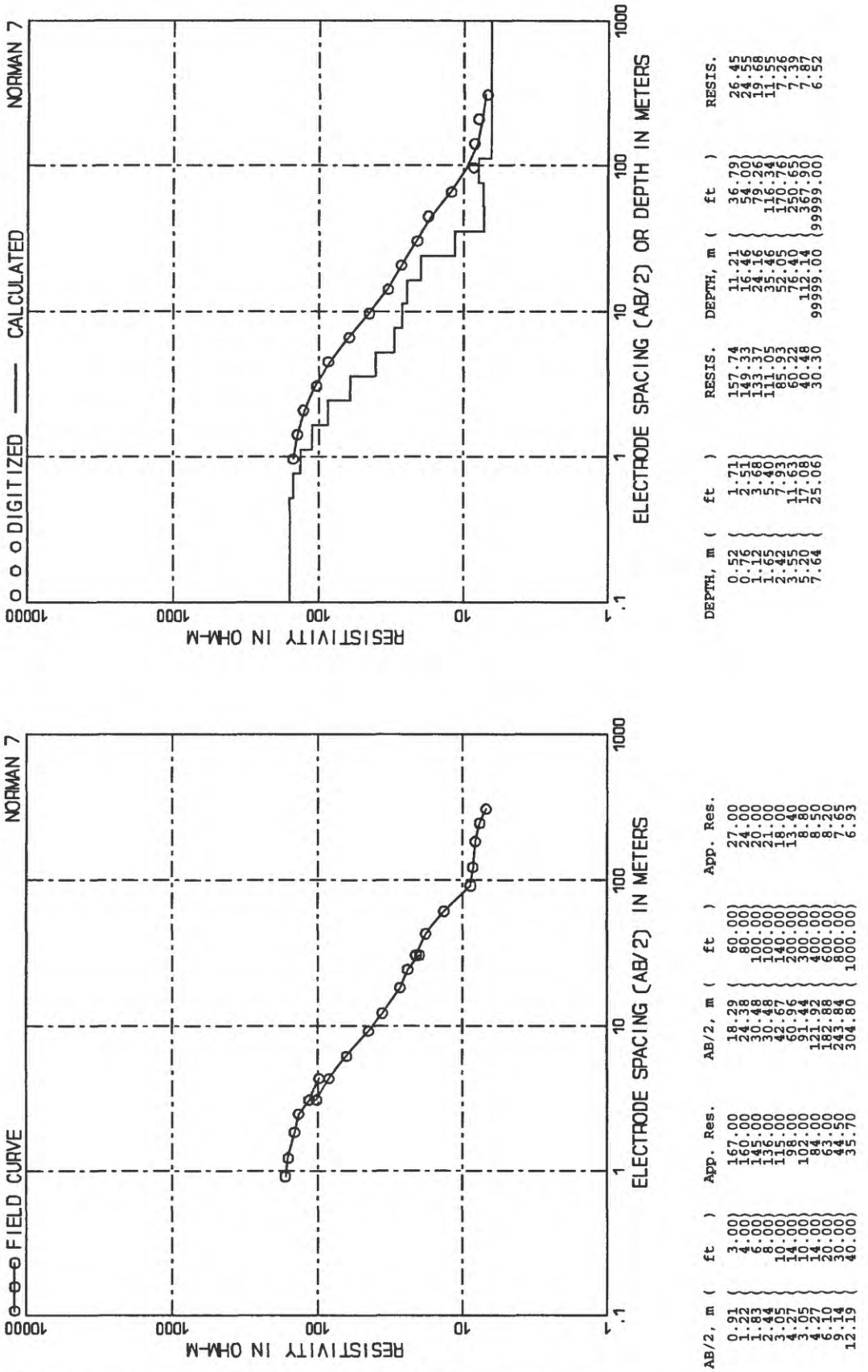

Figure A17. DC Resistivity sounding Norman 11 and interpretation.

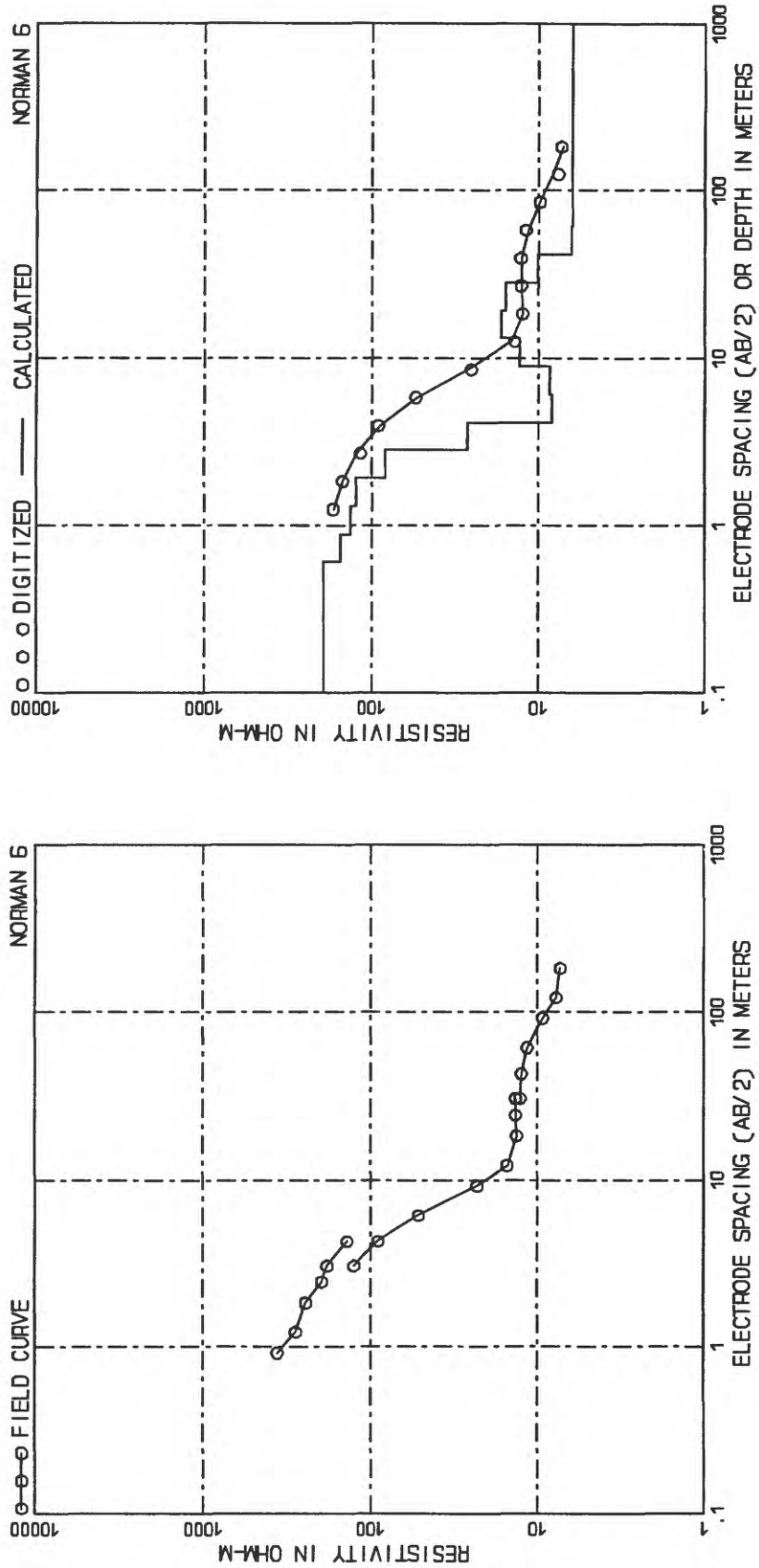

Figure A18. DC Resistivity sounding Norman 12 and interpretation.

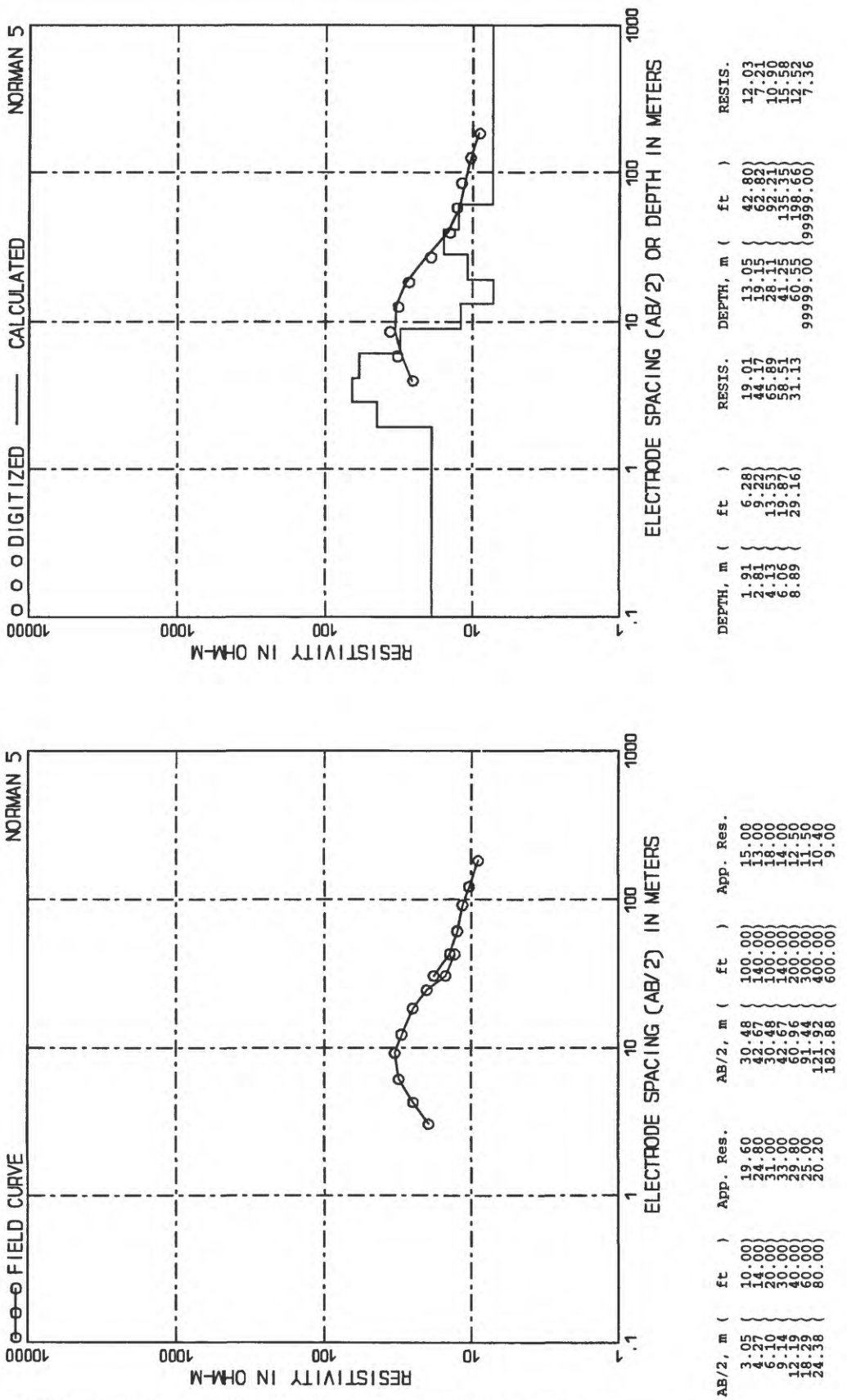

Figure A19. DC Resistivity sounding Norman 13 and interpretation.

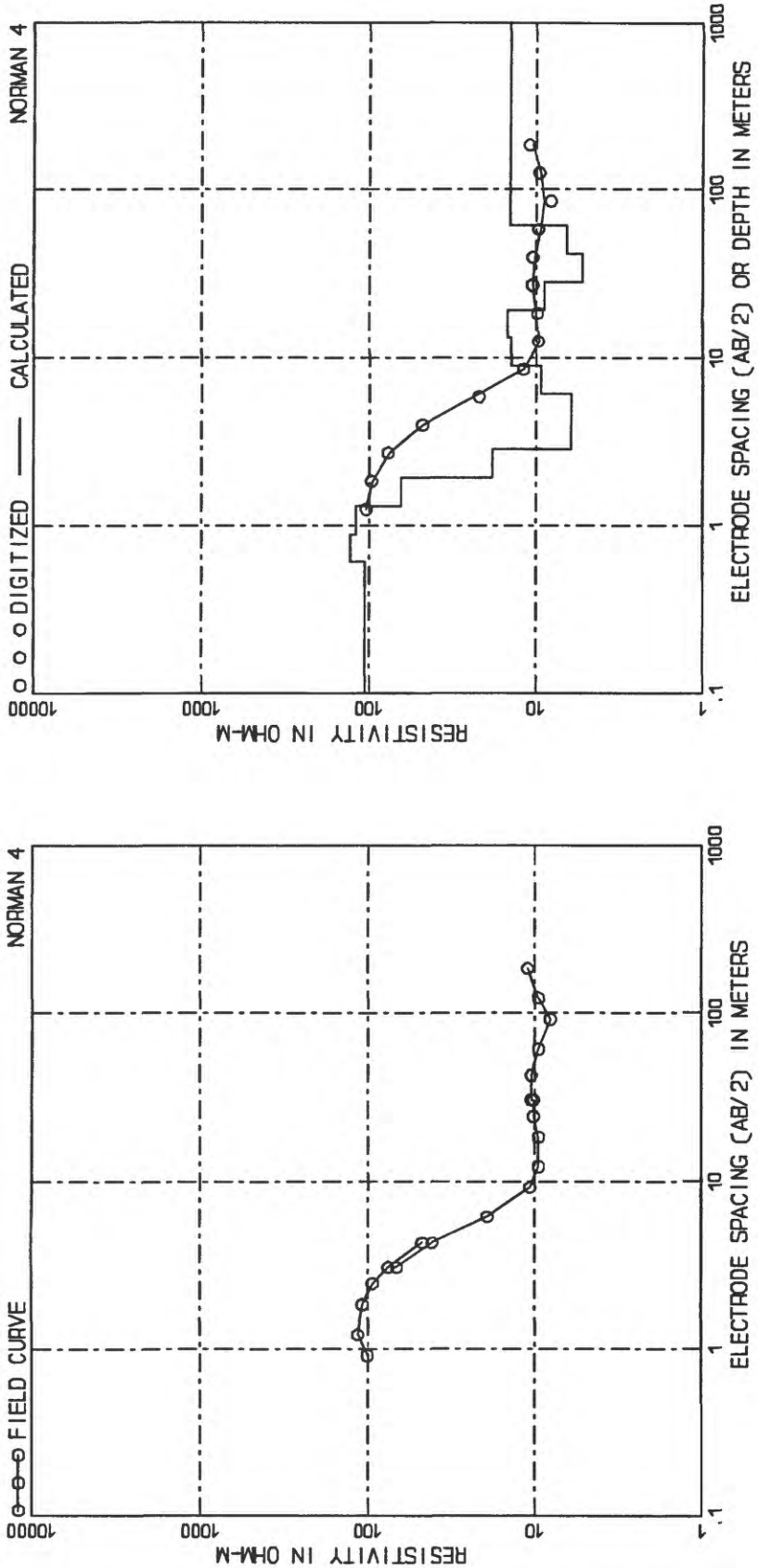

Figure A20. DC Resistivity sounding Norman 14 and interpretation.

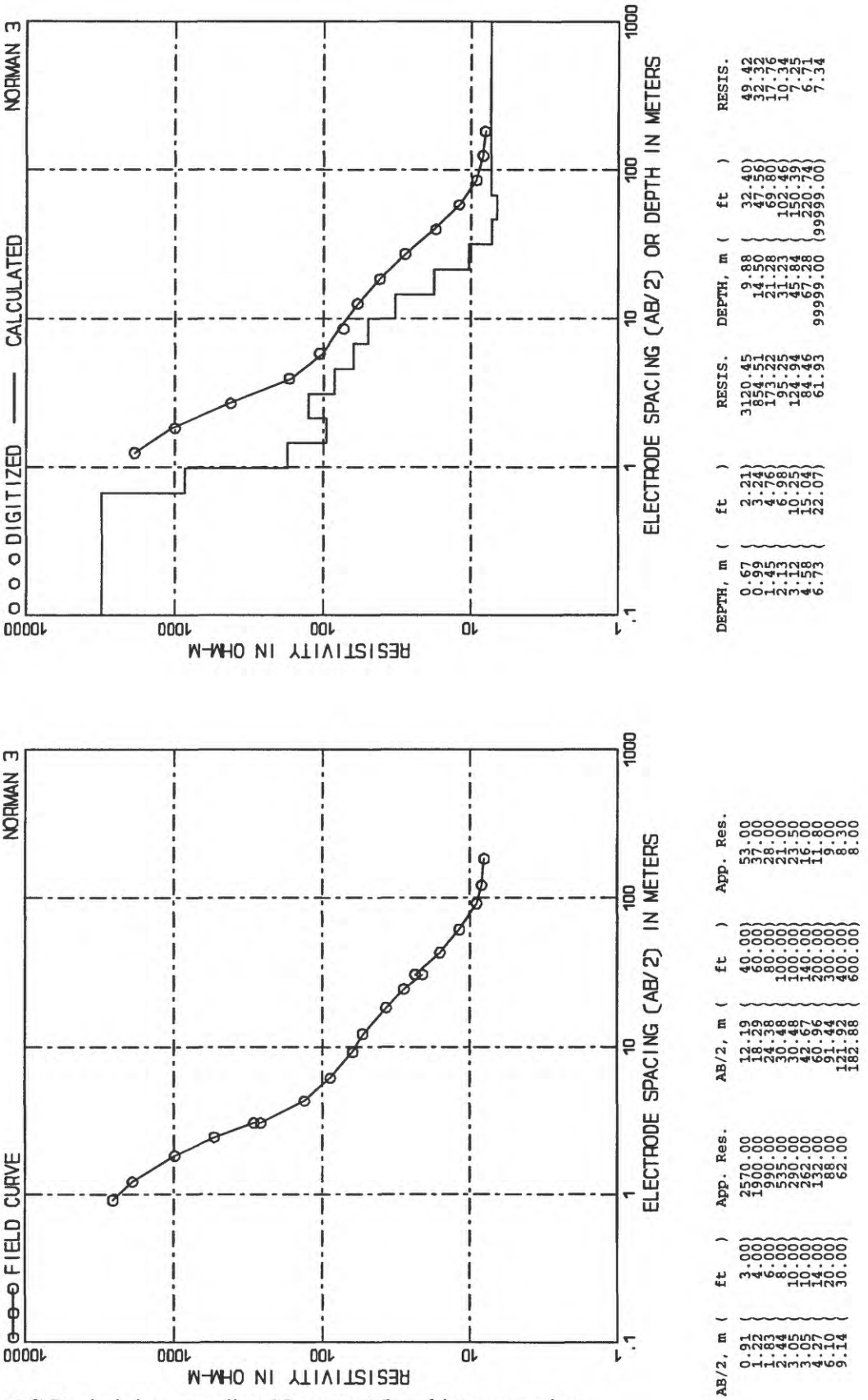

Figure A21. DC Resistivity sounding Norman 15 and interpretation.

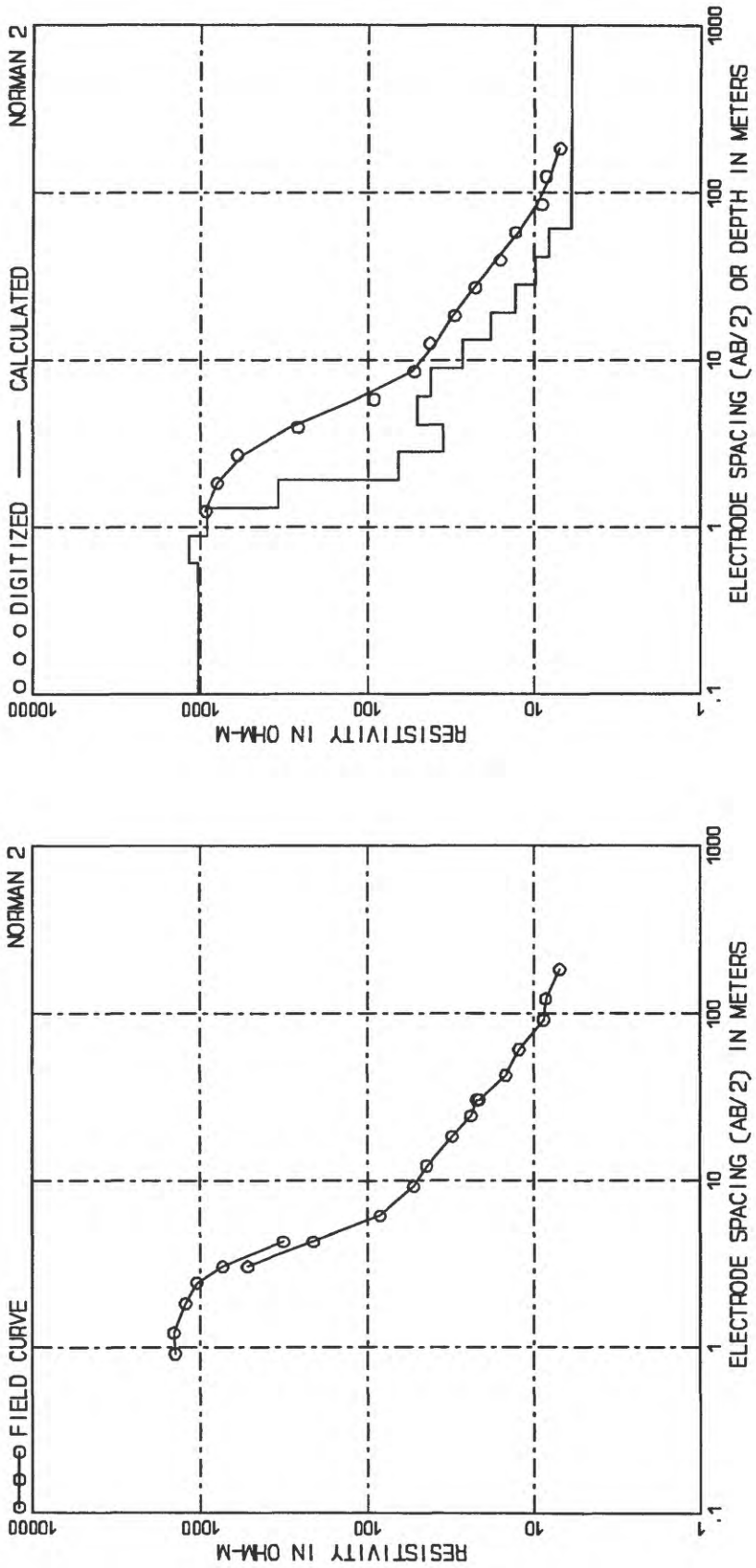

Figure A22. DC Resistivity sounding Norman 16 and interpretation.

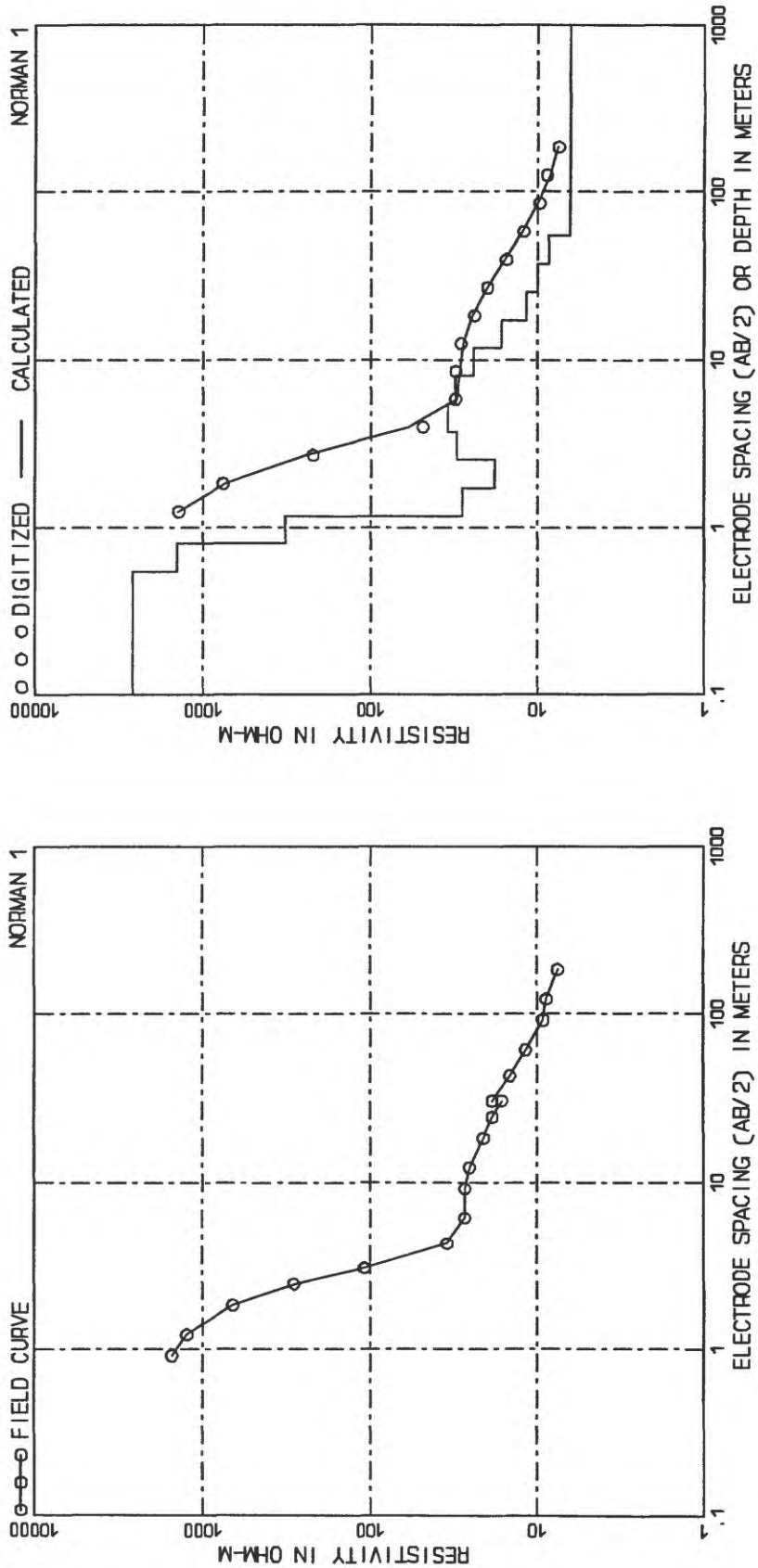

DEPTH, m (ft)	RESIS.	DEPTH, m (ft)	RESIS.
0.54 (1.79)	2602.29	8.00 (26.24)	31.17
0.80 (1.62)	1431.73	11.74 (38.52)	24.10
1.17 (3.85)	323.40	17.23 (56.54)	16.43
1.72 (5.65)	28.38	25.30 (82.99)	11.67
2.53 (8.30)	17.98	37.13 (121.81)	10.05
3.71 (12.18)	10.58	54.50 (178.80)	8.57
5.45 (17.88)	34.76	99999.00 (99999.00)	6.40

AB/2, m (ft)	App. Res.	AB/2, m (ft)	App. Res.
0.91 (3.00)	1520.00	12.19 (40.00)	25.50
1.22 (4.00)	1240.00	18.29 (60.00)	21.00
1.83 (6.00)	660.00	24.38 (80.00)	18.50
2.44 (8.00)	285.00	30.48 (100.00)	16.30
3.05 (10.00)	107.00	42.67 (140.00)	14.50
4.27 (14.00)	34.50	60.96 (200.00)	11.70
6.10 (20.00)	27.00	91.44 (300.00)	9.20
9.14 (30.00)		121.92 (400.00)	8.80
		182.88 (600.00)	7.50

Figure A23. DC Resistivity sounding Norman 17 and interpretation.

Relative Coordinates of GPR Test Grid 1

STATION ID:

ExxSyyy - xx is meters east of test line 1, yyy is meters south of test line 2

COORDINATES:

relative orthogonal in meters

ID	X	Y	Z
E00S300	-0.000	19.914	0.280
E01S300	1.078	19.955	0.277
E02S300	2.008	20.004	0.256
E03S300	3.005	20.057	0.242
E04S300	4.016	20.063	0.227
E05S300	5.029	20.102	0.220
E06S300	5.986	20.128	0.216
E07S300	6.983	20.175	0.215
E08S300	7.972	20.180	0.212
E09S300	8.990	20.233	0.204
E10S300	10.003	20.257	0.194
E00S302	0.039	17.941	0.255
E01S302	1.103	17.980	0.312
E02S302	2.044	18.061	0.287
E03S302	3.069	18.053	0.266
E04S302	4.058	18.079	0.274
E05S302	5.029	18.132	0.271
E06S302	6.043	18.168	0.274
E07S302	7.045	18.184	0.302
E08S302	8.019	18.241	0.305
E09S302	9.009	18.287	0.288
E10S302	10.054	18.288	0.334
E00S304	0.040	15.965	0.177
E01S304	1.134	16.013	0.194
E02S304	2.035	16.032	0.218
E03S304	3.067	16.020	0.252
E04S304	4.049	16.074	0.276
E05S304	5.026	16.118	0.320
E06S304	6.085	16.152	0.363
E07S304	7.040	16.174	0.413
E08S304	8.092	16.271	0.467
E09S304	9.018	16.250	0.431
E10S304	10.022	16.197	0.398
E00S306	0.018	13.943	0.158
E01S306	1.177	13.997	0.207
E02S306	2.063	14.031	0.228
E03S306	3.092	14.034	0.251
E04S306	4.015	14.092	0.303
E05S306	5.059	14.149	0.366
E06S306	6.054	14.140	0.419
E07S306	7.059	14.161	0.460
E08S306	8.070	14.236	0.551
E09S306	9.044	14.250	0.520
E10S306	10.039	14.277	0.473

ID	X	Y	Z
E00S308	-0.024	11.991	0.279
E01S308	1.217	12.010	0.272
E02S308	2.105	12.000	0.272
E03S308	3.117	12.041	0.289
E04S308	4.113	12.086	0.359
E05S308	5.082	12.113	0.438
E06S308	6.116	12.155	0.610
E07S308	7.096	12.197	0.542
E08S308	8.101	12.206	0.482
E09S308	9.085	12.259	0.452
E10S308	10.048	12.293	0.418
E00S310	-0.052	9.963	0.188
E01S310	1.226	9.990	0.297
E02S310	2.132	10.043	0.429
E03S310	3.210	10.040	0.391
E04S310	4.145	10.088	0.359
E05S310	5.144	10.111	0.399
E06S310	6.083	10.194	0.401
E07S310	7.111	10.188	0.404
E08S310	8.087	10.216	0.407
E09S310	9.082	10.262	0.420
E10S310	10.031	10.300	0.397
E00S312	0.015	7.974	0.082
E01S312	1.215	8.018	0.189
E02S312	2.087	8.058	0.250
E03S312	3.164	8.065	0.247
E04S312	4.166	8.075	0.277
E05S312	5.132	8.151	0.275
E06S312	6.111	8.189	0.238
E07S312	7.089	8.205	0.206
E08S312	8.069	8.224	0.185
E09S312	9.103	8.295	0.204
E10S312	10.045	8.277	0.207
E00S314	-0.002	6.002	0.005
E01S314	1.244	6.051	0.076
E02S314	2.150	6.055	0.107
E03S314	3.230	6.085	0.153
E04S314	4.164	6.079	0.166
E05S314	5.177	6.109	0.158
E06S314	6.125	6.183	0.155
E07S314	7.113	6.187	0.148
E08S314	8.084	6.222	0.119
E09S314	9.112	6.295	0.101
E10S314	10.088	6.328	0.084

ID	X	Y	Z
E00S316	0.010	4.032	-0.016
E01S316	1.272	4.021	-0.003
E02S316	2.148	4.048	0.014
E03S316	3.253	4.105	0.043
E04S316	4.184	4.082	0.063
E05S316	5.173	4.154	0.078
E06S316	6.156	4.216	0.085
E07S316	7.111	4.234	0.087
E08S316	8.102	4.247	0.085
E09S316	9.110	4.355	0.102
E10S316	10.091	4.335	0.224
E00S318	0.053	2.041	-0.042
E01S318	1.299	2.019	-0.022
E02S318	2.181	2.056	-0.008
E03S318	3.275	2.064	0.019
E04S318	4.208	2.109	0.043
E05S318	5.245	2.183	0.049
E06S318	6.194	2.196	0.069
E07S318	7.098	2.232	0.083
E08S318	8.141	2.261	0.103
E09S318	9.107	2.354	0.108
E10S318	10.136	2.329	0.143
E00S320	0.000	0.000	0.000
E01S320	1.284	0.048	0.012
E02S320	2.236	0.074	0.035
E03S320	3.246	0.116	0.053
E04S320	4.204	0.112	0.054
E05S320	5.269	0.129	0.112
E06S320	6.169	0.208	0.100
E07S320	7.118	0.231	0.163
E08S320	8.137	0.257	0.147
E09S320	9.118	0.302	0.171
E10S320	10.131	0.311	0.158

GPR Test Grid 1 Images

Ground penetrating radar data were collected along parallel profiles arranged as a grid. The figure below shows the relative positions and names of each profile. Figures A24 through A67 present gray-scale images of the GPR data from 300 MHz, 500 MHz, and 900 MHz GSSI antennas. The upper image in each figure shows the raw data as recorded to disk. The lower image, or images for the 900 MHz data, show the processed data (static background removed and static geometric correction applied). Only 500 MHz data were collected along lines 0N through 20N.

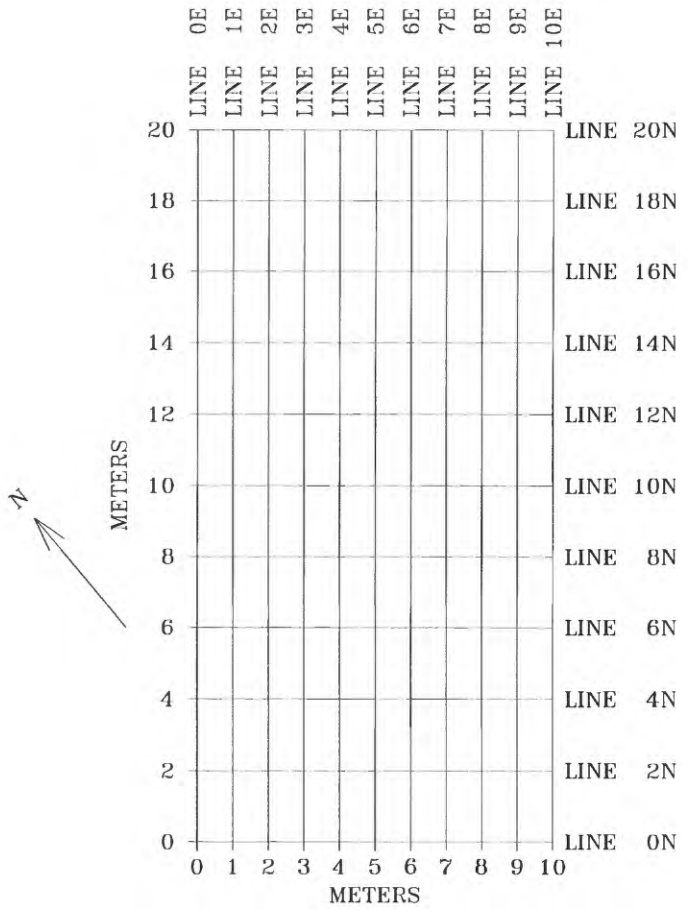

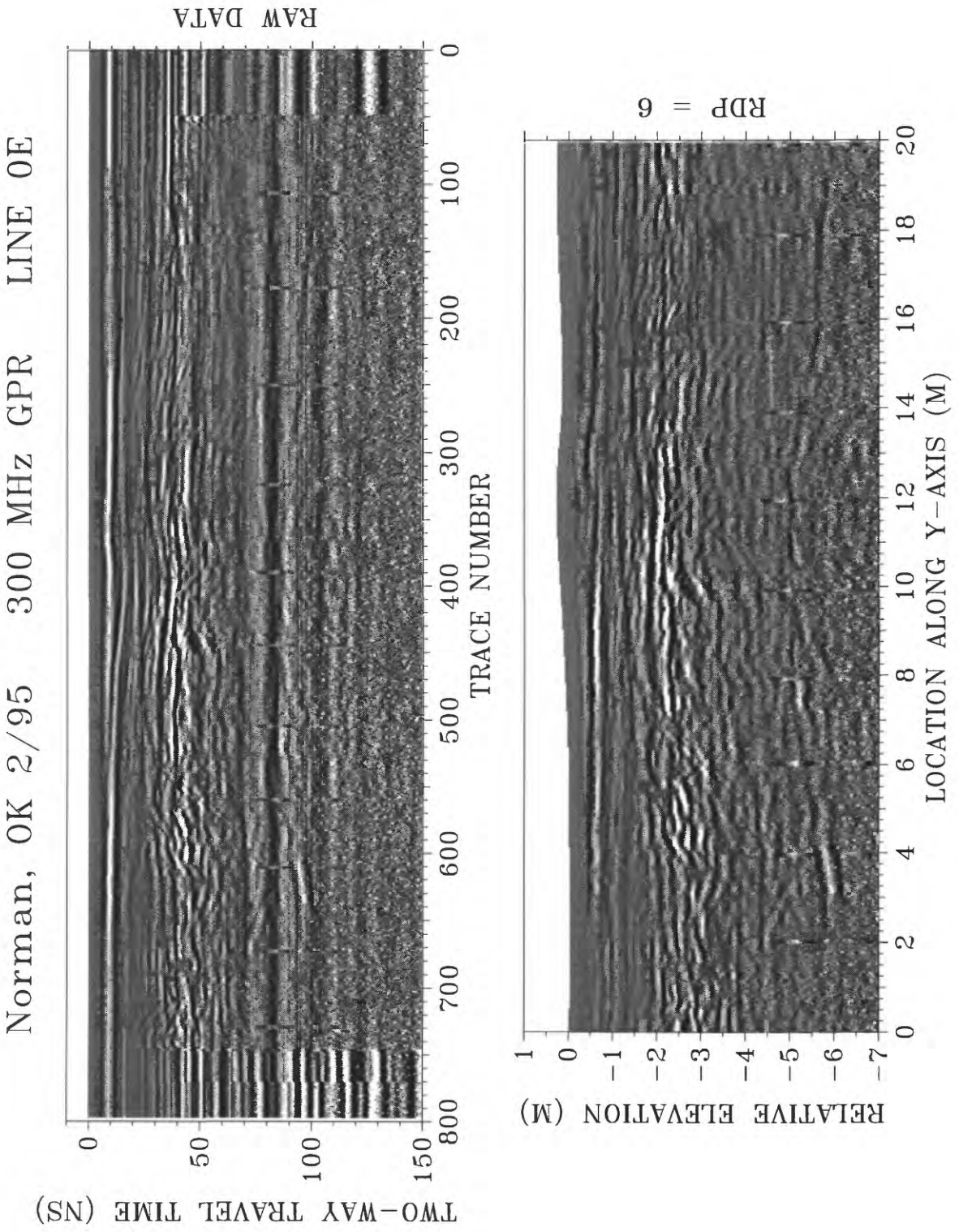

Figure A24. GPR images from 300 MHz antennas from Norman Landfill GPR test grid 1.

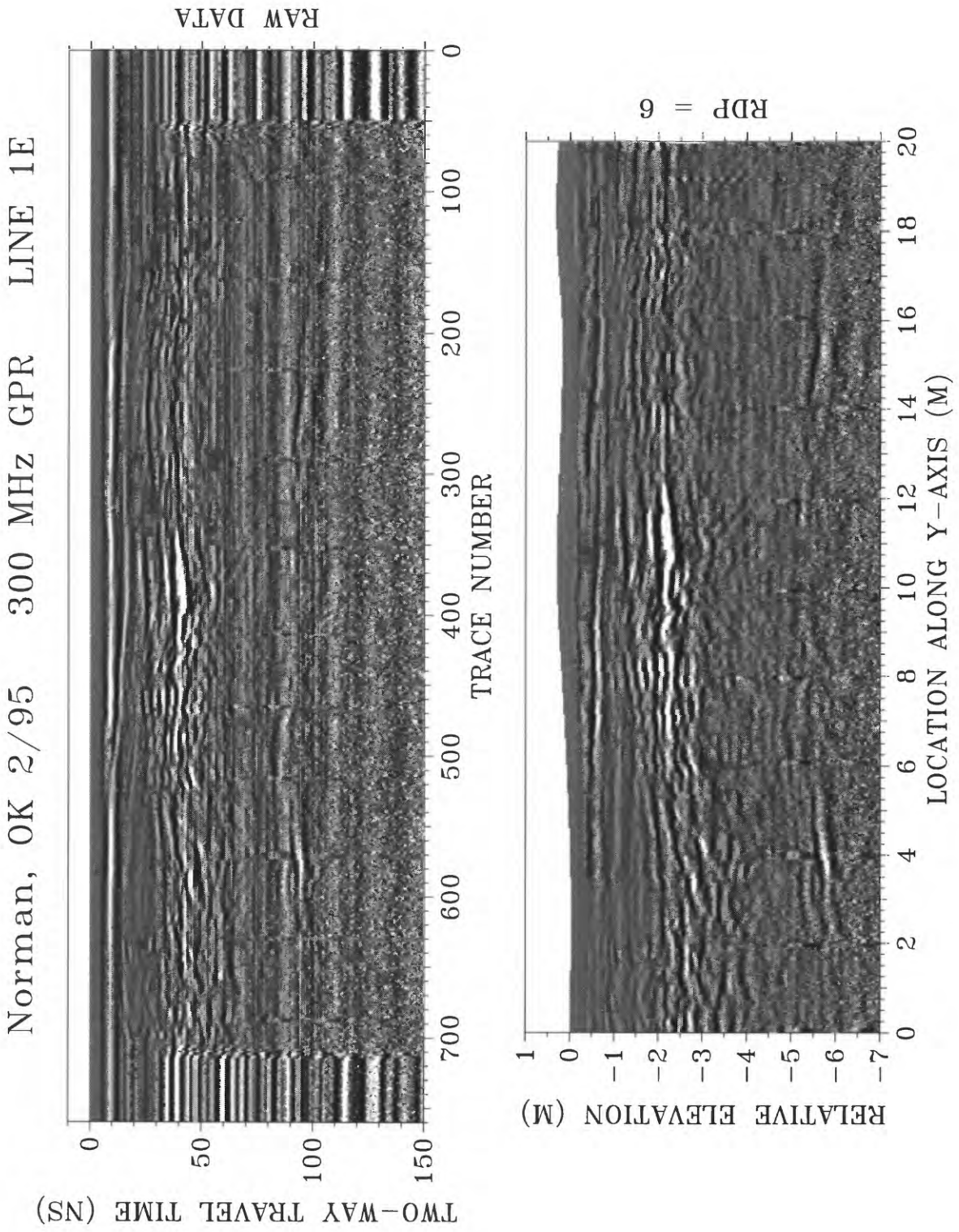

Figure A25. GPR images from 300 MHz antennas from Norman Landfill GPR test grid 1.

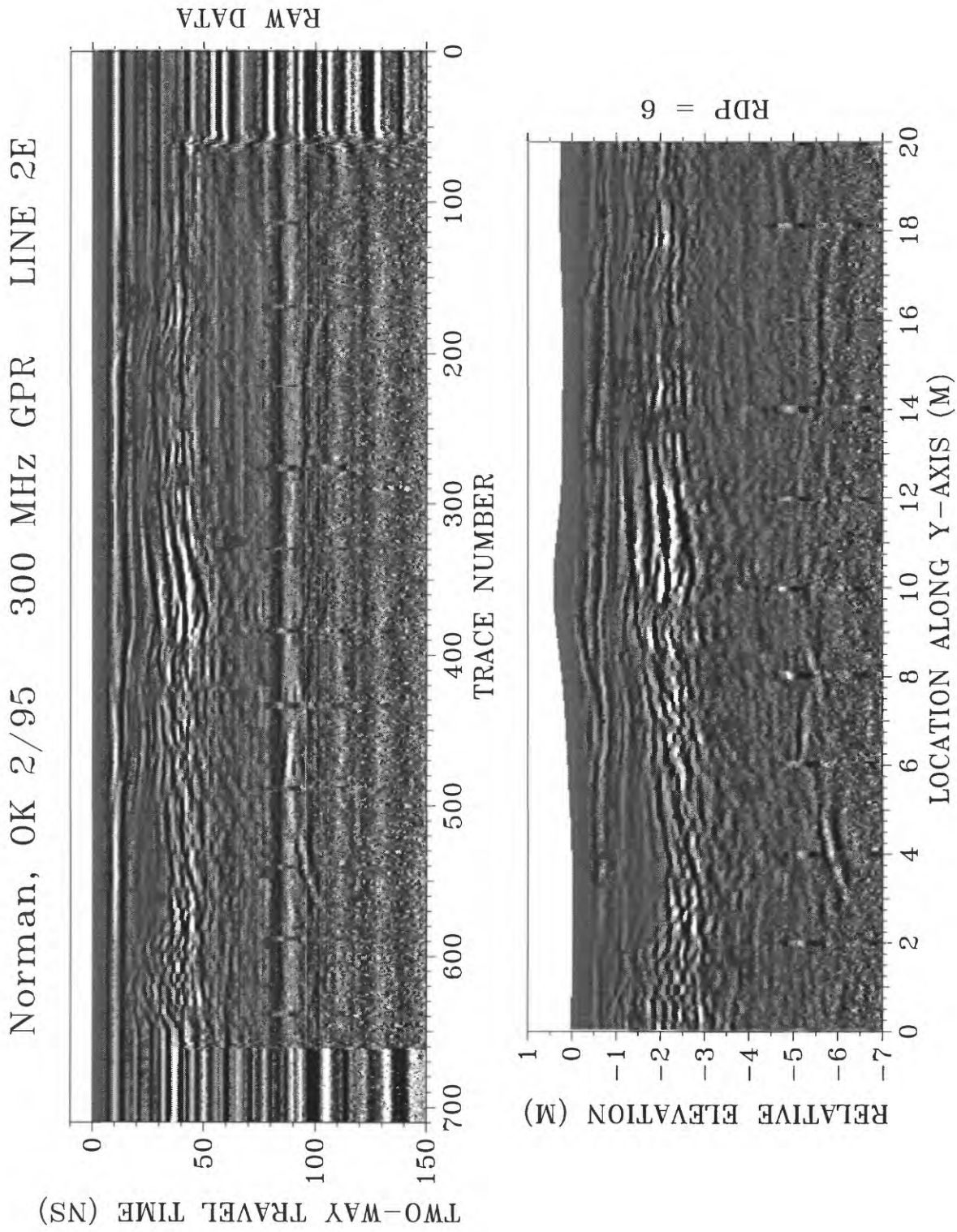

Figure A26. GPR images from 300 MHz antennas from Norman Landfill GPR test grid 1.

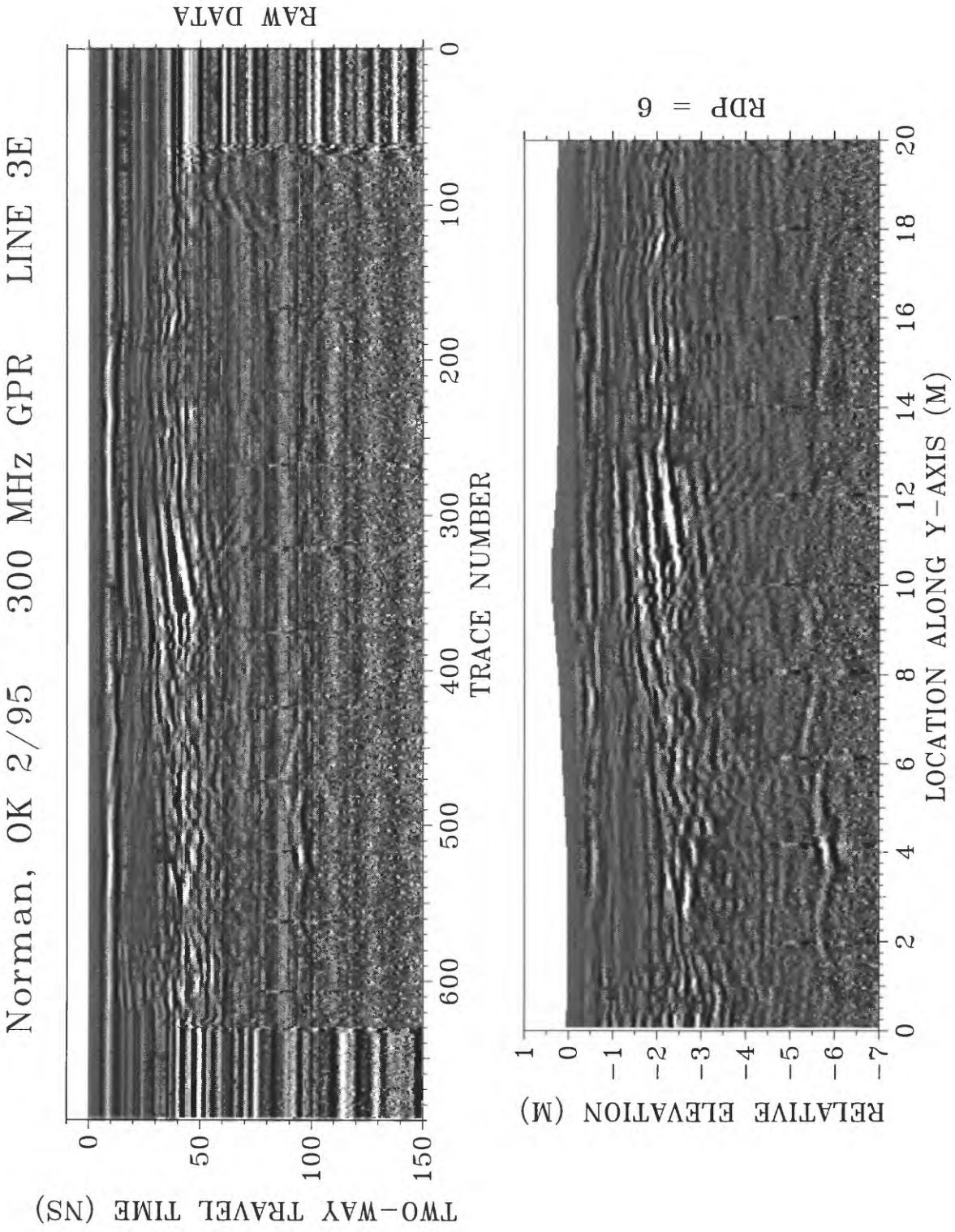

Figure A27. GPR images from 300 MHz antennas from Norman Landfill GPR test grid 1.

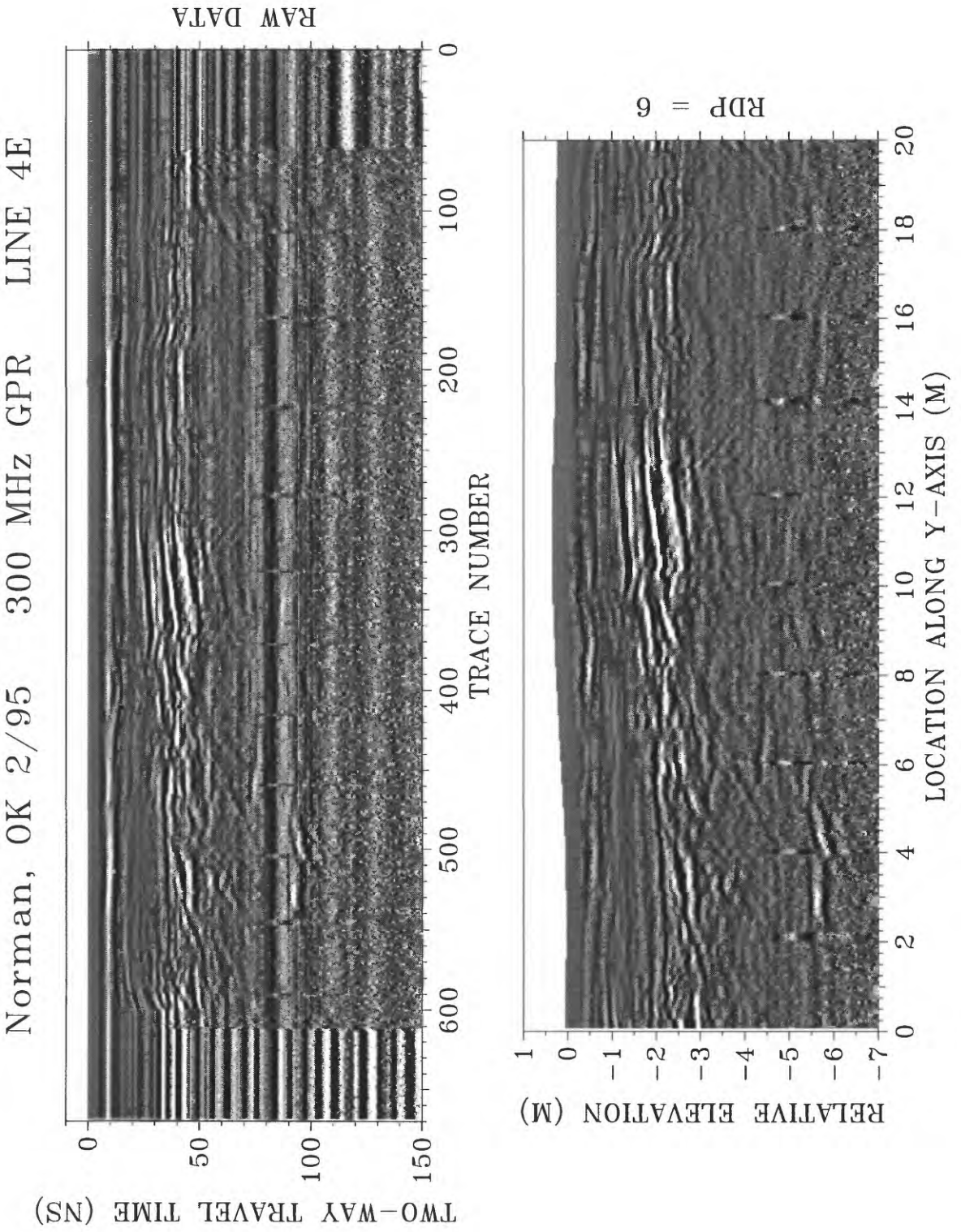

Figure A28. GPR images from 300 MHz antennas from Norman Landfill GPR test grid 1.

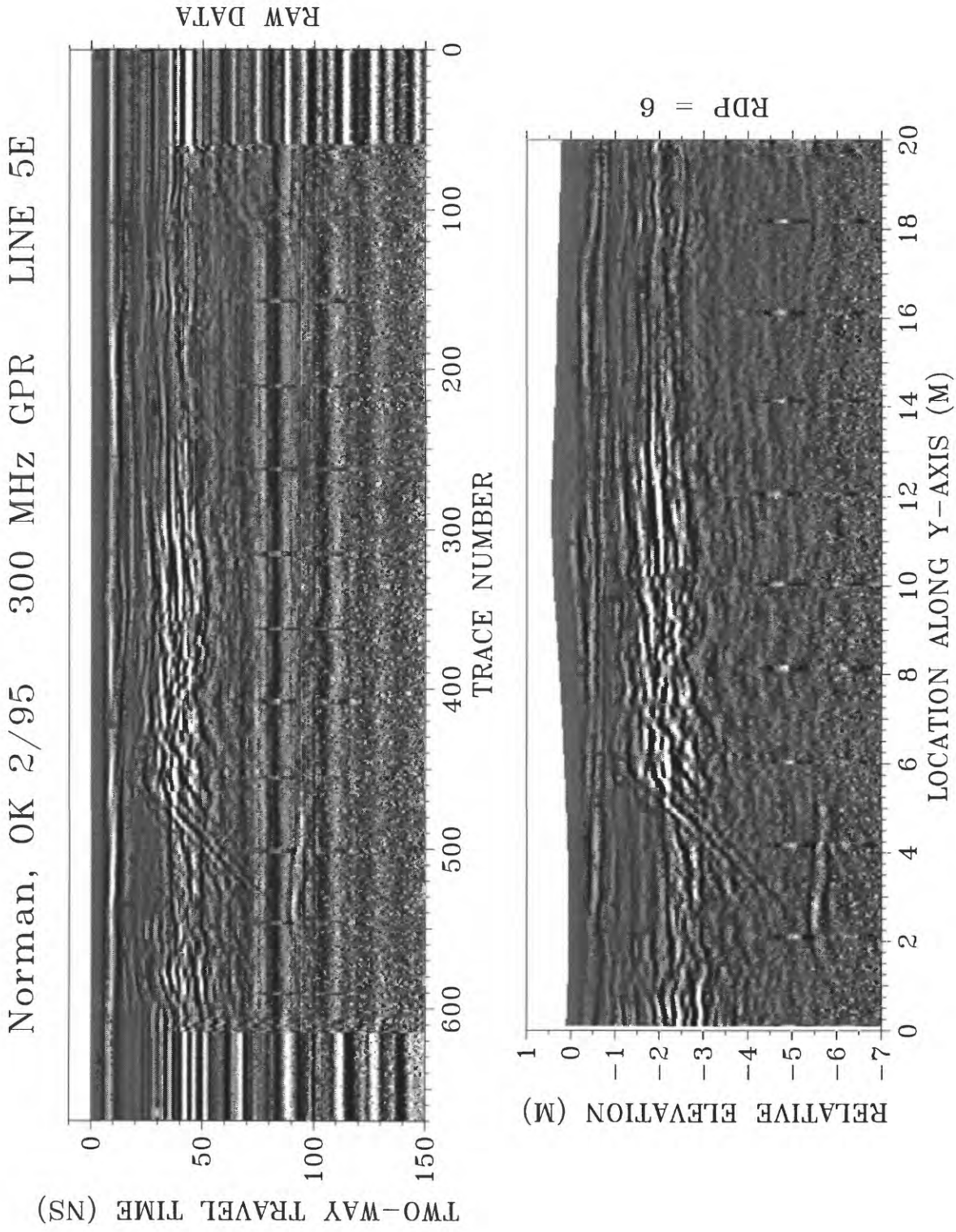

Figure A29. GPR images from 300 MHz antennas from Norman Landfill GPR test grid 1.

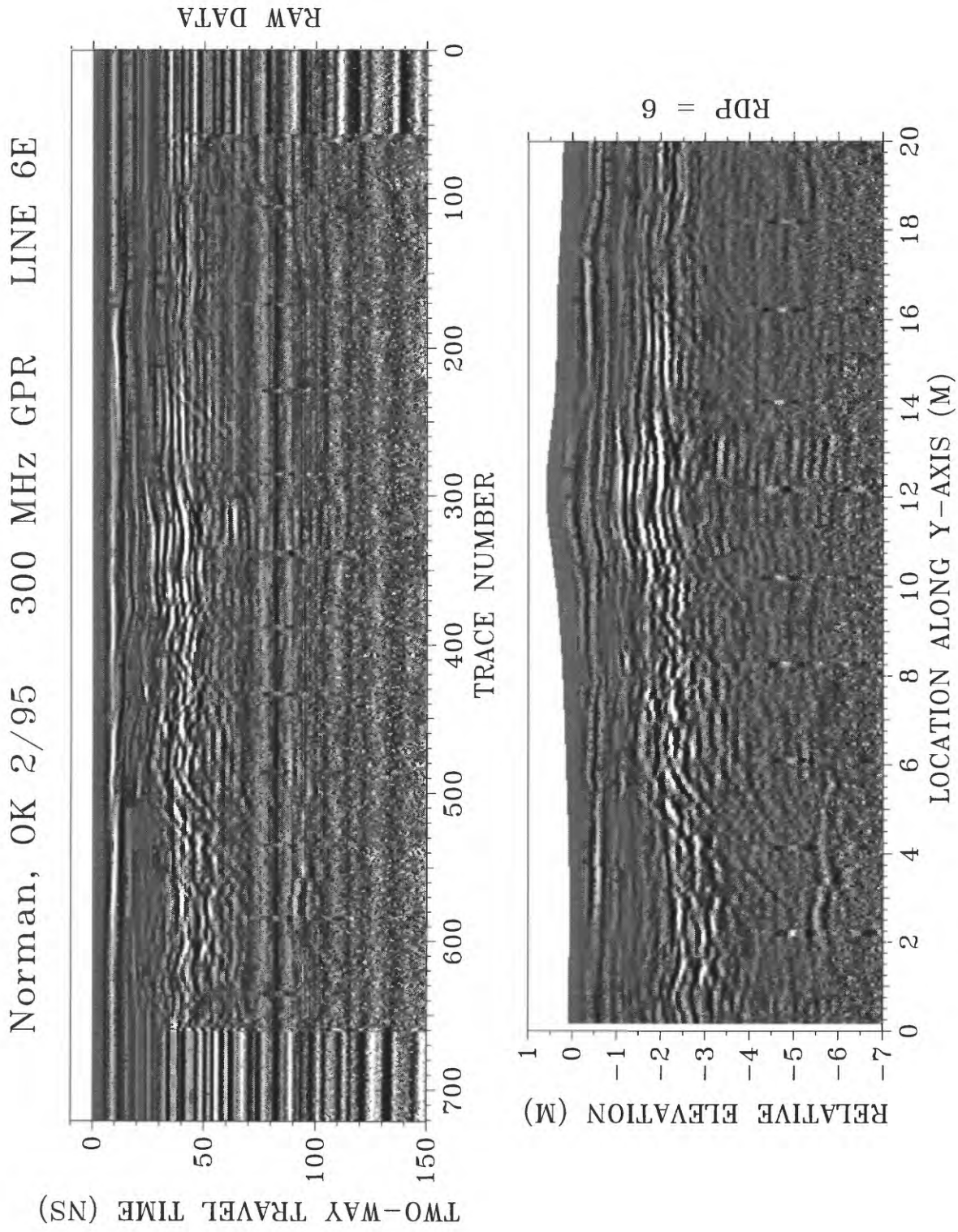

Figure A30. GPR images from 300 MHz antennas from Norman Landfill GPR test grid 1.

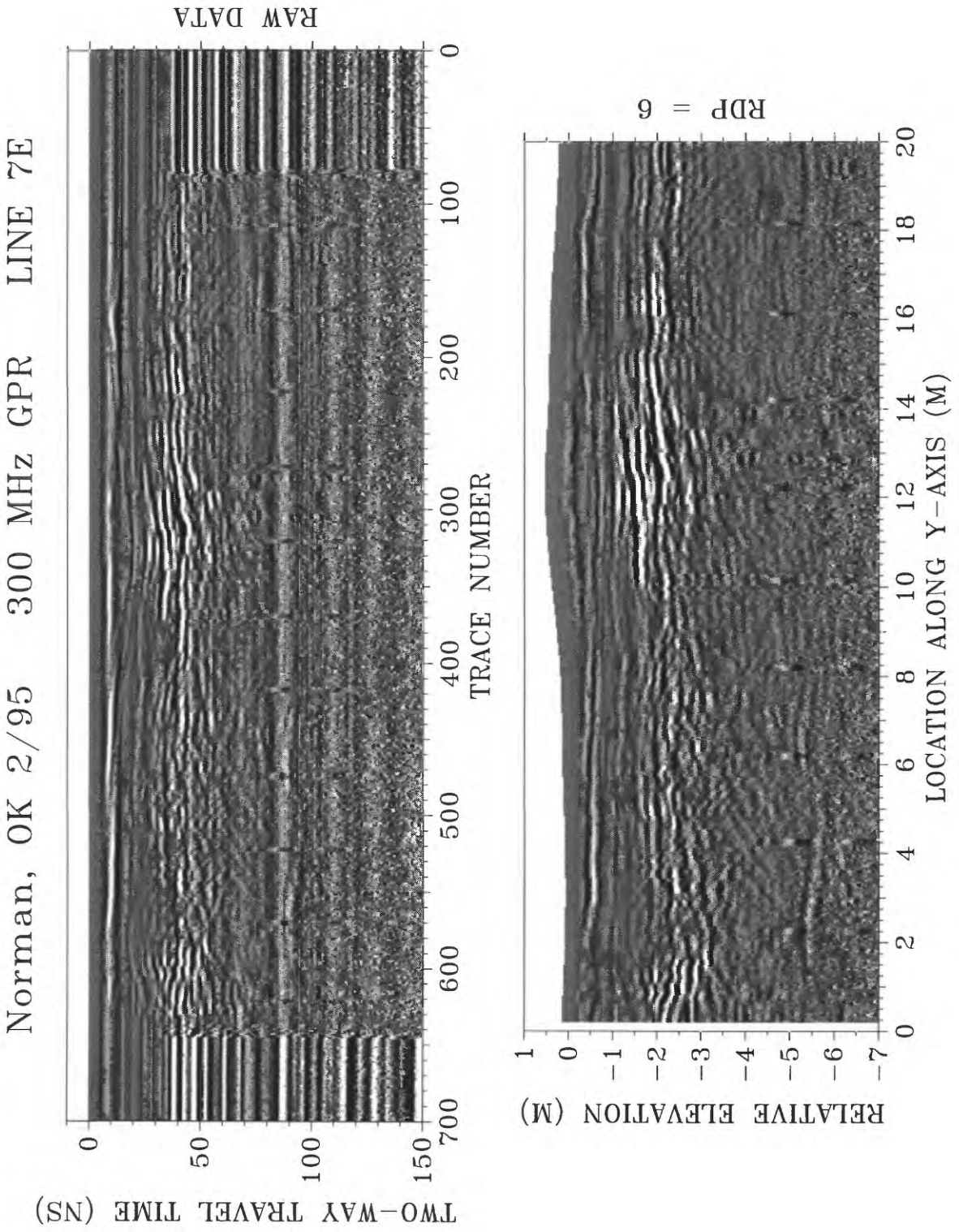

Figure A31. GPR images from 300 MHz antennas from Norman Landfill GPR test grid 1.

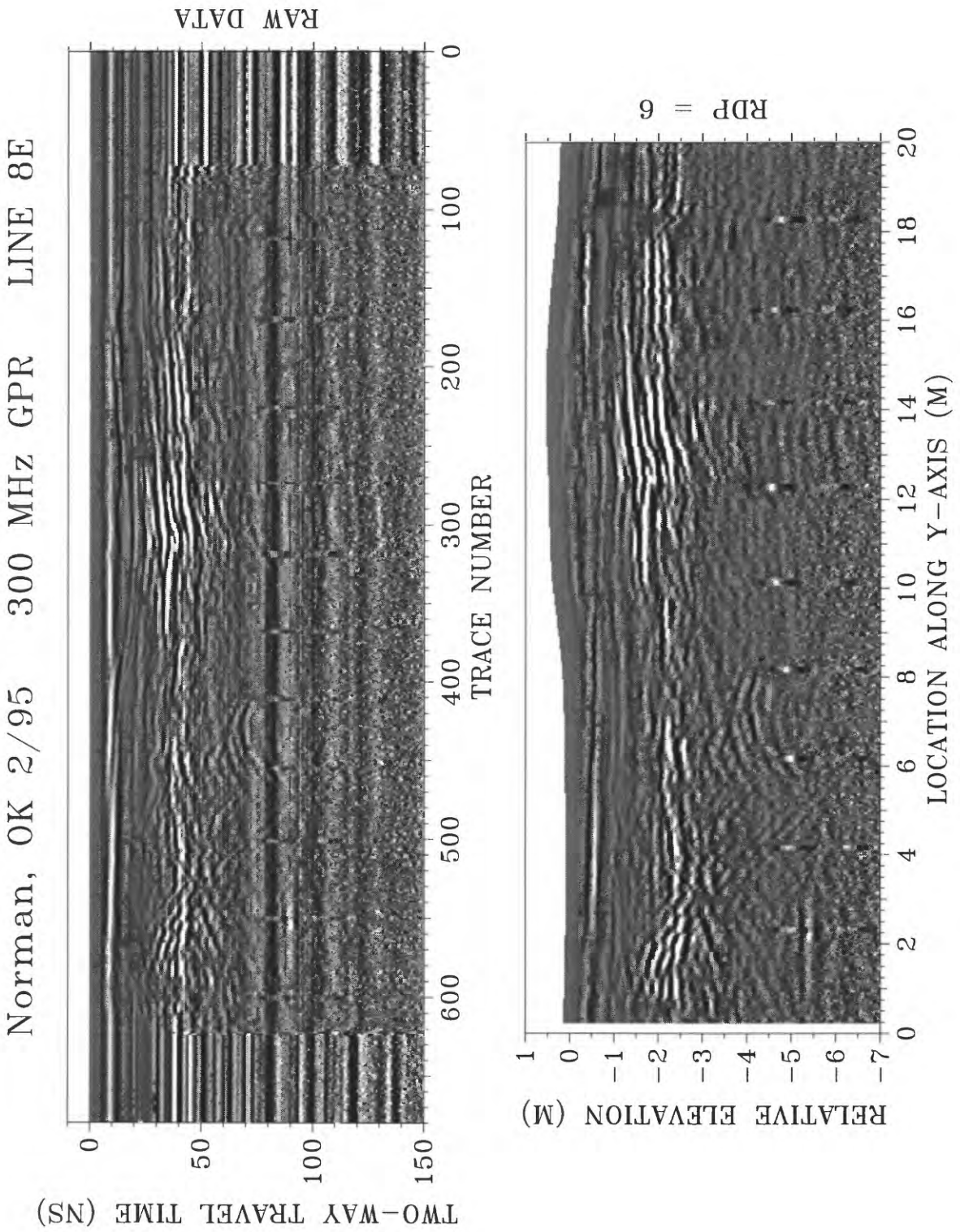

Figure A32. GPR images from 300 MHz antennas from Norman Landfill GPR test grid 1.

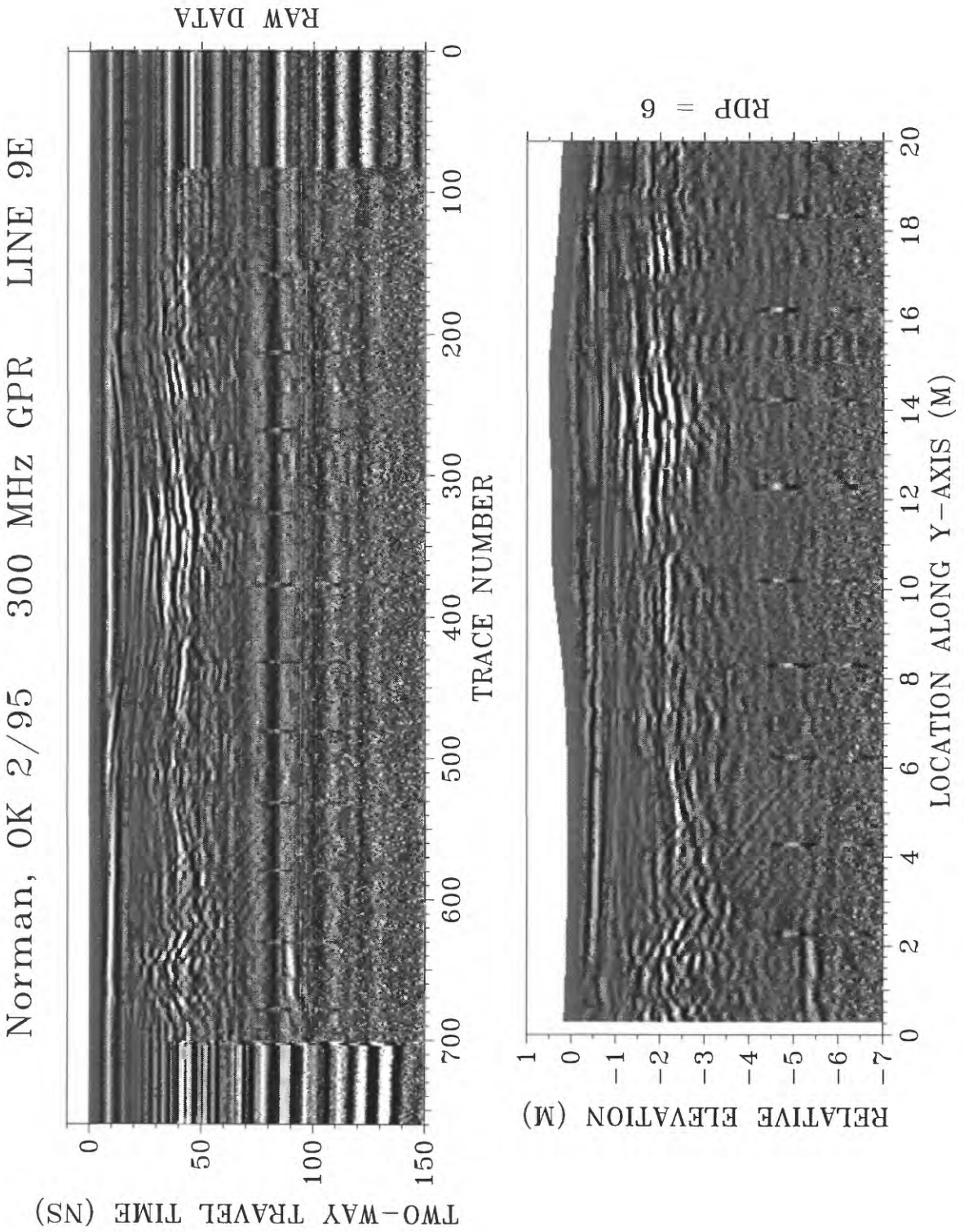

Figure A33. GPR images from 300 MHz antennas from Norman Landfill GPR test grid 1.

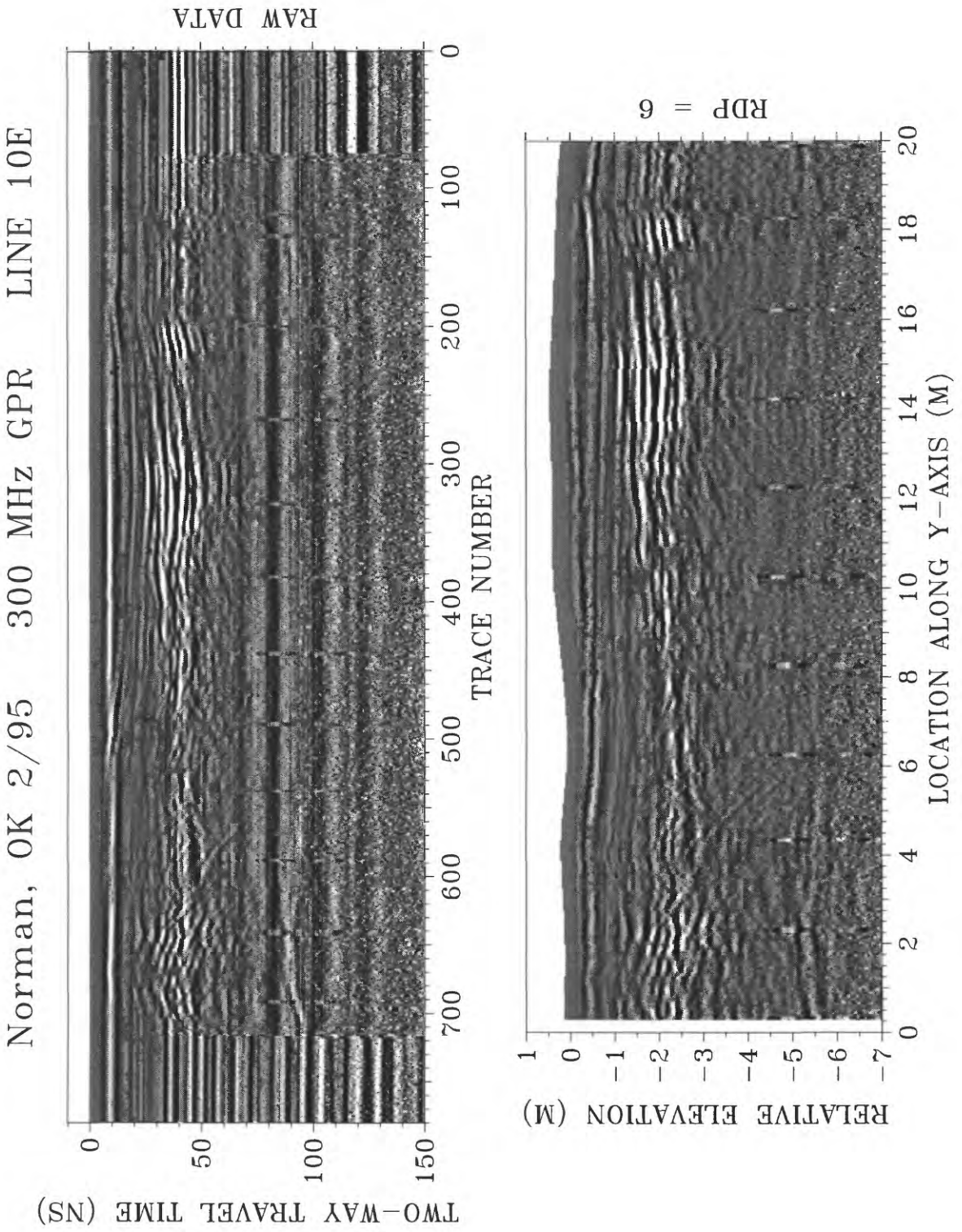

Figure A34. GPR images from 300 MHz antennas from Norman Landfill GPR test grid 1.

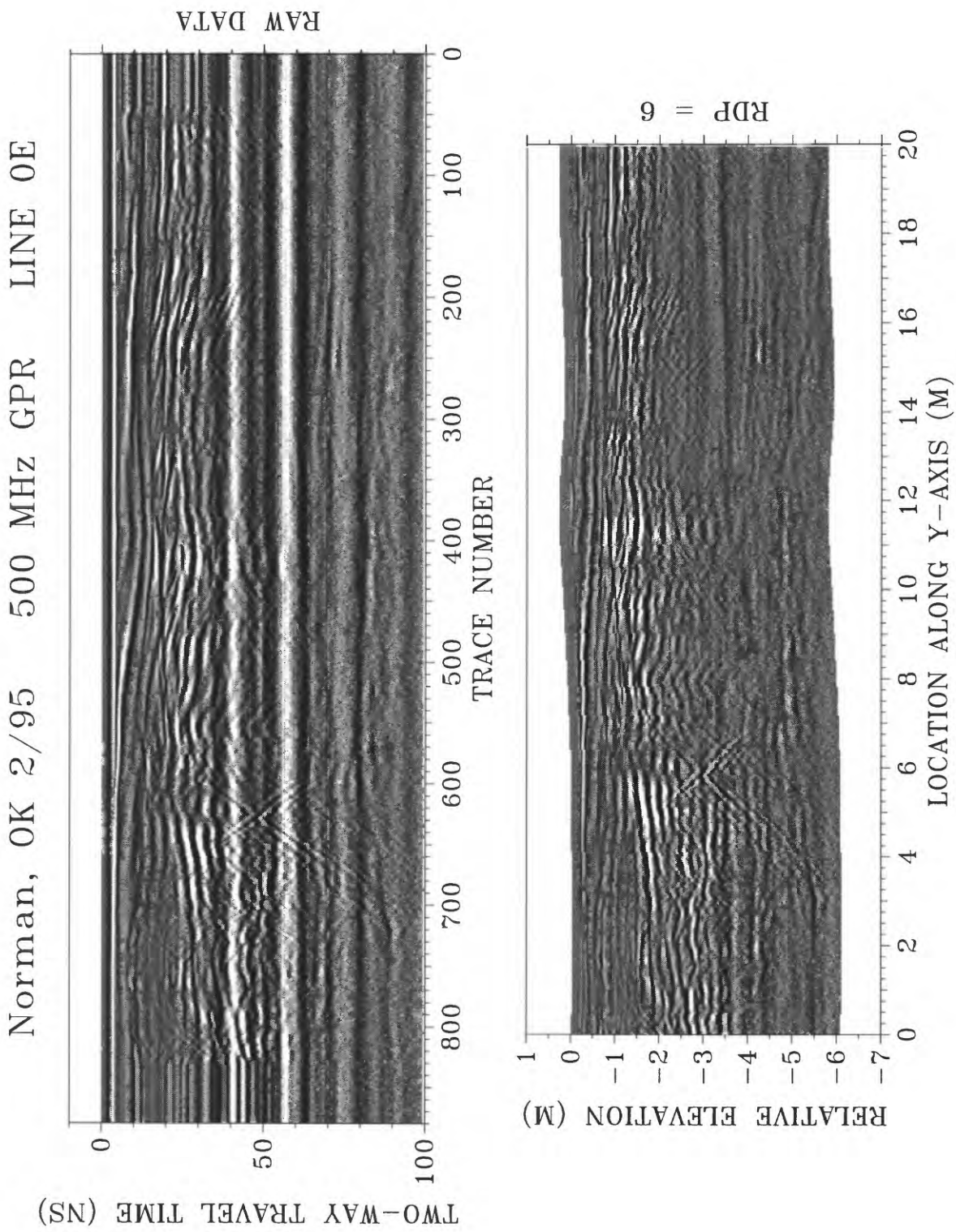

Figure A35. GPR images from 500 MHz antennas from Norman Landfill GPR test grid 1.

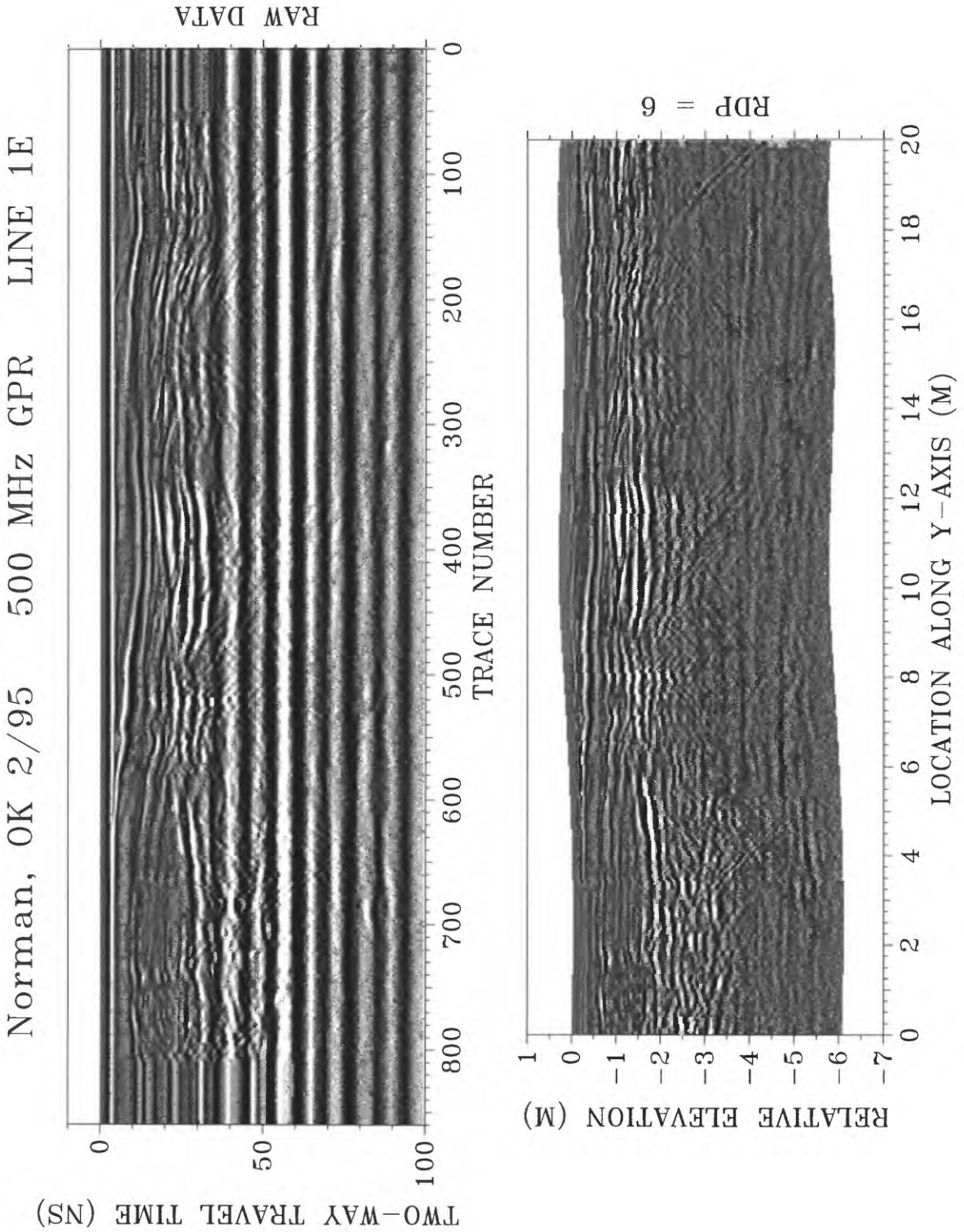

Figure A36. GPR images from 500 MHz antennas from Norman Landfill GPR test grid 1.

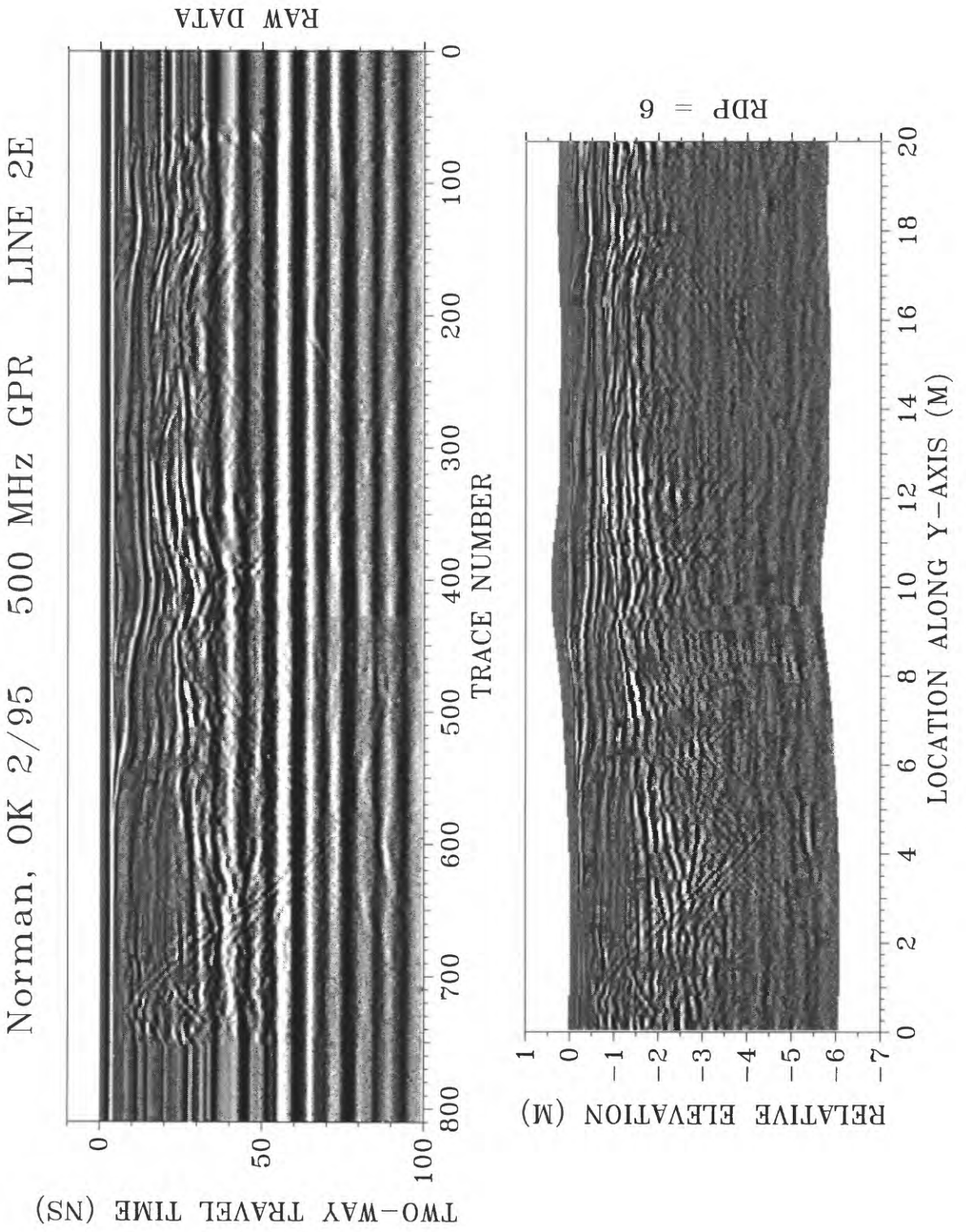

Figure A37. GPR images from 500 MHz antennas from Norman Landfill GPR test grid 1.

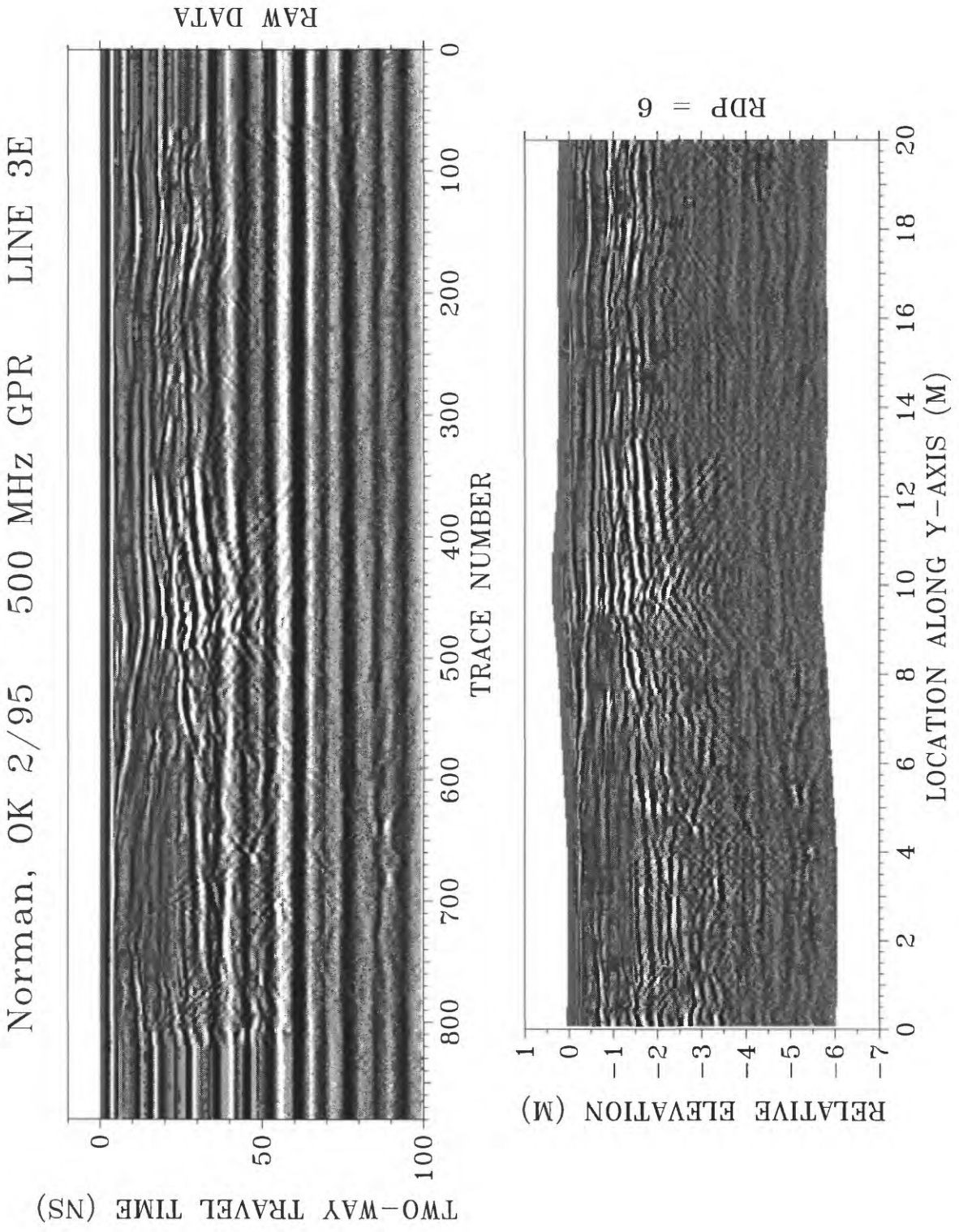

Figure A38. GPR images from 500 MHz antennas from Norman Landfill GPR test grid 1.

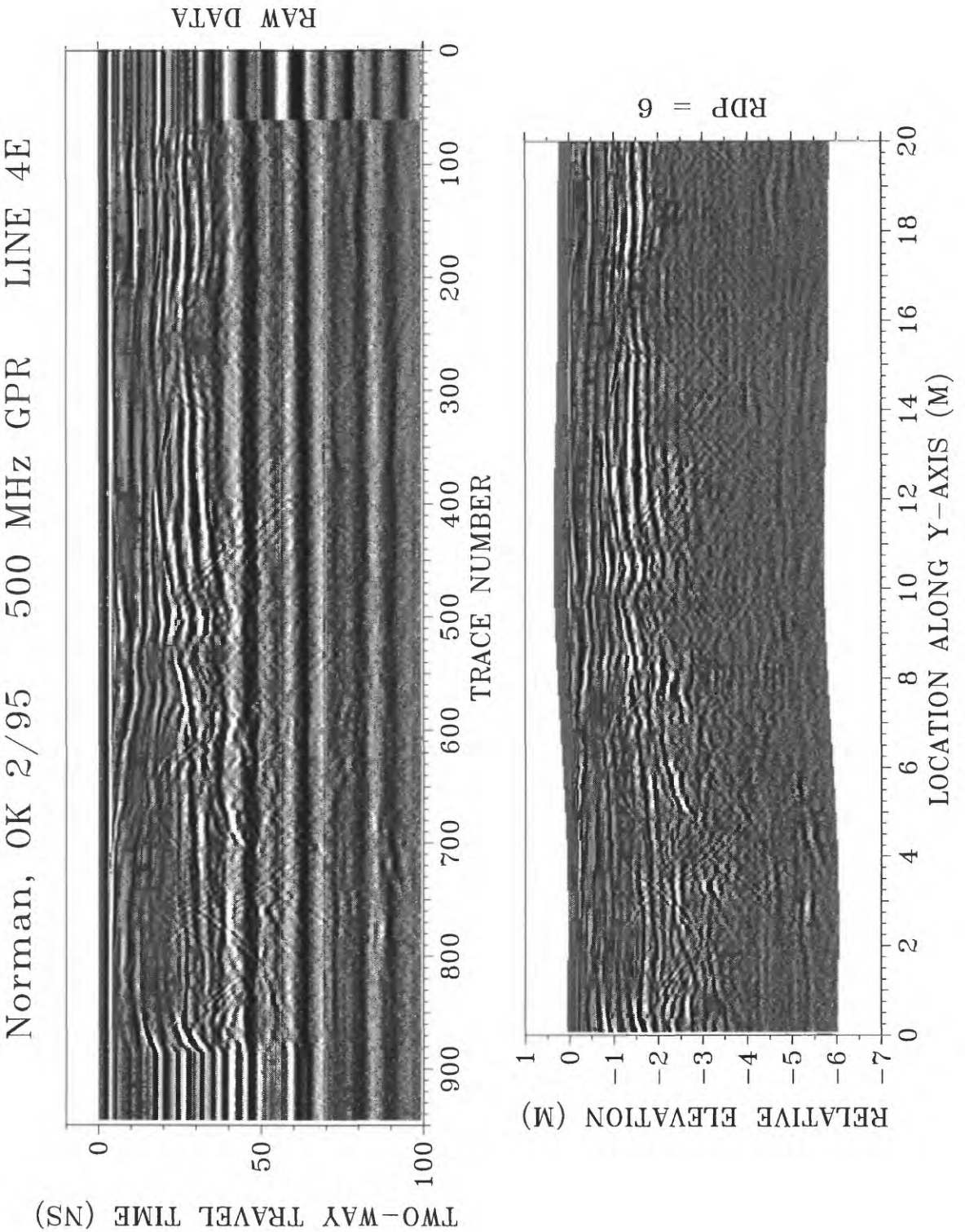

Figure A39. GPR images from 500 MHz antennas from Norman Landfill GPR test grid 1.

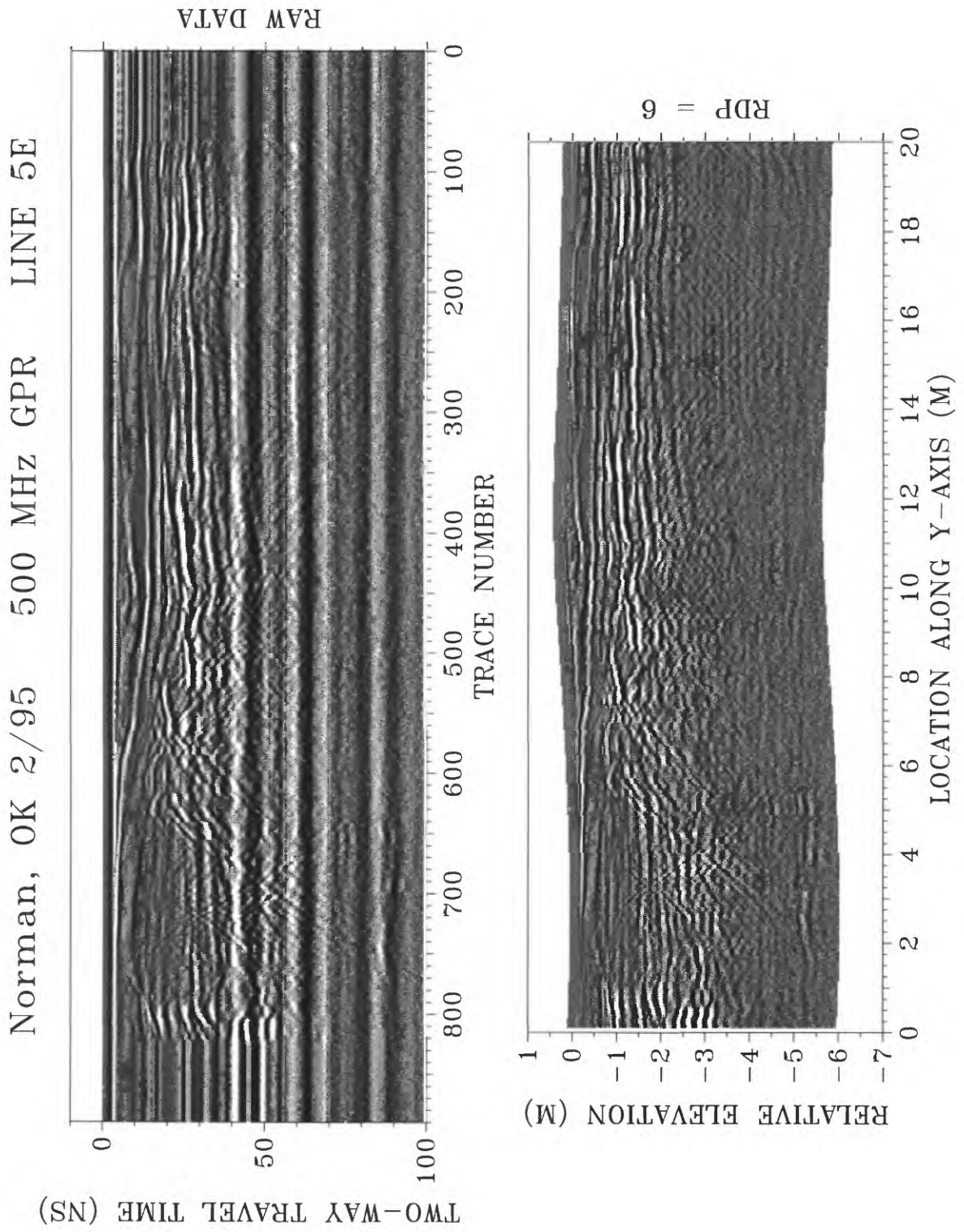

Figure A40. GPR images from 500 MHz antennas from Norman Landfill GPR test grid 1.

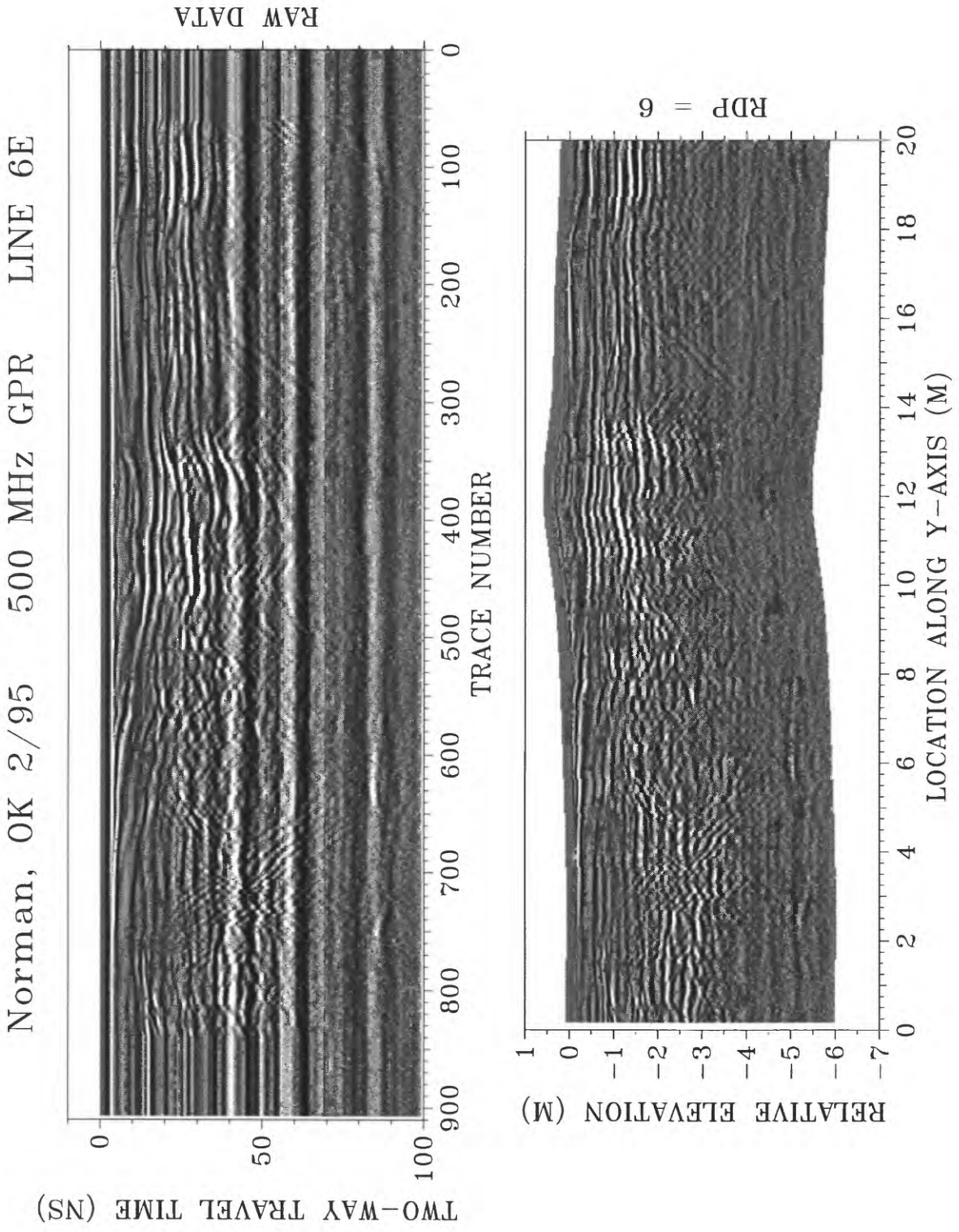

Figure A41. GPR images from 500 MHz antennas from Norman Landfill GPR test grid 1.

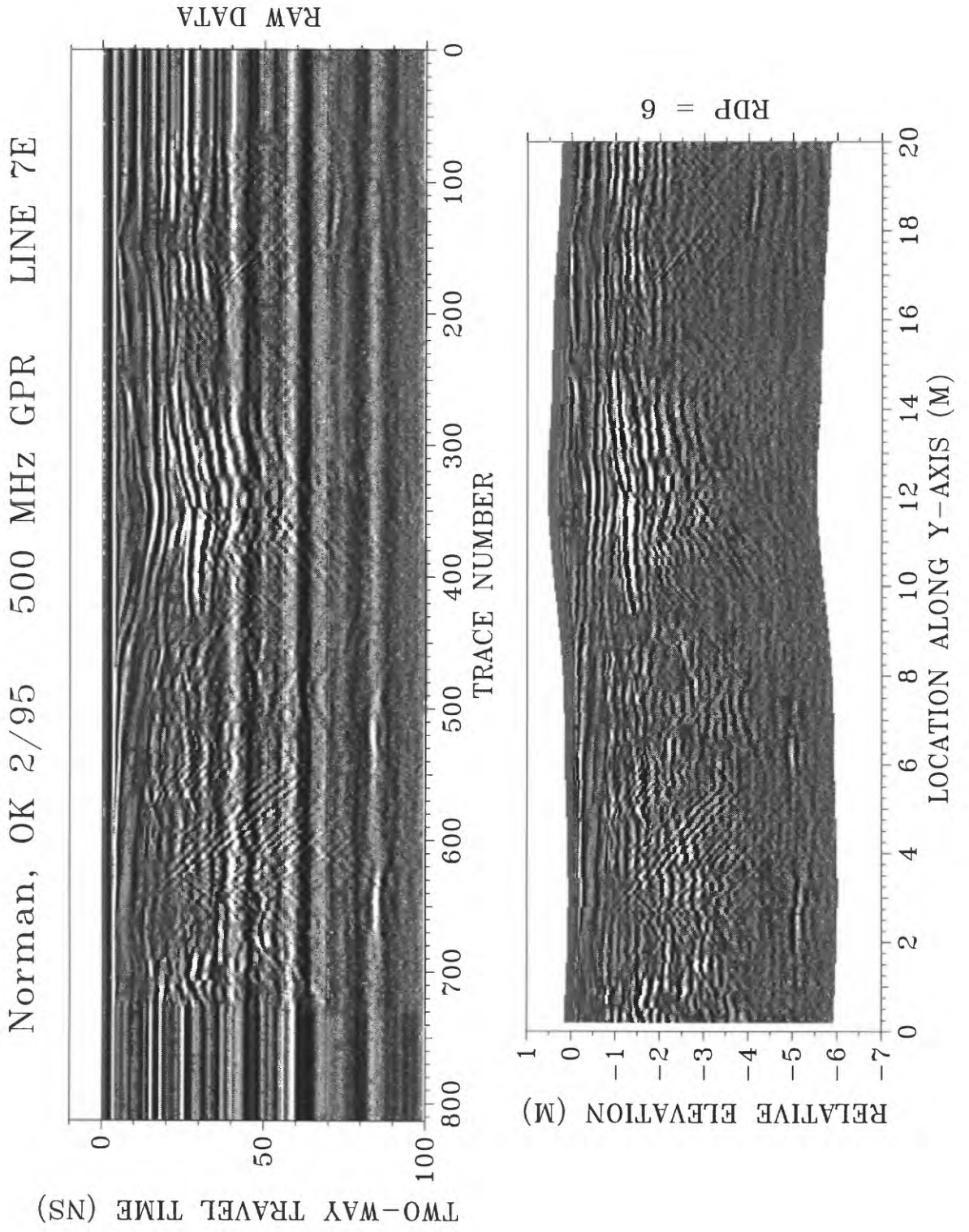

Figure A42. GPR images from 500 MHz antennas from Norman Landfill GPR test grid 1.

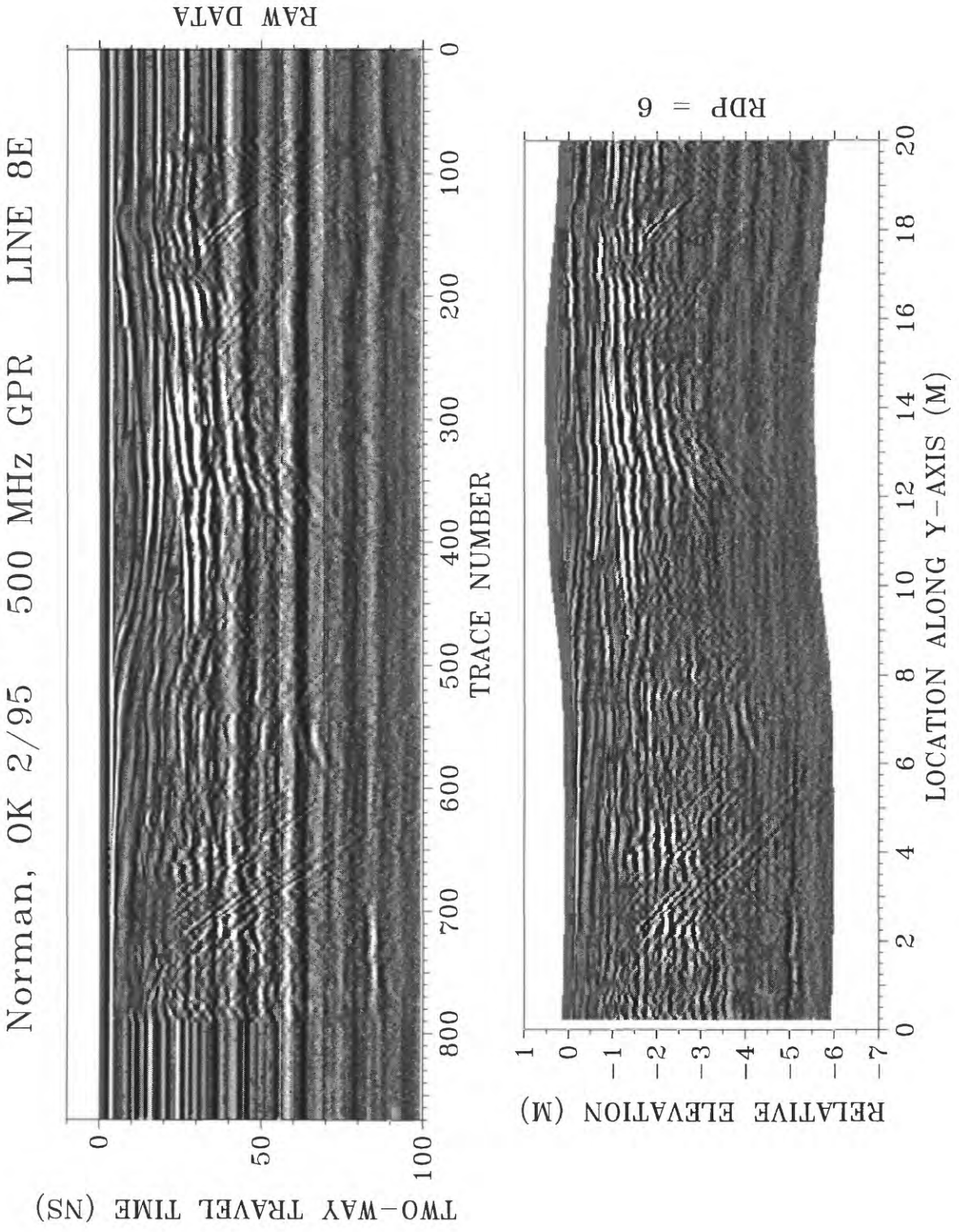

Figure A43. GPR images from 500 MHz antennas from Norman Landfill GPR test grid 1.

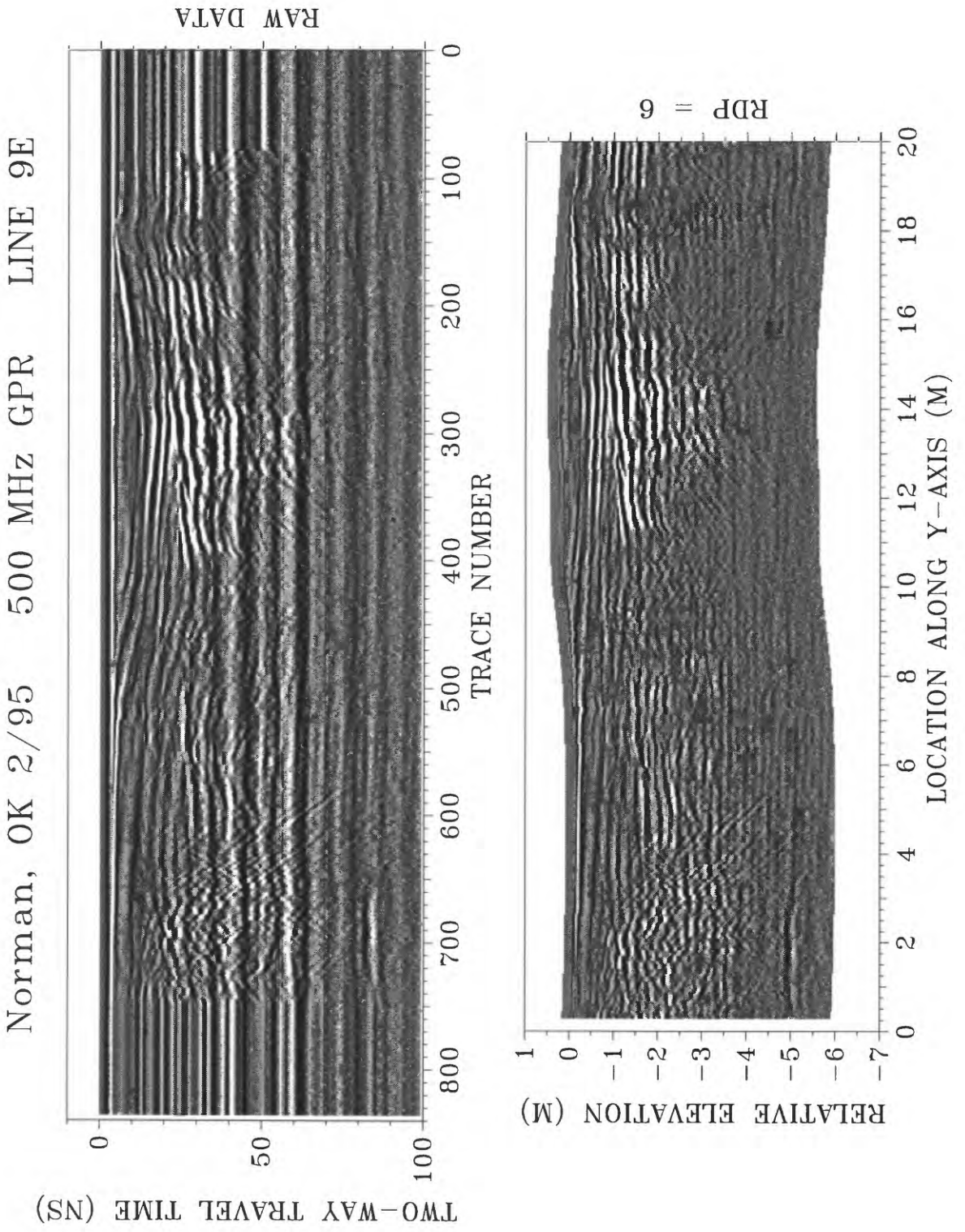

Figure A44. GPR images from 500 MHz antennas from Norman Landfill GPR test grid 1.

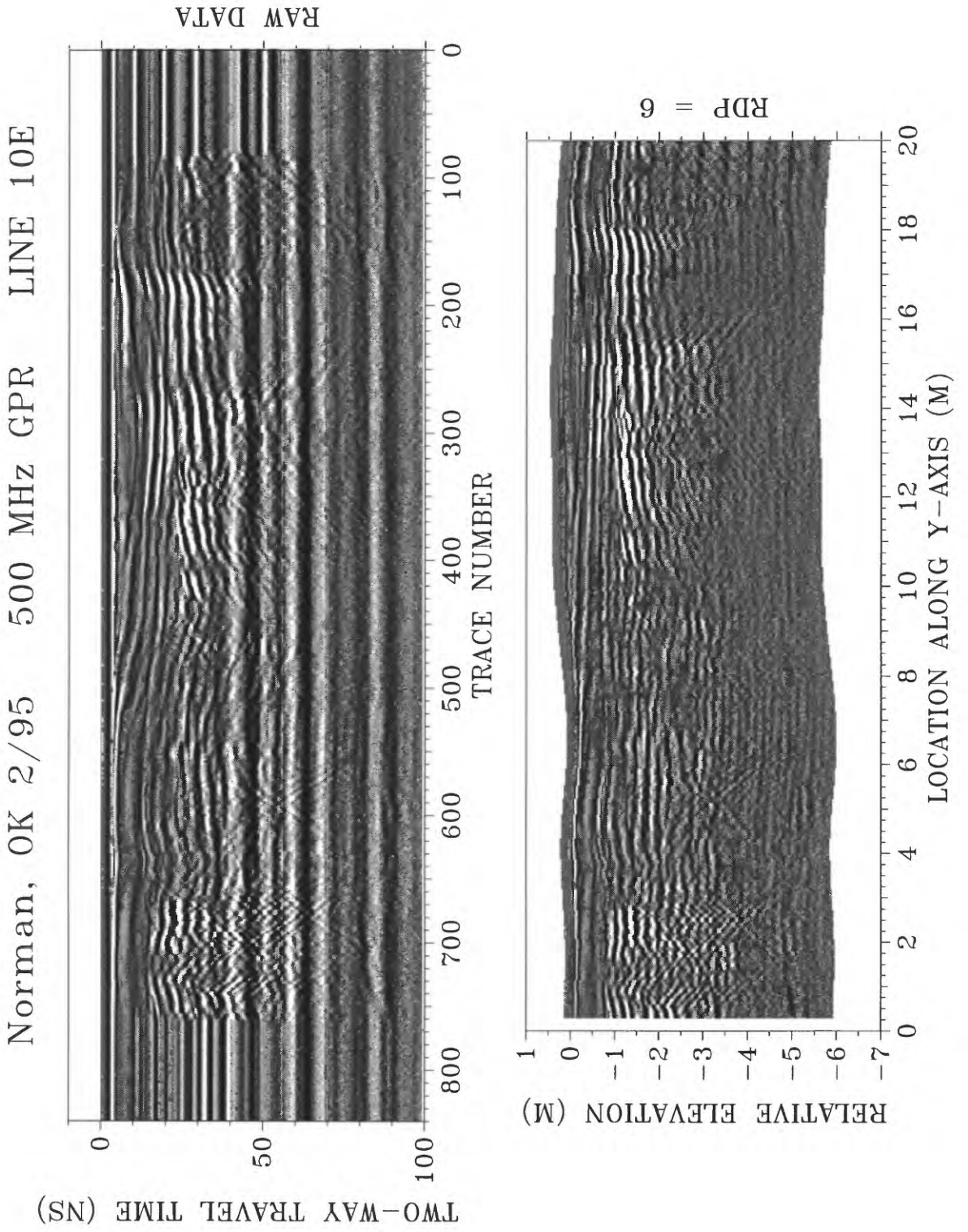

Figure A45. GPR images from 500 MHz antennas from Norman Landfill GPR test grid 1.

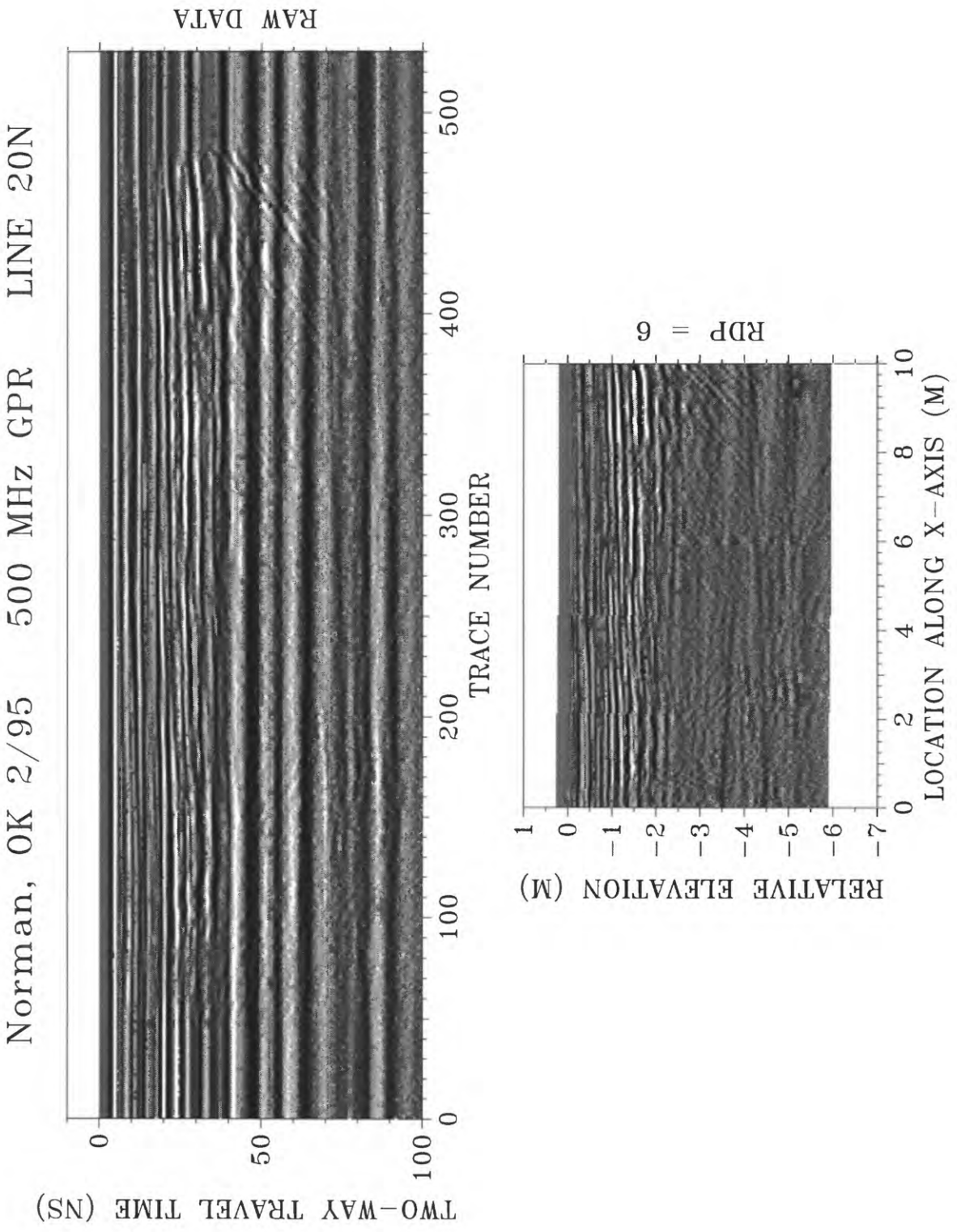

Figure A46. GPR images from 500 MHz antennas from Norman Landfill GPR test grid 1.

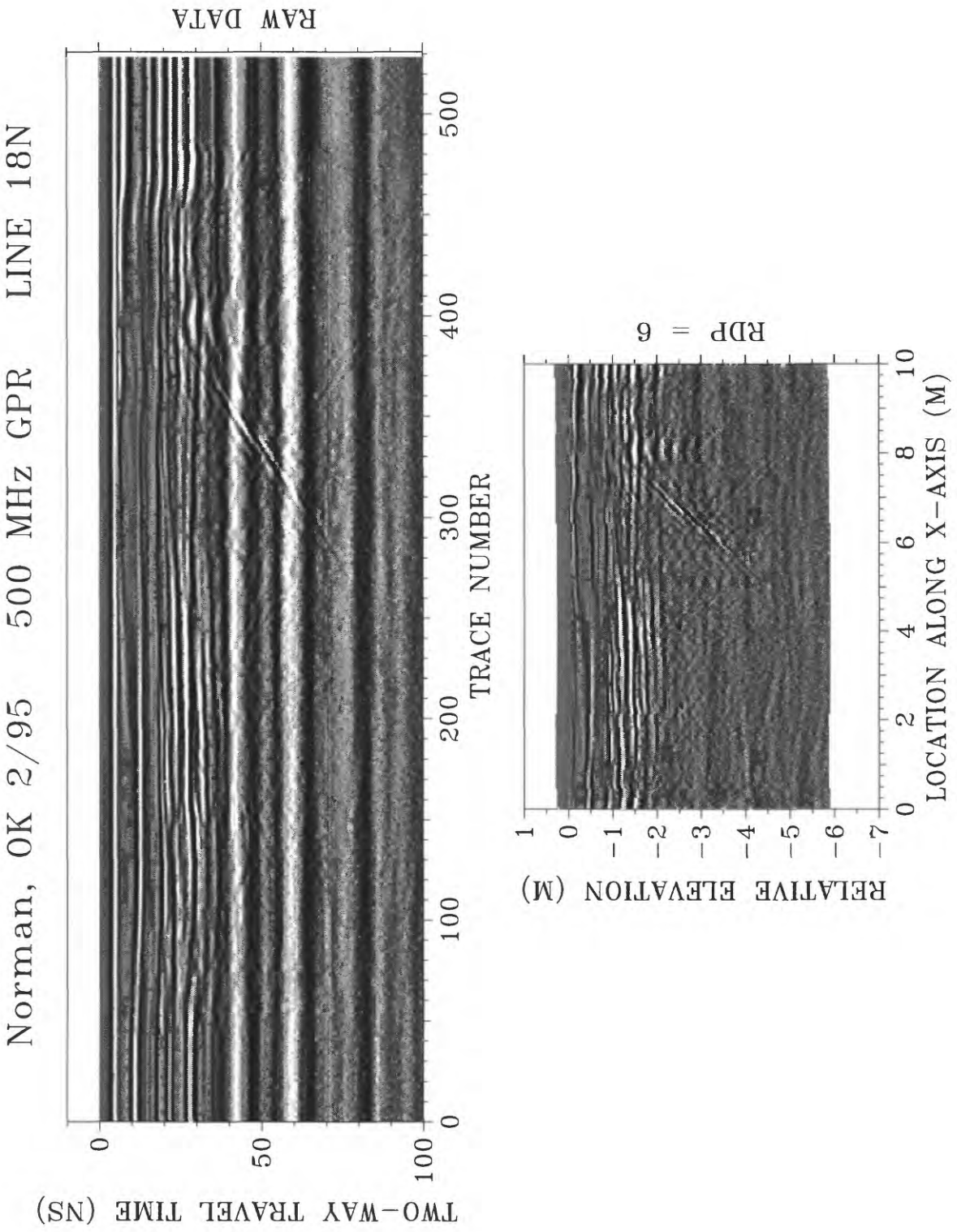

Figure A47. GPR images from 500 MHz antennas from Norman Landfill GPR test grid 1.

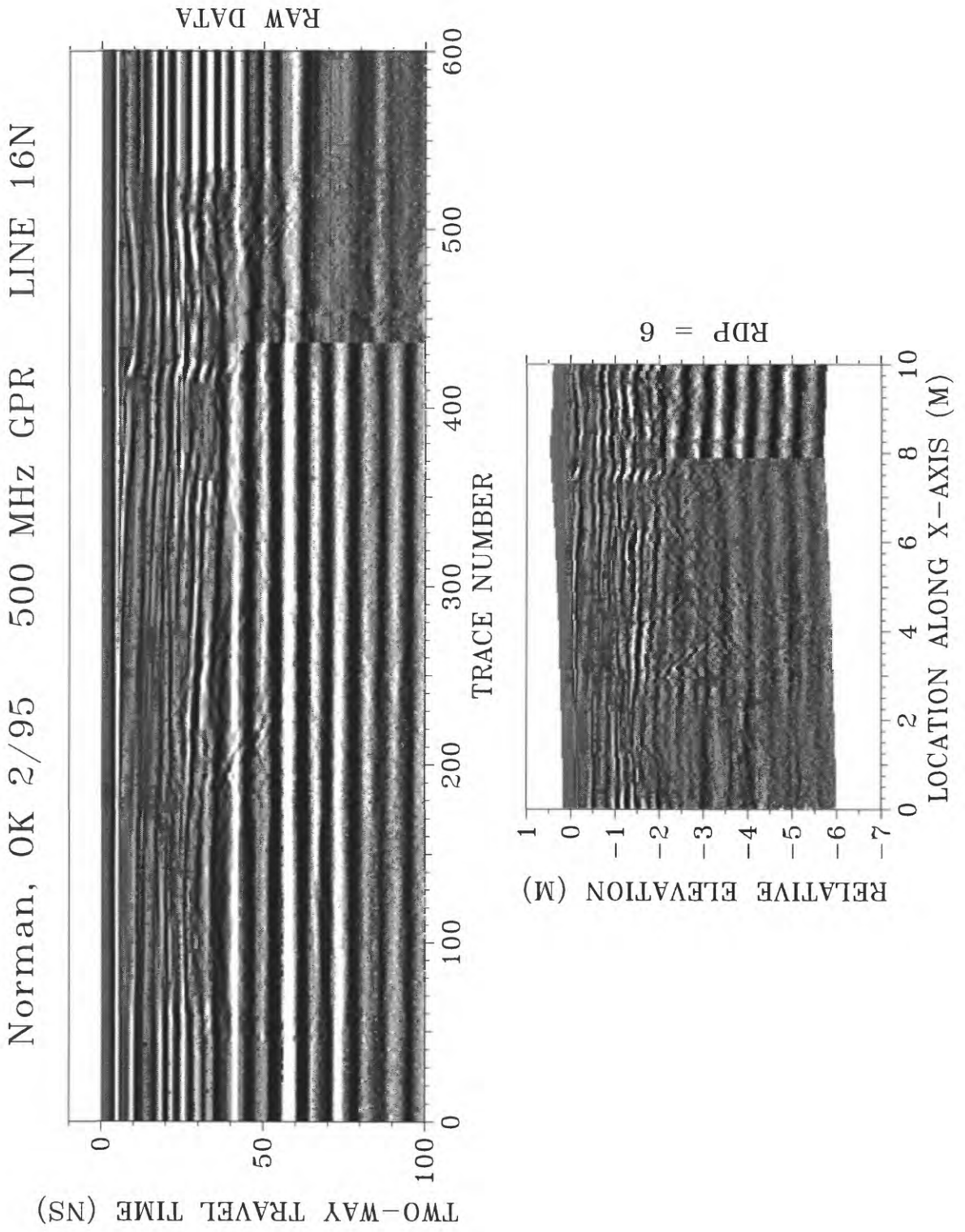

Figure A48. GPR images from 500 MHz antennas from Norman Landfill GPR test grid 1.

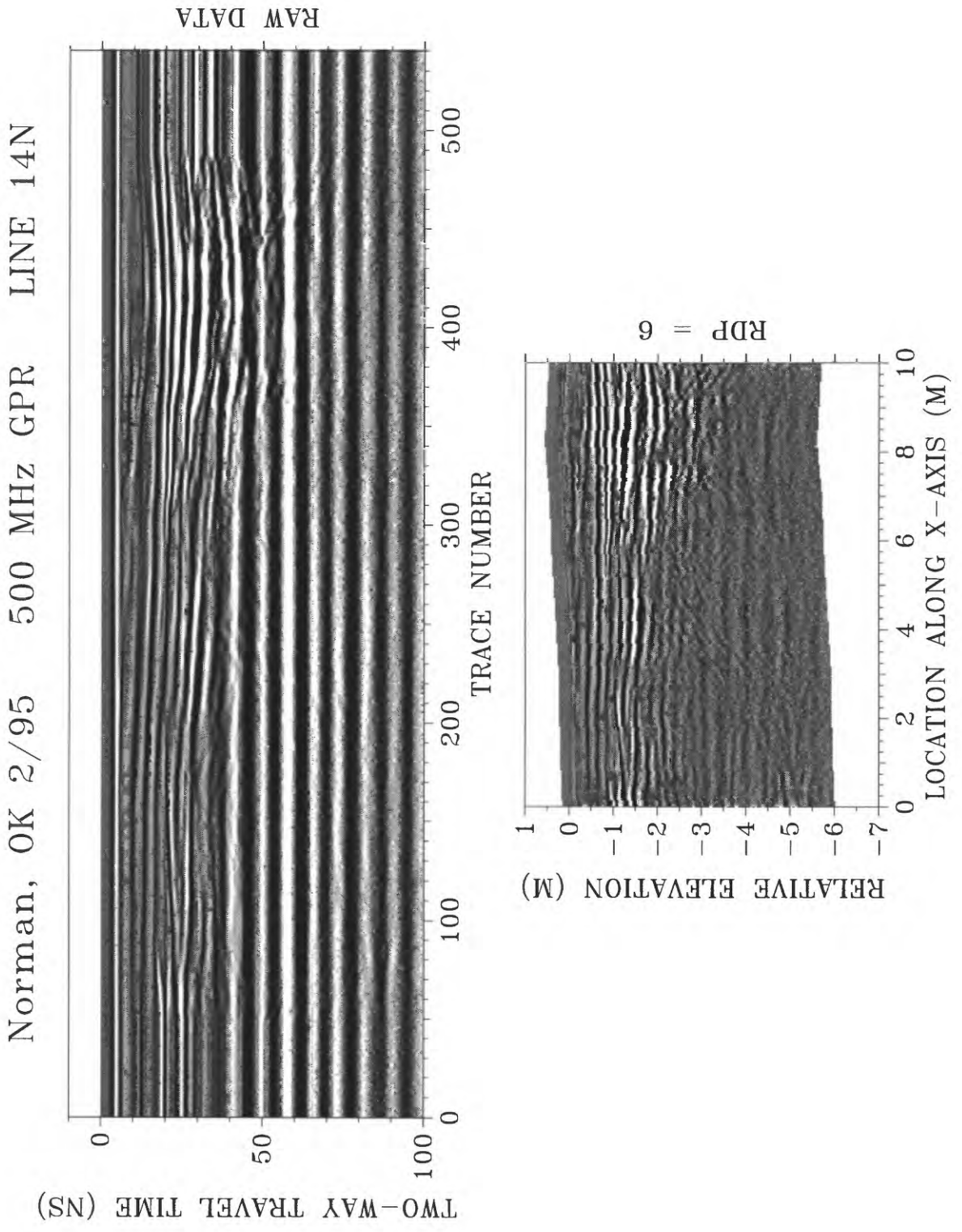

Figure A49. GPR images from 500 MHz antennas from Norman Landfill GPR test grid 1.

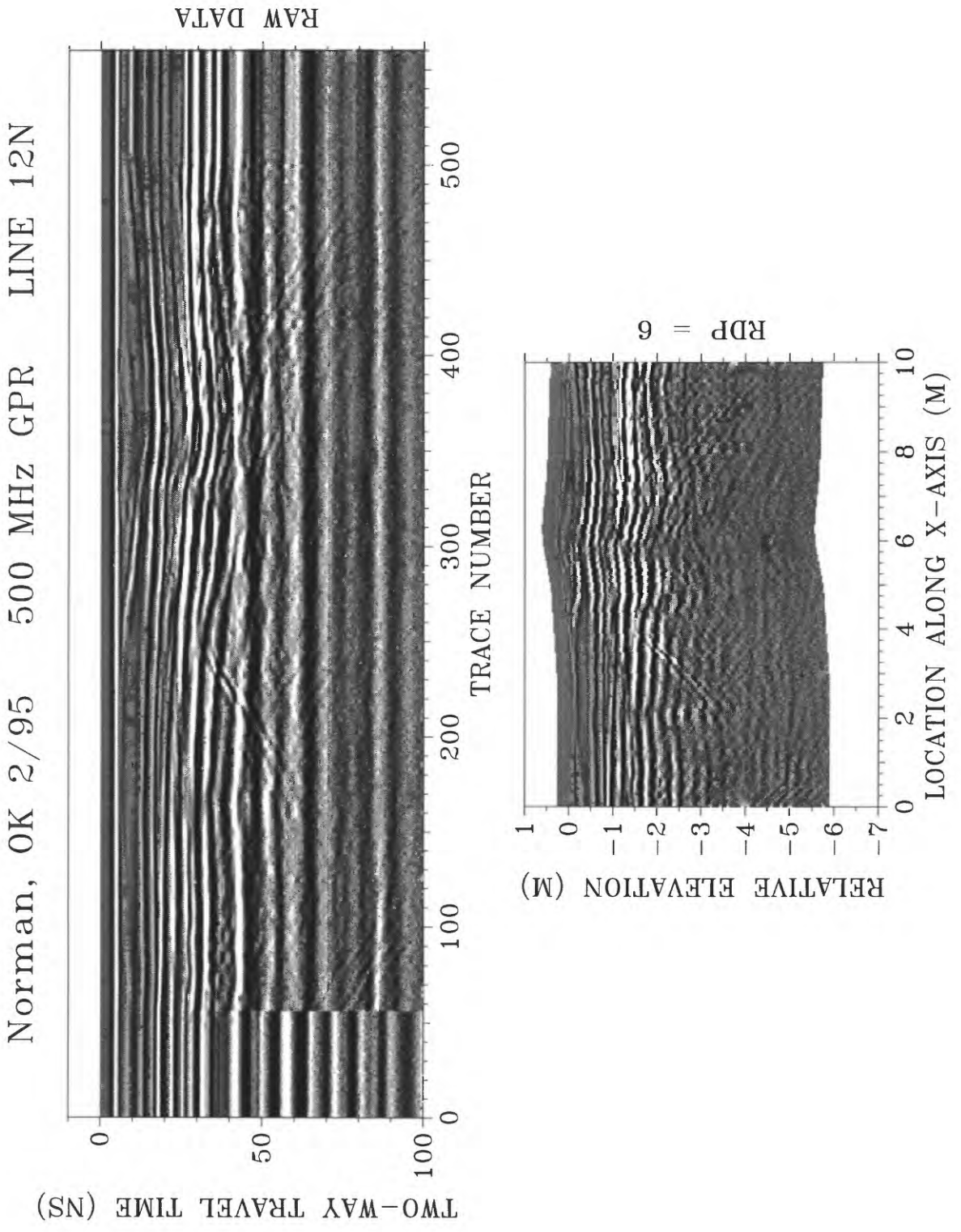

Figure A50. GPR images from 500 MHz antennas from Norman Landfill GPR test grid 1.

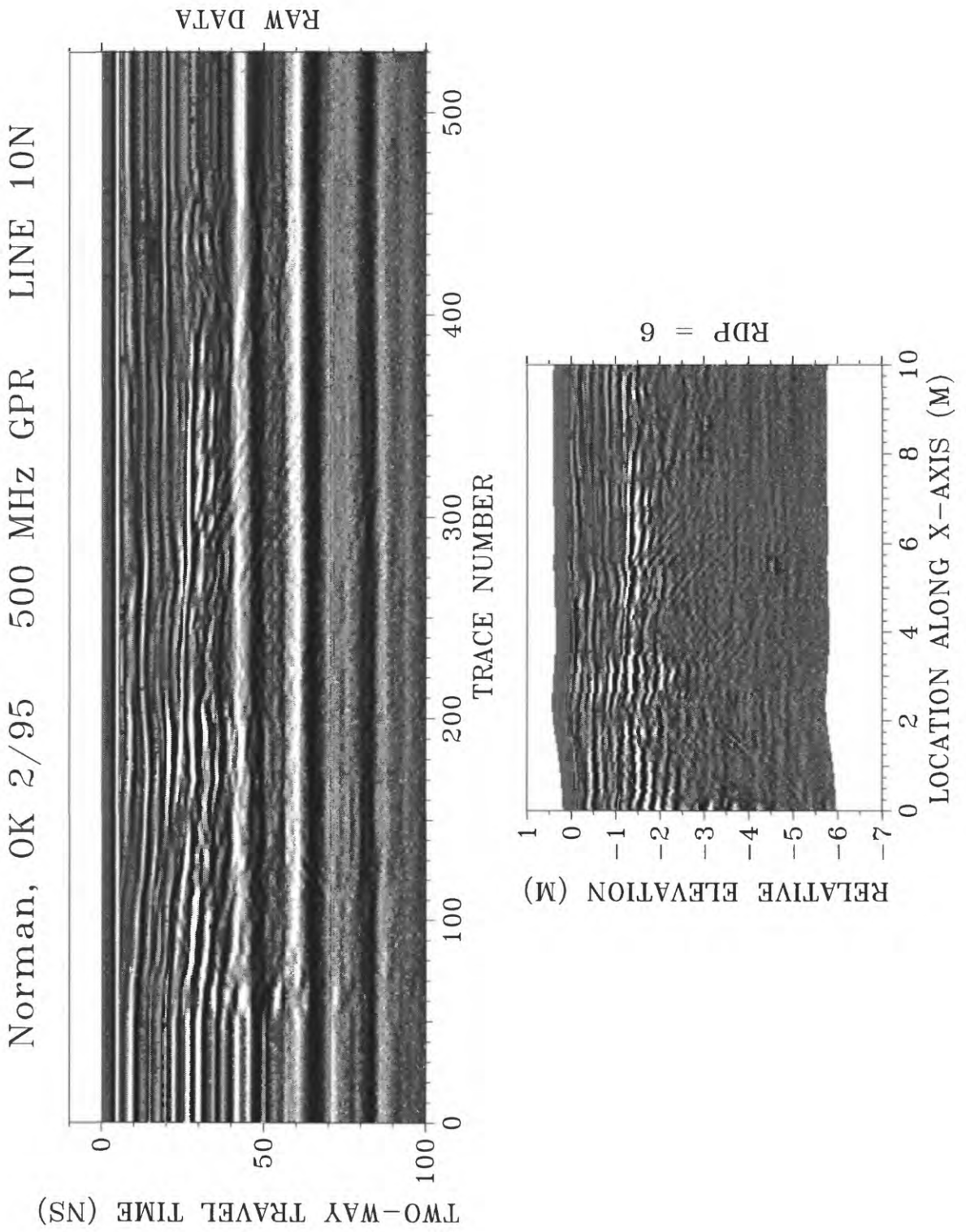

Figure A51. GPR images from 500 MHz antennas from Norman Landfill GPR test grid 1.

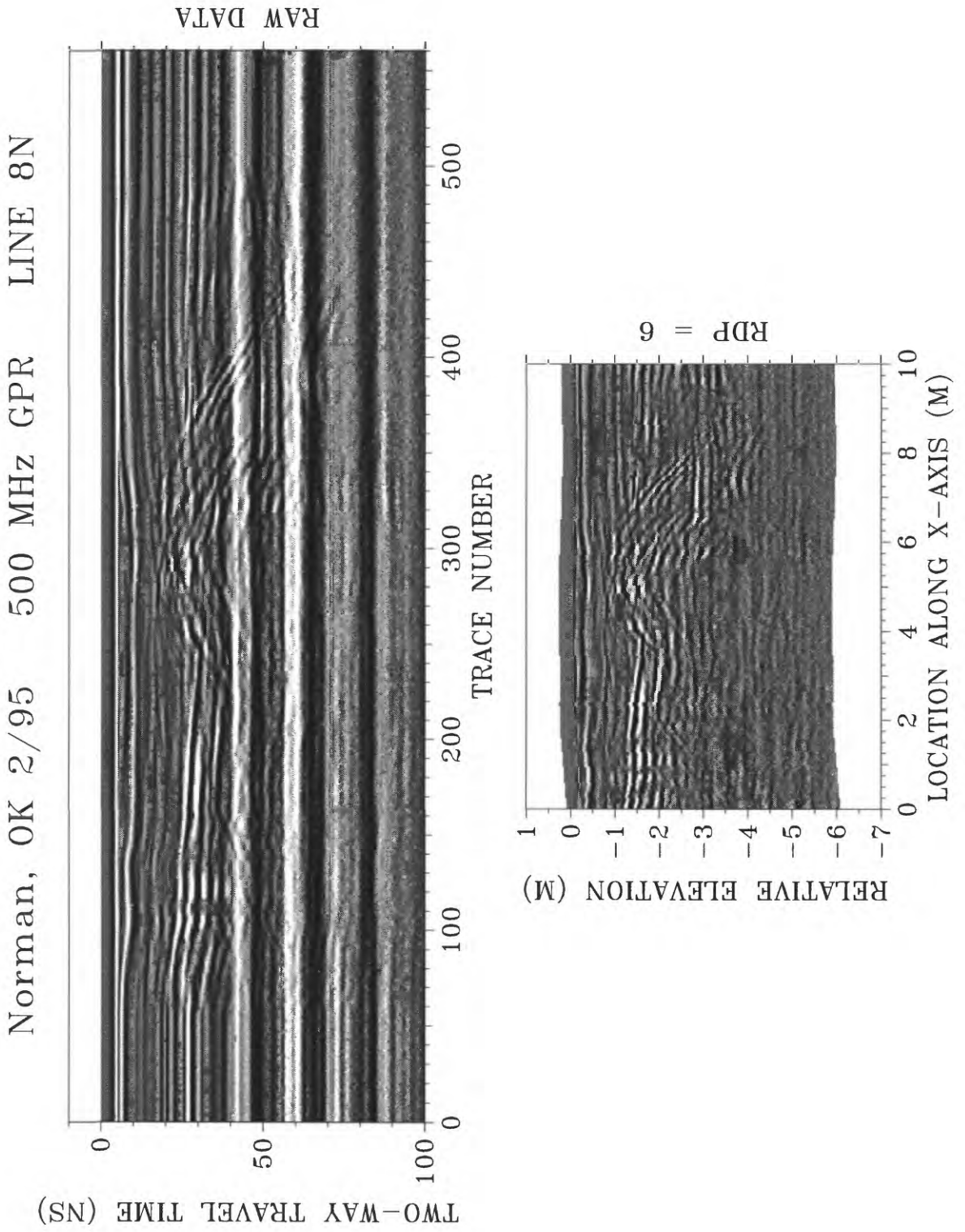

Figure A52. GPR images from 500 MHz antennas from Norman Landfill GPR test grid 1.

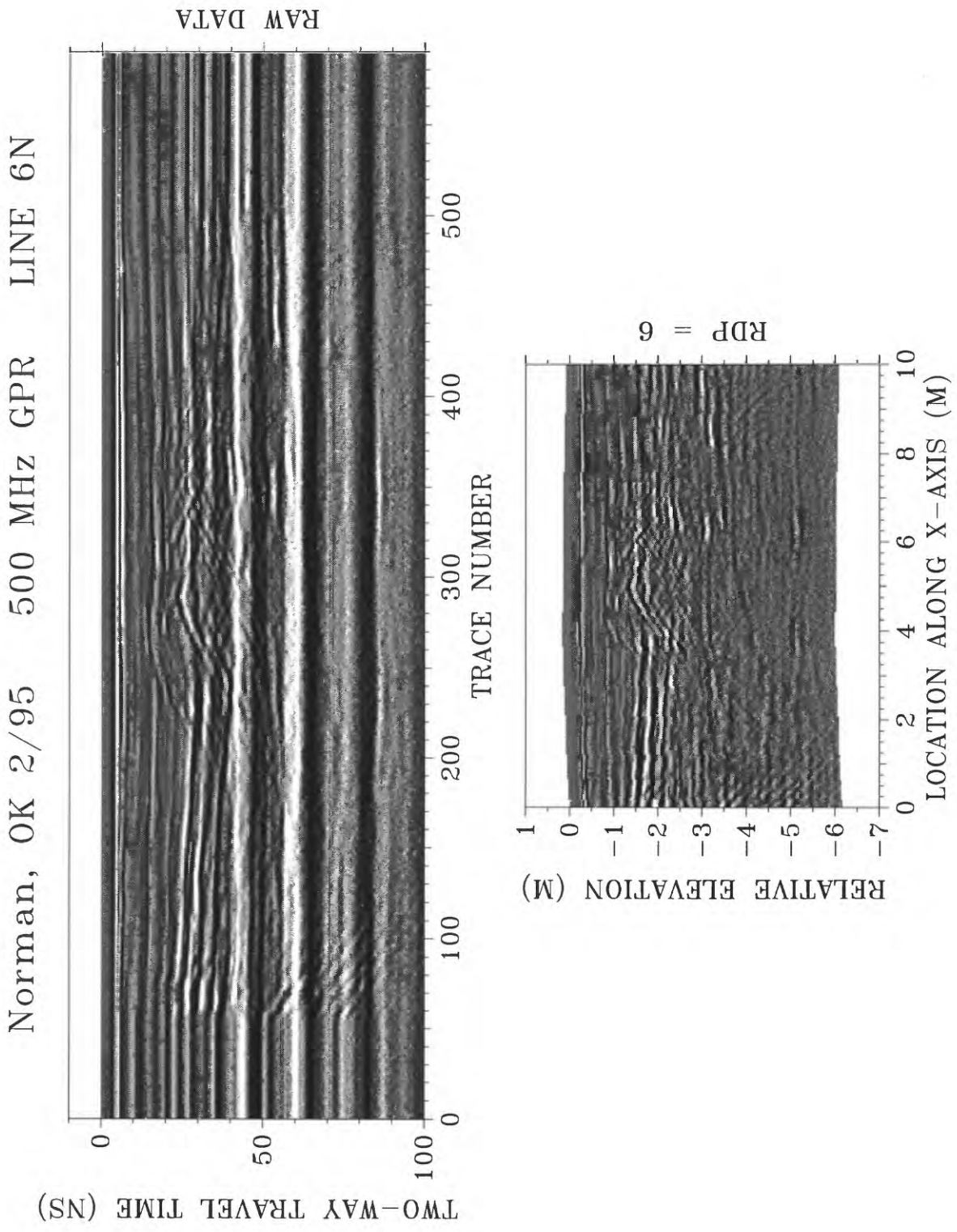

Figure A53. GPR images from 500 MHz antennas from Norman Landfill GPR test grid 1.

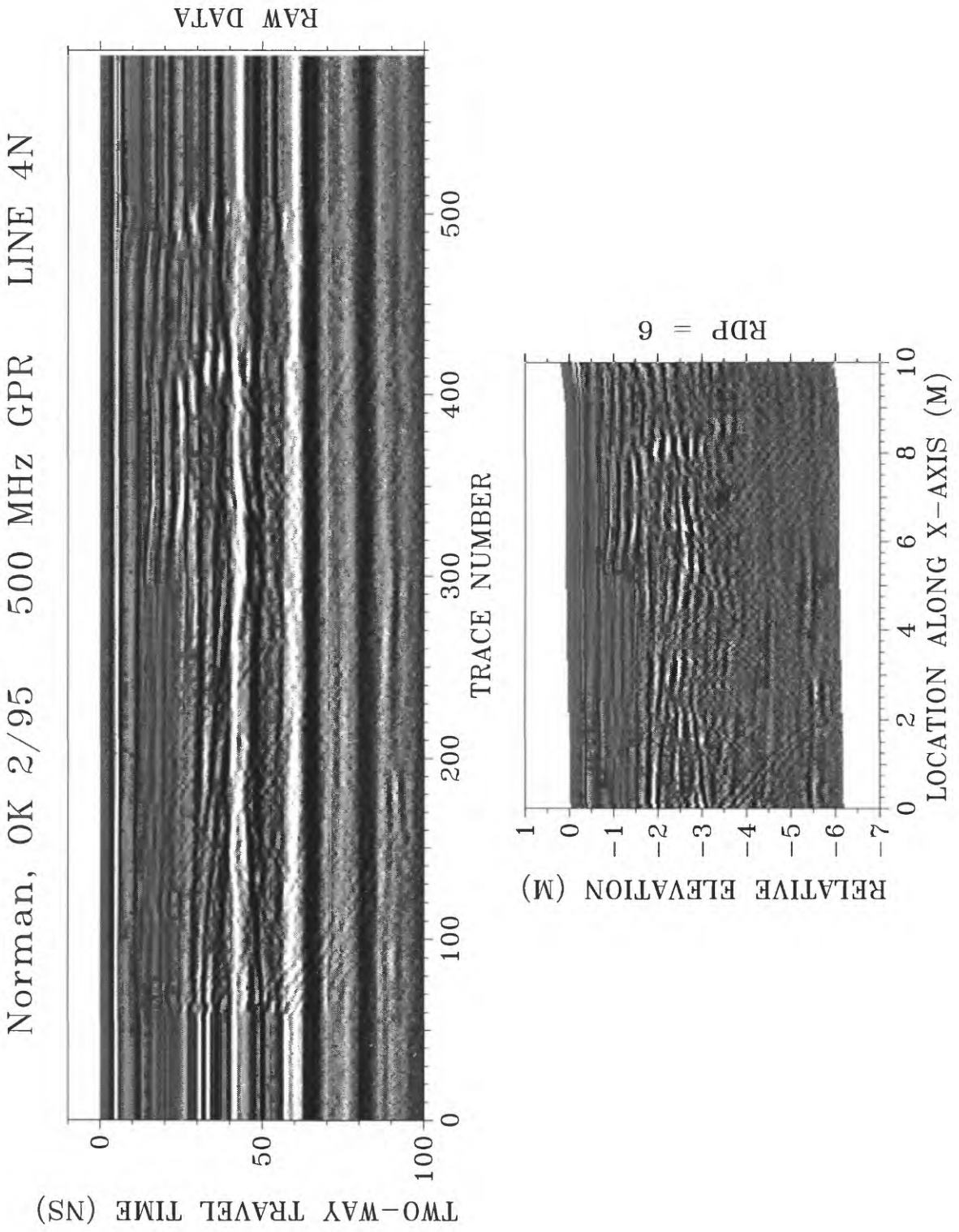

Figure A54. GPR images from 500 MHz antennas from Norman Landfill GPR test grid 1.

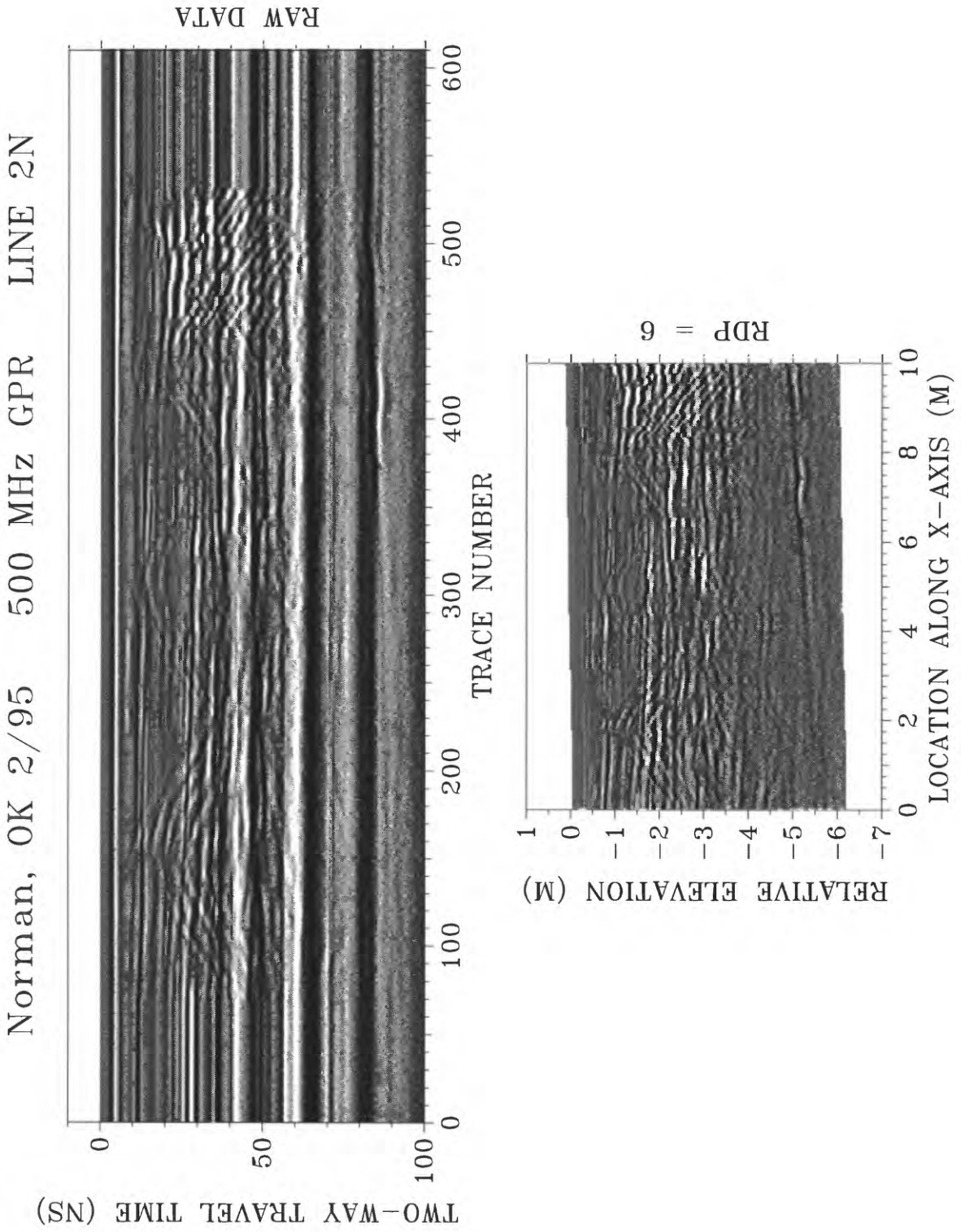

Figure A55. GPR images from 500 MHz antennas from Norman Landfill GPR test grid 1.

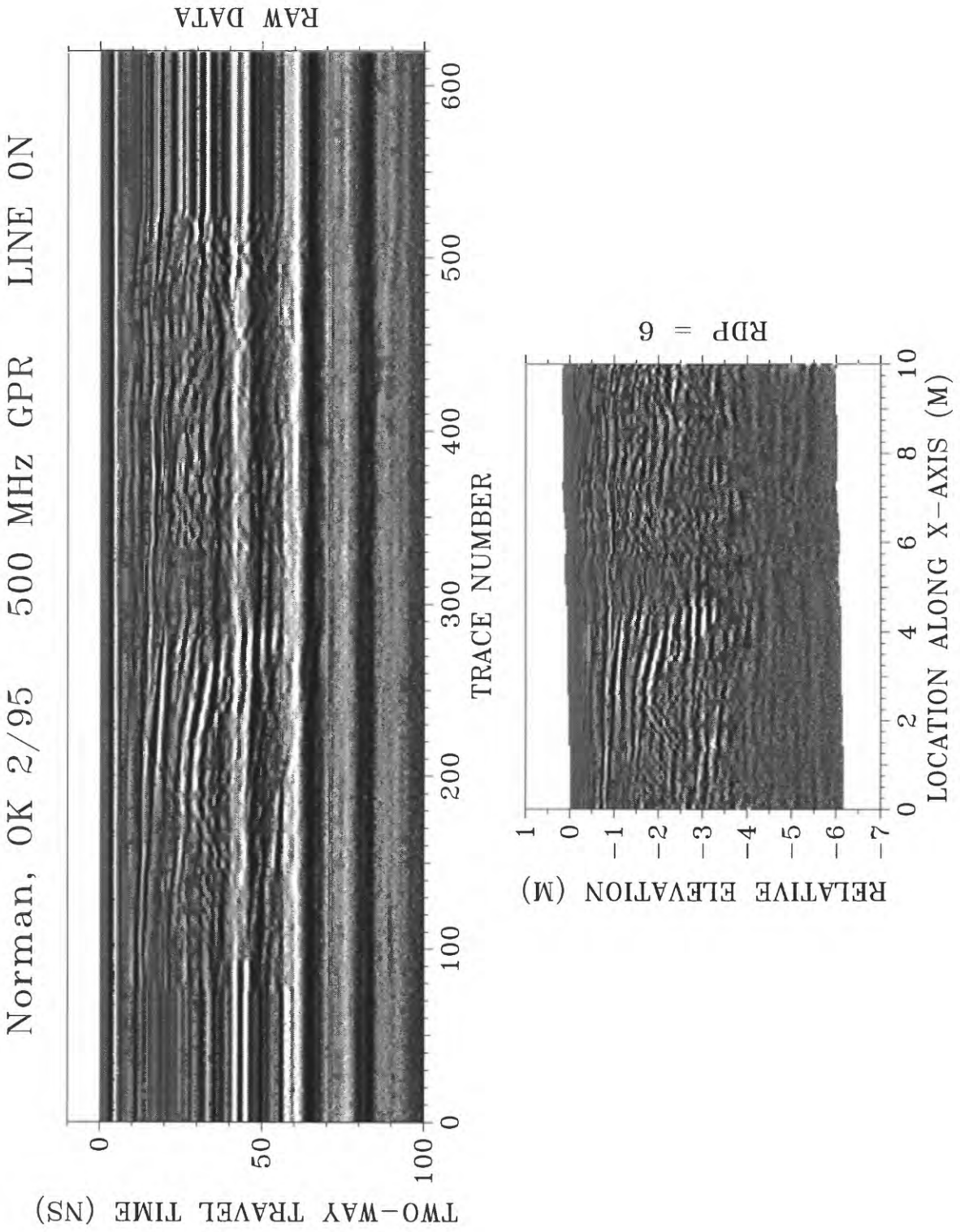

Figure A56. GPR images from 500 MHz antennas from Norman Landfill GPR test grid 1.

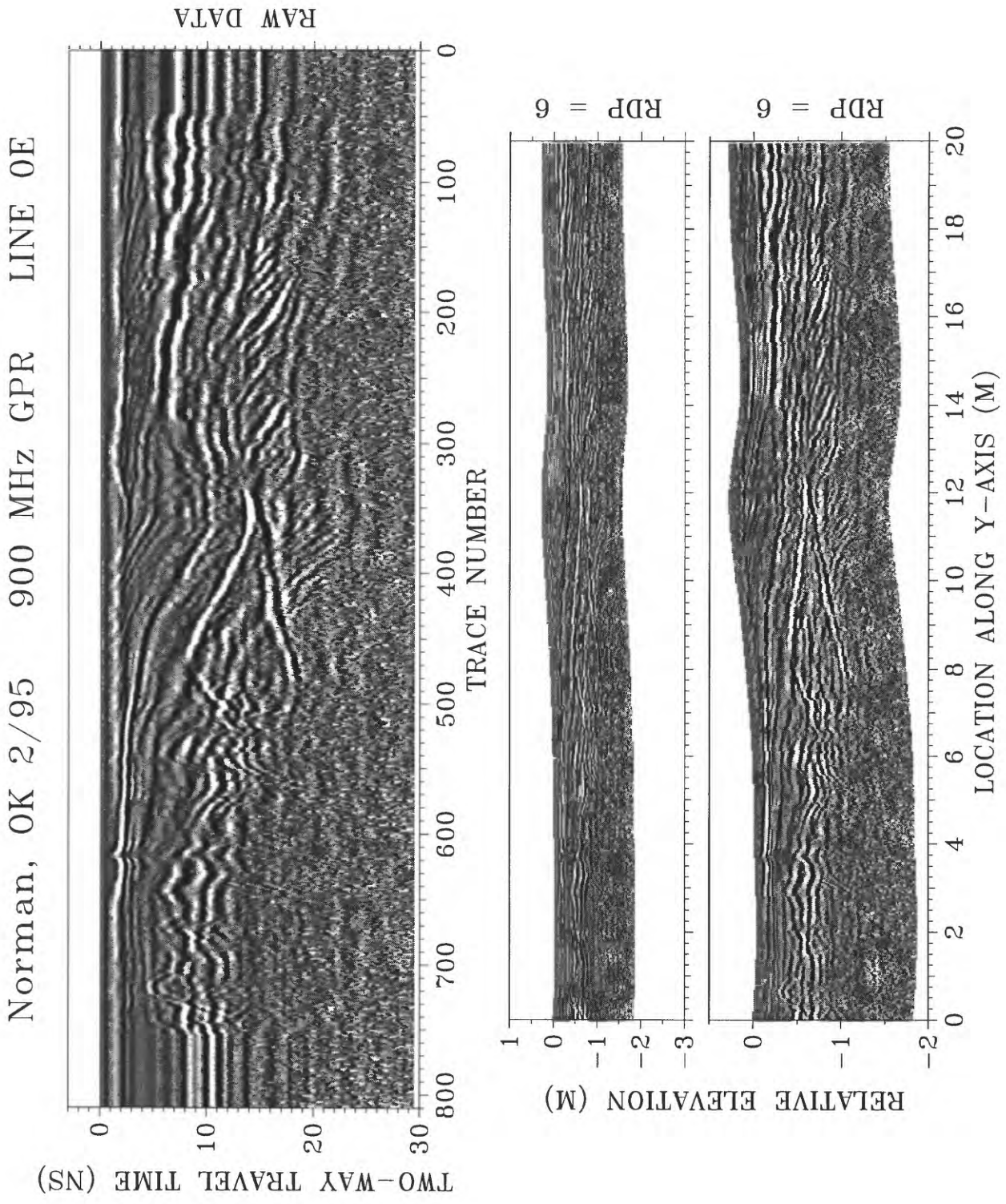

Figure A57. GPR images from 900 MHz antennas from Norman Landfill GPR test grid 1.

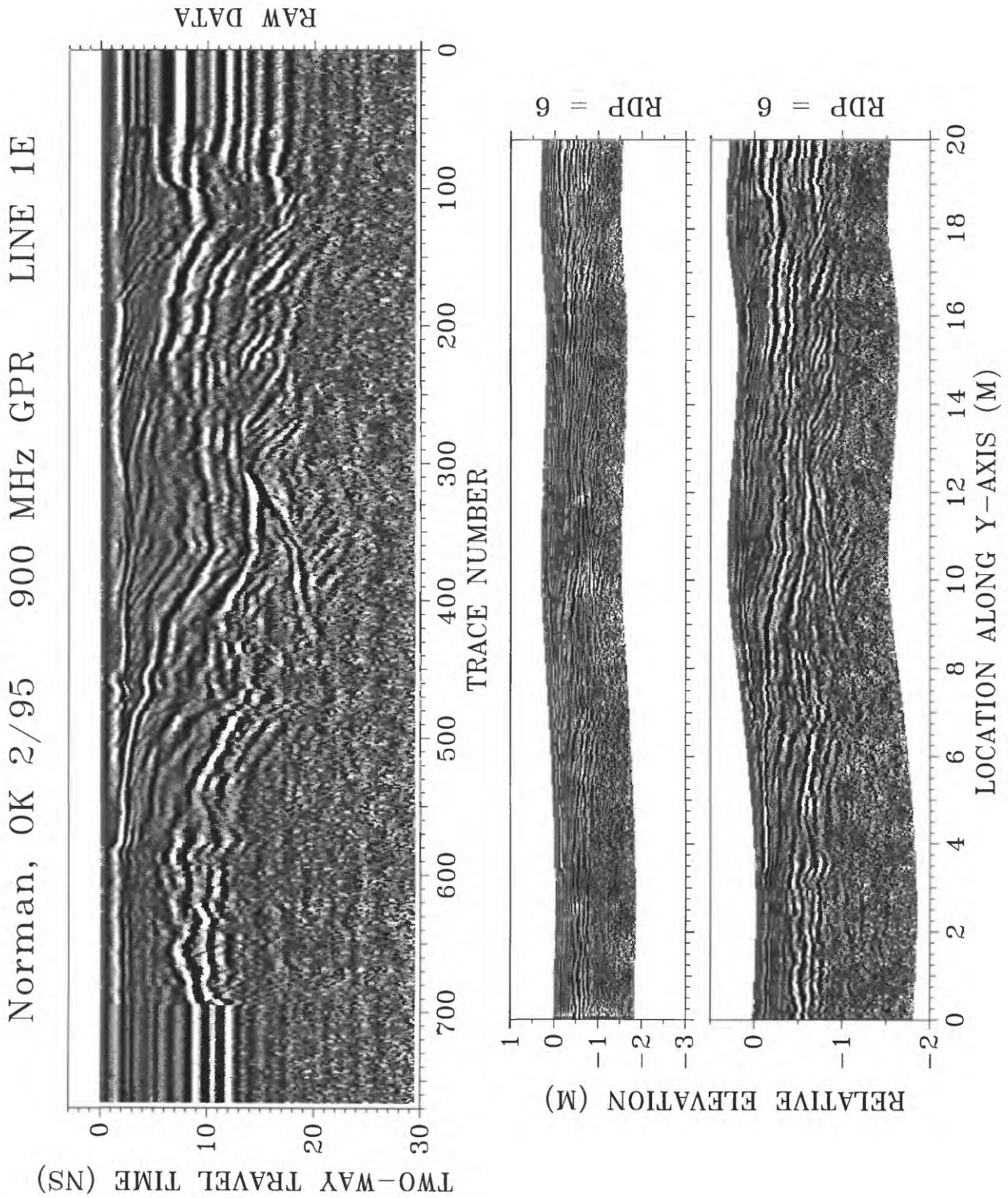

Figure A58. GPR images from 900 MHz antennas from Norman Landfill GPR test grid 1.

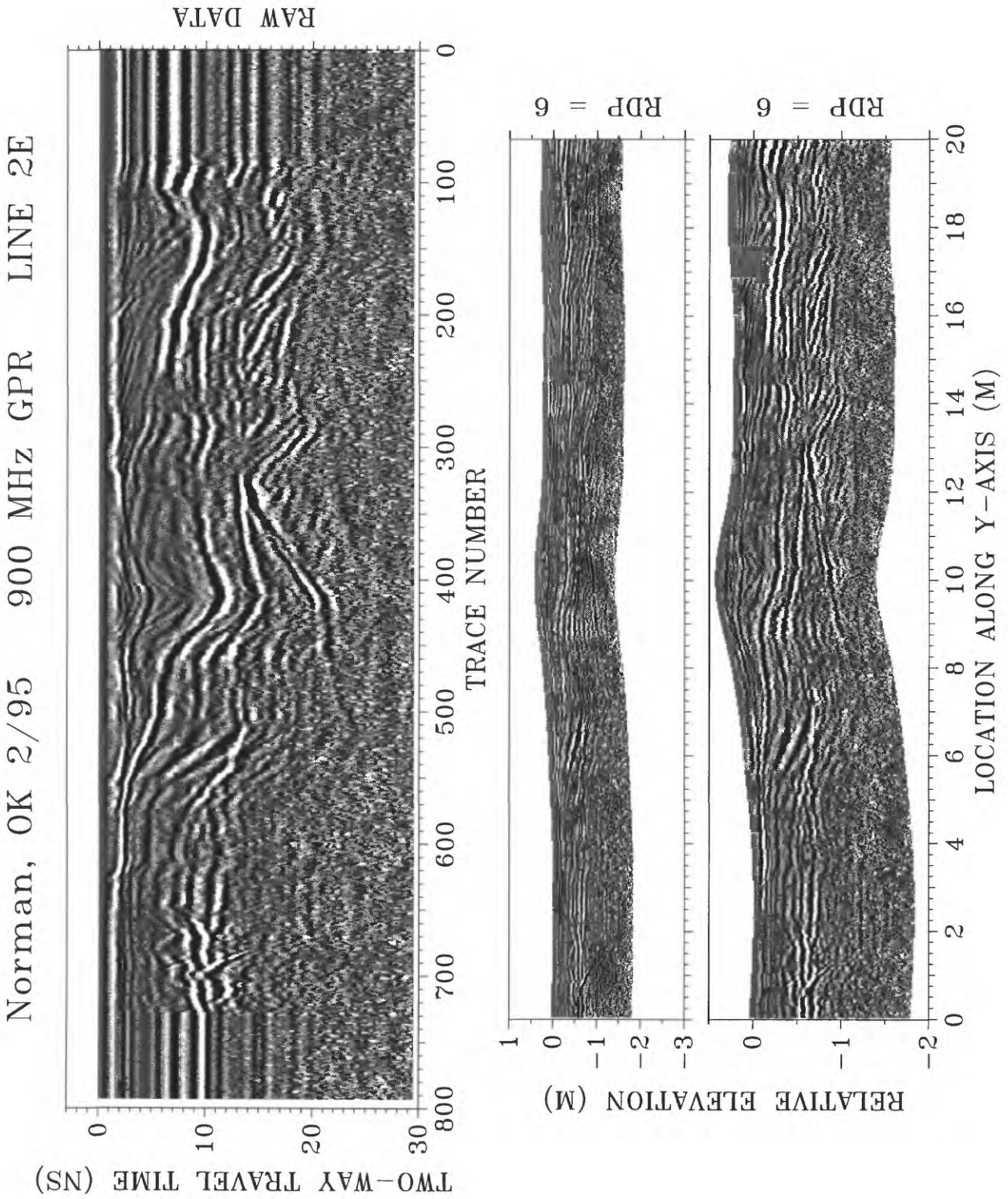

Figure A59. GPR images from 900 MHz antennas from Norman Landfill GPR test grid 1.

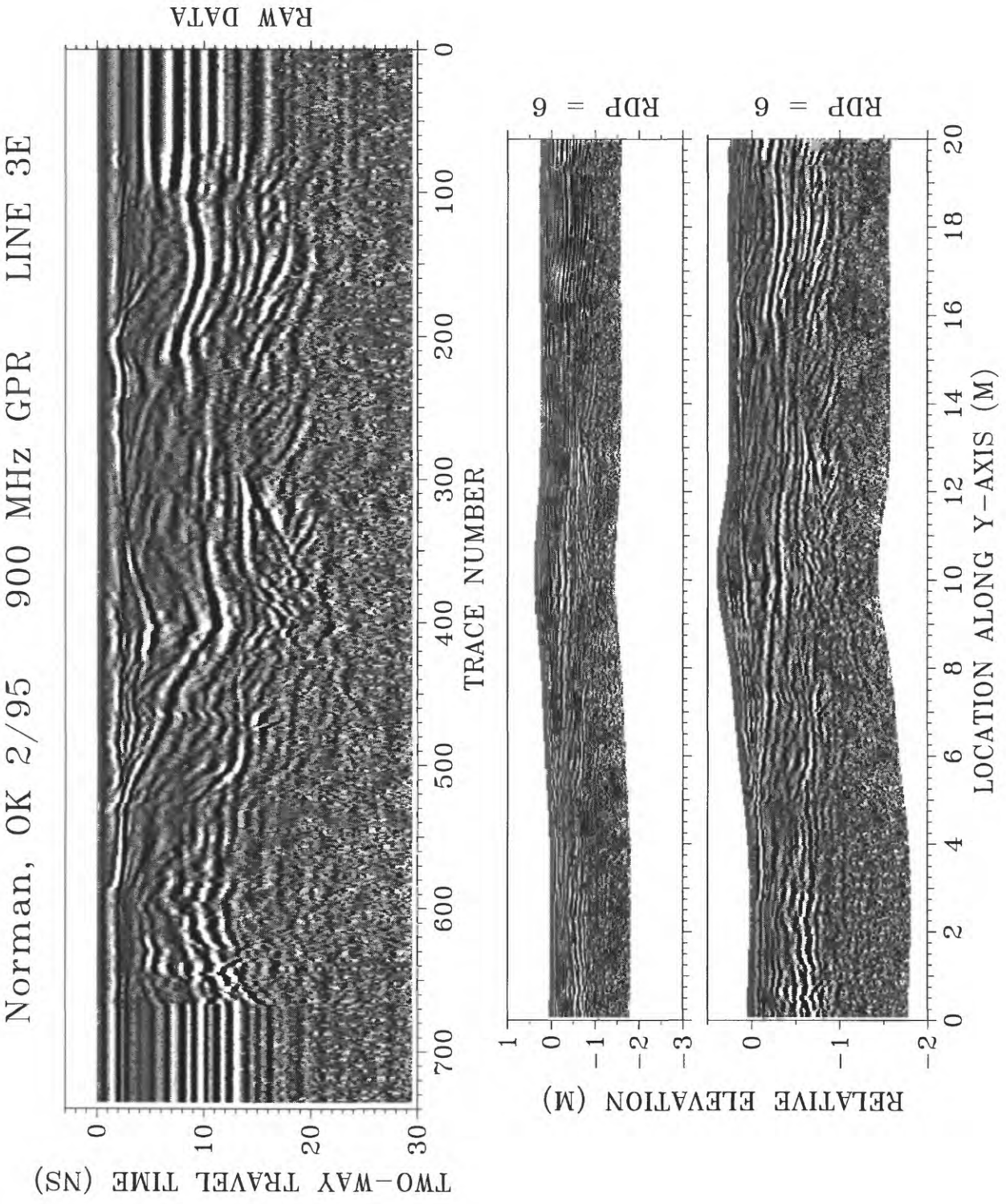

Figure A60. GPR images from 900 MHz antennas from Norman Landfill GPR test grid 1.

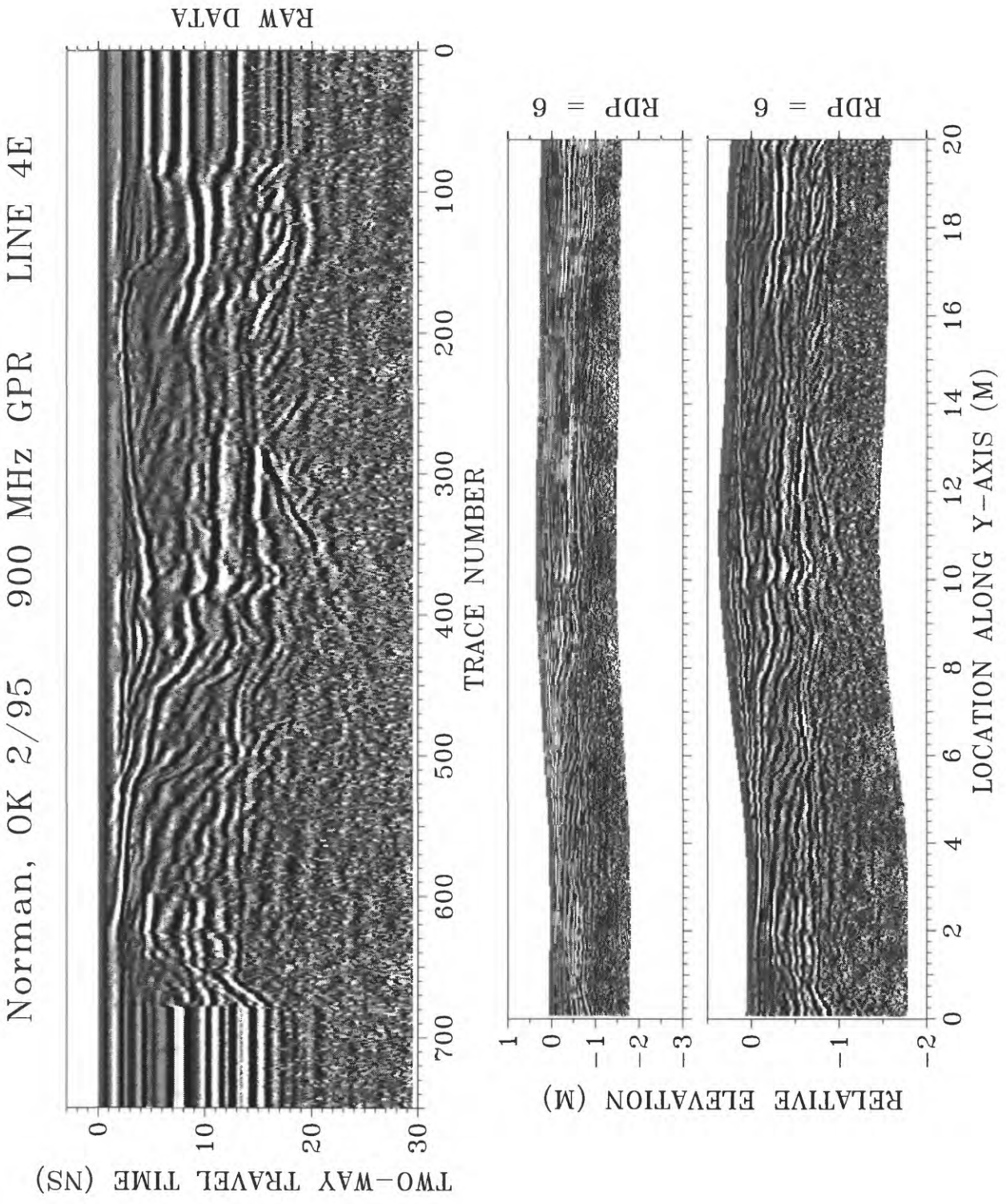

Figure A61. GPR images from 900 MHz antennas from Norman Landfill GPR test grid 1.

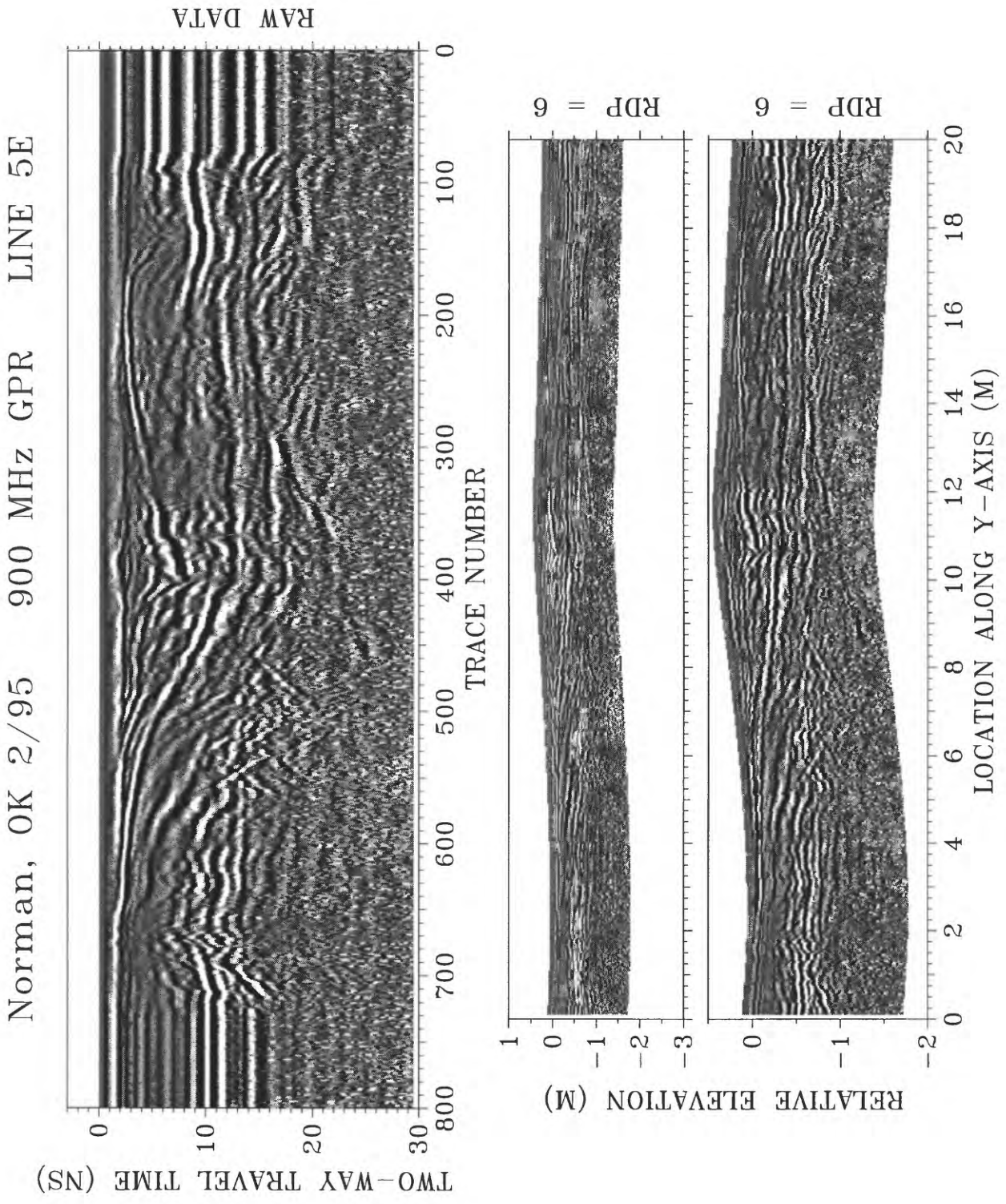

Figure A62. GPR images from 900 MHz antennas from Norman Landfill GPR test grid 1.

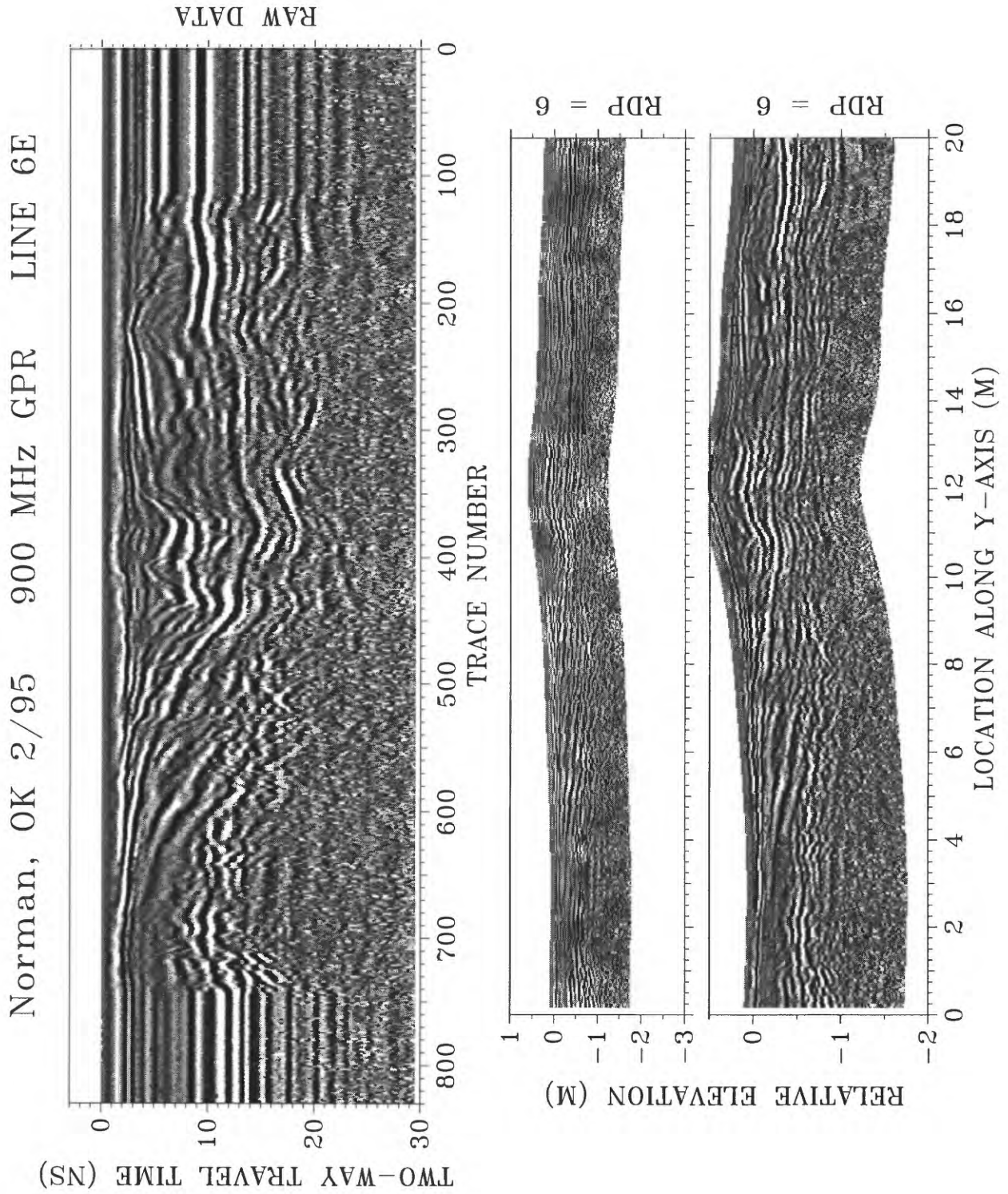

Figure A63. GPR images from 900 MHz antennas from Norman Landfill GPR test grid 1.

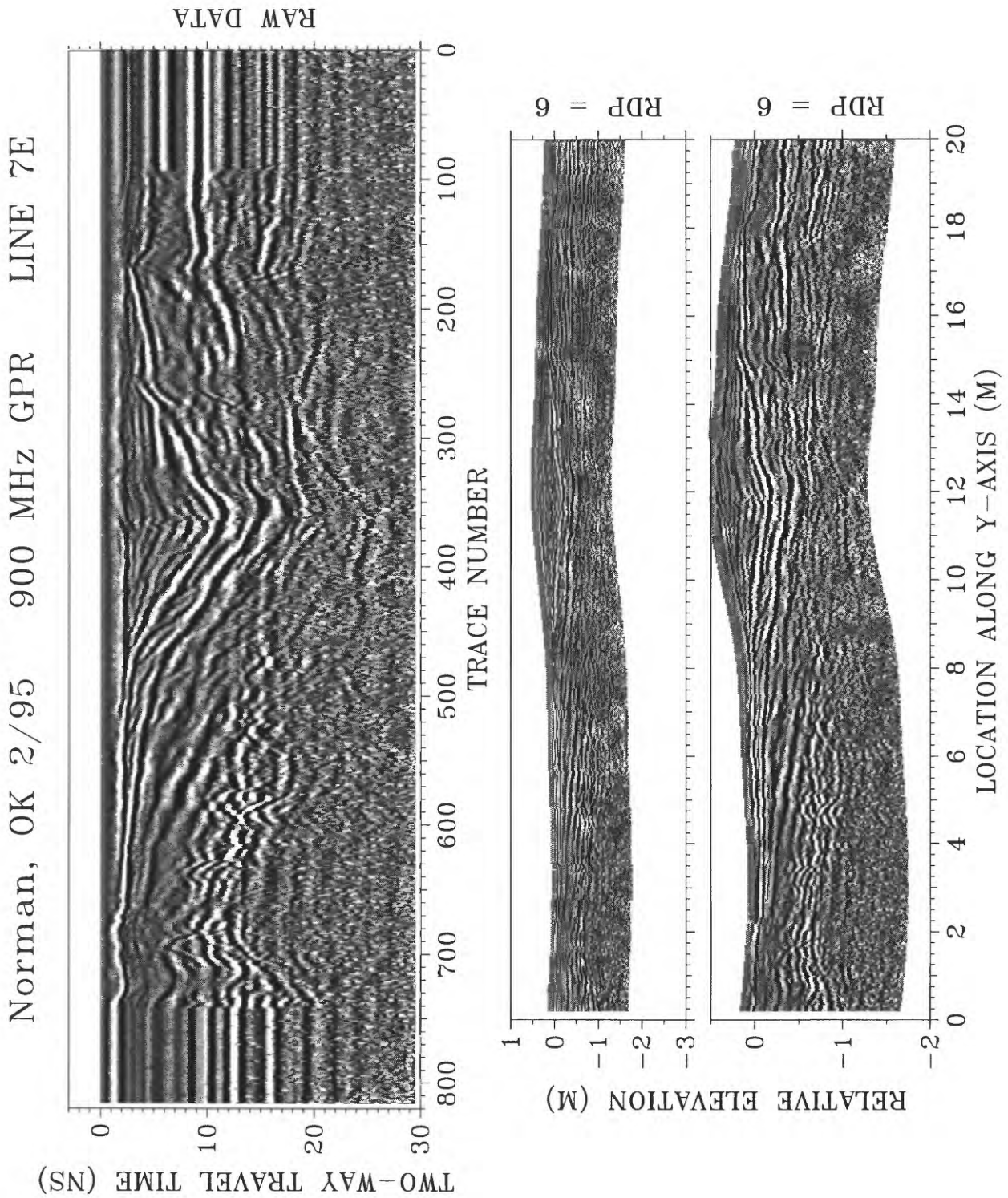

Figure A64. GPR images from 900 MHz antennas from Norman Landfill GPR test grid 1.

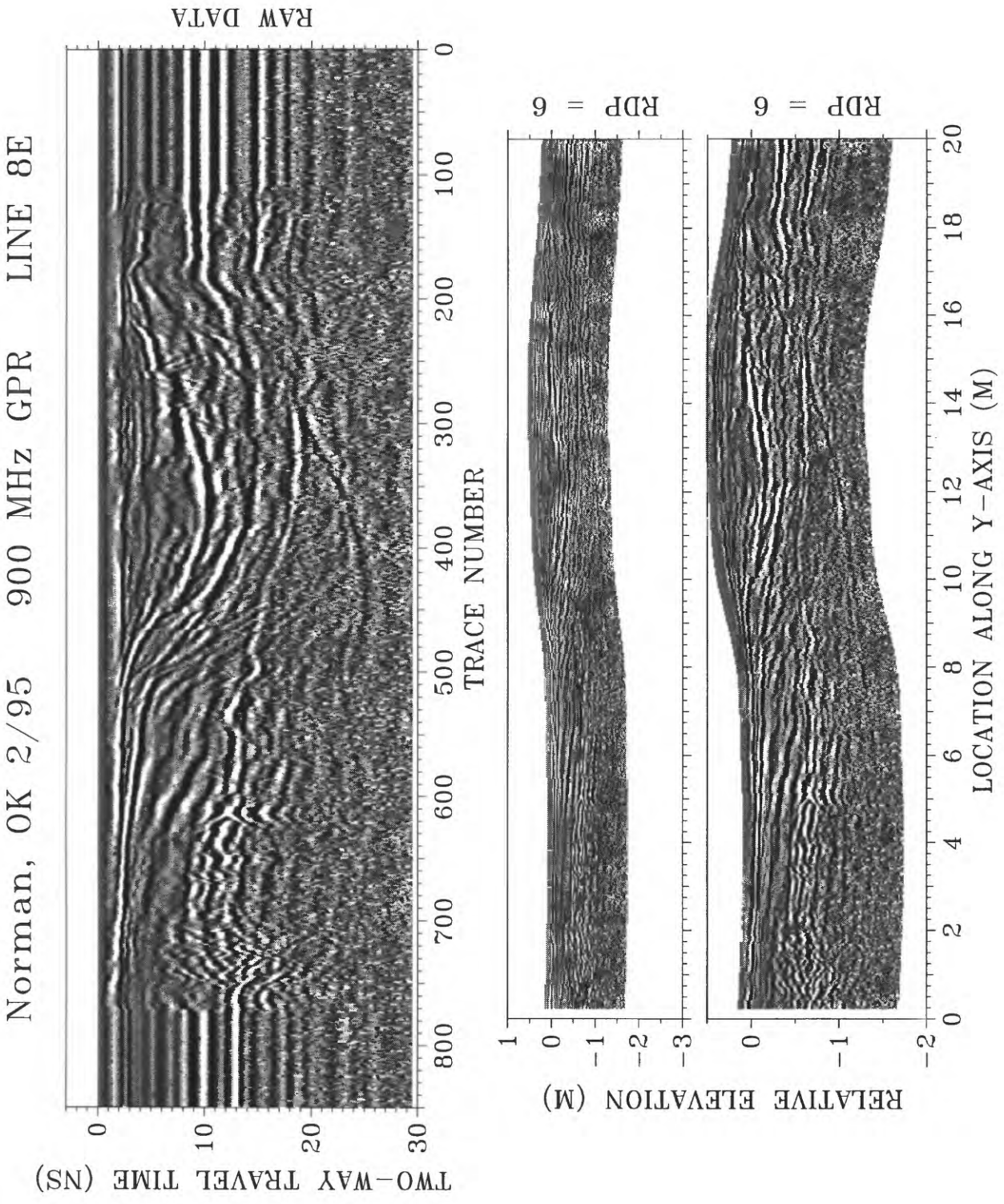

Figure A65. GPR images from 900 MHz antennas from Norman Landfill GPR test grid 1.

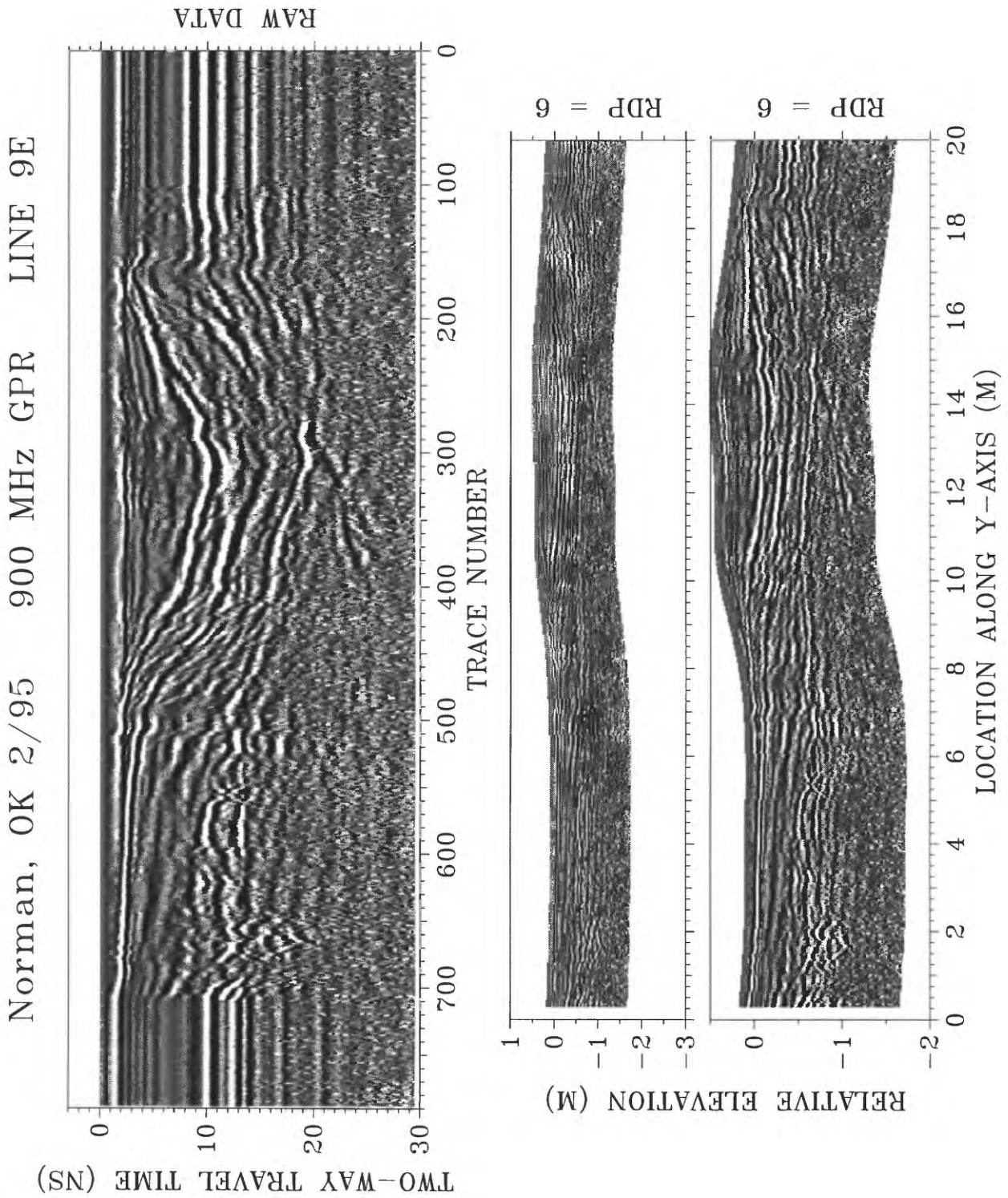

Figure A66. GPR images from 900 MHz antennas from Norman Landfill GPR test grid 1.

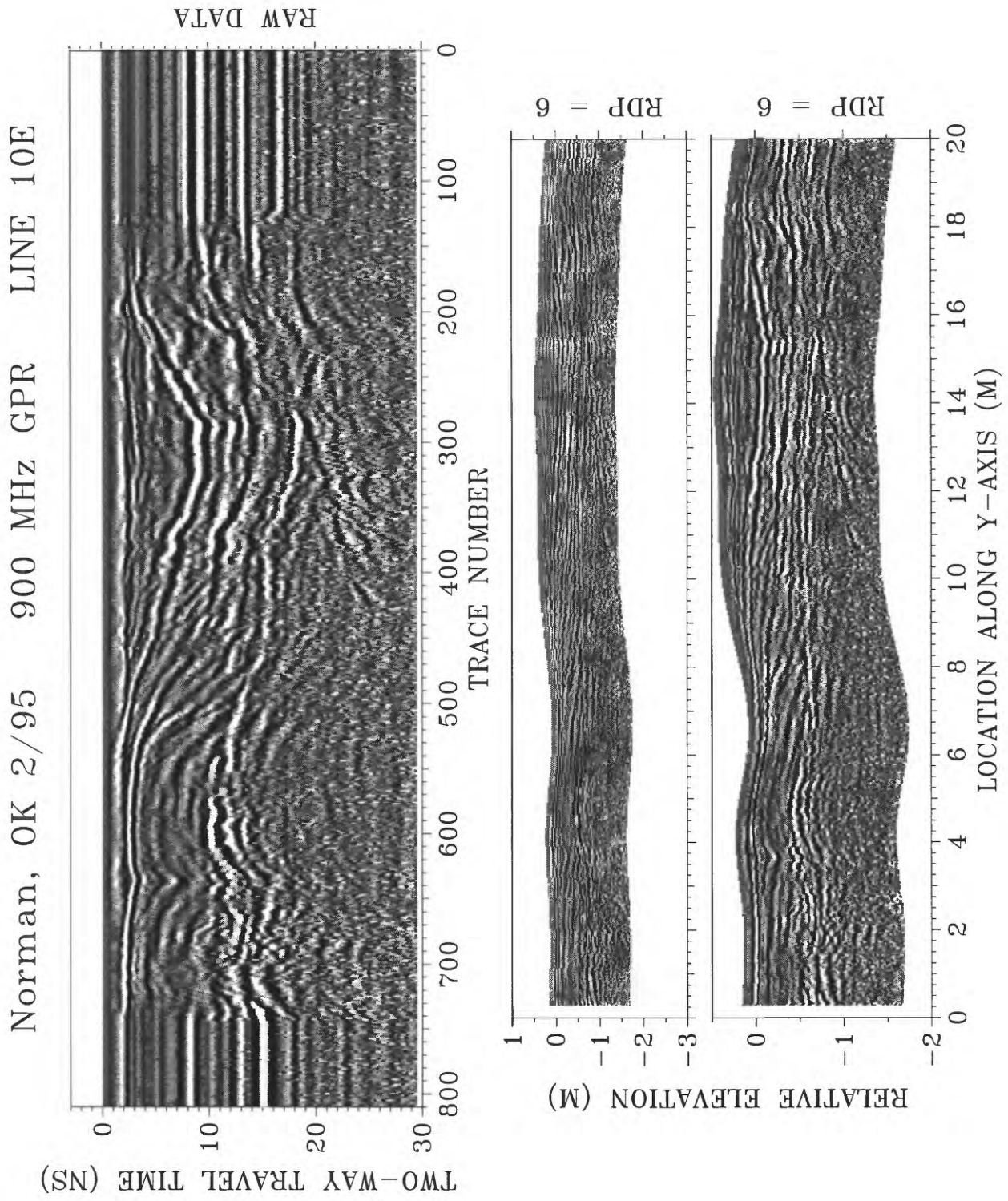

Figure A67. GPR images from 900 MHz antennas from Norman Landfill GPR test grid 1.